QC
1
.U54
vol 63C
no. 2

THE UNIVERSITY
OF MICHIGAN
NOV 25 1959
LIBRARY

Volume 63C
Number 2
Oct.–Dec. 1959

Journal of Research

of the

NATIONAL BUREAU OF STANDARDS

C. ENGINEERING AND INSTRUMENTATION

Journal of Research

of the

National Bureau of Standards

C. Engineering and Instrumentation

OCT.–DEC. • 1959

VOLUME • 63C

NUMBER • 2

Editor: W. A. Wildhack

Associate Editors: G. F. Montgomery, R. B. Jacobs

Publication dates: Aug. 15, Nov. 15, 1959

JOURNAL OF RESEARCH

The National Bureau of Standards Journal of Research reports research and development in the fields of activity shown at right. Also included from time to time are survey articles and compilations of information on topics closely related to the Bureau's scientific and technical program.

The Journal is published in four separate sections as follows:

A. Physics and Chemistry

Contains papers of interest primarily to scientists working in these fields. Issued six times a year. Annual subscription: domestic, $4.00; foreign, $4.75.

B. Mathematics and Mathematical Physics

Presents studies and compilations designed mainly for the mathematician and the theoretical physicist. Issued quarterly. Annual subscription: domestic, $2.25; foreign, $2.75.

C. Engineering and Instrumentation

Reports research and development results of interest chiefly to the engineer and the applied scientist. Issued quarterly. Annual subscription: domestic, $2.25; foreign, $2.75.

D. Radio Propagation

Reports work in radio propagation physics and upper atmospheric research. Issued six times a year. Annual subscription: domestic, $4.00; foreign, $4.75.

U.S. DEPARTMENT OF COMMERCE
Frederick H. Mueller, Secretary

NATIONAL BUREAU OF STANDARDS
A. V. Astin, Director

Functions and Activities

The functions of the National Bureau of Standards are set forth in the Act of Congress, March 3, 1901, as amended. These include the development and maintenance of the national standards of measurement and the provision of means and methods for making measurements consistent with these standards; the determination of physical constants and properties of materials; the development of methods and instruments for testing materials, devices, and structures; advisory services to government agencies on scientific and technical problems; invention and development of devices to serve special needs of the Government; and the development of standard practices, codes, and specifications. The work includes basic and applied research, development, engineering, instrumentation, testing, evaluation, calibration services, and various consultation and information services. The Bureau also serves as the Federal technical research center in a number of specialized fields. The scope of activities of the National Bureau of Standards is suggested in the following listing of the divisions and sections engaged in technical work.

Washington, D.C

Electricity and Electronics. Resistance and Reactance. Electron Devices. Electrical Instruments. Magnetic Measurements. Dielectrics. Engineering Electronics. Electronic Instrumentation. Electrochemistry.

Optics and Metrology. Photometry and Colorimetry. Optical Instruments. Photographic Technology. Length. Engineering Metrology.

Heat. Temperature Physics. Thermodynamics. Cryogenic Physics. Rheology. Engine Fuels. Free Radicals Research.

Atomic and Radiation Physics. Spectroscopy. Radiometry. Mass Spectrometry. Solid State Physics. Electron Physics. Atomic Physics. Neutron Physics. Radiation Theory. Radioactivity. X-ray. High Energy Radiation. Nucleonic Instrumentation. Radiological Equipment.

Chemistry. Organic Coatings. Surface Chemistry. Organic Chemistry. Analytical Chemistry. Inorganic Chemistry. Electrodeposition. Molecular Structure and Properties of Gases. Physical Chemistry. Thermochemistry. Spectrochemistry. Pure Substances.

Mechanics. Sound. Mechanical Instruments. Fluid Mechanics. Engineering Mechanics. Mass and Scale. Capacity, Density, and Fluid Meters. Combustion Controls.

Organic and Fibrous Materials. Rubber. Textiles. Paper. Leather. Testing and Specifications. Polymer Structure. Plastics. Dental Research.

Metallurgy. Thermal Metallurgy. Chemical Metallurgy. Mechanical Metallurgy. Corrosion. Metal Physics.

Mineral Products. Engineering Ceramics. Glass. Refractories. Enameled Metals. Concreting Materials. Constitution and Microstructure.

Building Technology. Structural Engineering. Fire Protection. Air Conditioning, Heating, and Refrigeration. Floor, Roof, and Wall Coverings. Codes and Safety Standards. Heat Transfer.

Applied Mathematics. Numerical Analysis. Computation. Statistical Engineering. Mathematical Physics.

Data Processing Systems. SEAC Engineering Group. Components and Techniques. Digital Circuitry. Digital Systems. Analog Systems. Applications Engineering.

• Office of Basic Instrumentation. • Office of Weights and Measures

Boulder, Colorado

Cryogenic Engineering. Cryogenic Equipment. Cryogenic Processes. Properties of Materials. Gas Liquefaction.

Radio Propagation Physics. Upper Atmosphere Research. Ionosphere Research. Regular Prediction Services. Sun-Earth Relationships. VHF Research. Radio Warning Services. Airglow and Aurora. Radio Astronomy and Arctic Propagation.

Radio Propagation Engineering. Data Reduction Instrumentation. Radio Noise. Tropospheric Measurements. Tropospheric Analysis. Propagation-Terrain Effects. Radio-Meteorology. Lower Atmosphere Physics.

Radio Standards. High Frequency Electrical Standards. Radio Broadcast Service. Radio and Microwave Materials. Electronic Calibration Center. Microwave Circuit Standards.

Radio Communication and Systems. Low Frequency and Very Low Frequency Research. High Frequency and Very High Frequency Research. Modulation Systems. Antenna Research. Navigation Systems. Systems Analysis. Field Operations.

Order all publications from the Superintendent of Documents
U.S. Government Printing Office, Washington 25, D.C.

Use of funds for printing this publication approved by the Director of the Bureau of the Budget (June 24, 1958).

DEPOSITED BY THE
UNITED STATES OF AMERICA

Journal of Research of the National Bureau of Standards—C. Engineering and Instrumentation

Vol. 63C, No. 2, October–December 1959

Conical Coaxial Capacitors and Their Advantages

M. C. Selby

(June 16, 1959)

Adjustable capacitors having electrodes in the form of coaxial cones or frustums have been used on rare occasions in the past, but their potential superiority to other types of capacitors for some important applications has been overlooked. The advantage of this geometry over cylindrical or disk forms is that the practical capacitance range is several times larger. An example cites the capacitance ranges for the same mechanical and percentage accuracy of a disk, cylindrical and conical type to be 10, 40, and 168 to 1, respectively. An approximate equation was derived for this conical capacitor and close agreement is shown between computed and measured values of capacitance versus electrode displacement. Multiple cone and specially shaped electrodes are suggested to obtain large values of capacitance with an appreciable saving of space and further increased range of capacitance.

1. Introduction

Adjustable capacitors of coaxial form are frequently more suitable for a given application than the conventional rotary or compression types.[1] Variation of capacitance in the former is obtained by linear displacement of one electrode, usually a cylinder or a disk, with respect to another similar stationary electrode. Unfortunately, cylindrical- and disk-type electrodes have a relatively limited capacity range. Conical electrodes are intuitively attractive because they represent an intermediate case between cylindrical and disk electrodes. So far as the author is aware, no expression for the capacity of a conical structure has been derived. Such an expression is given below and will be of help in determining the effect of the dimensions and angle of the cone on capacity values and particularly on the range of capacity.[2] This range is affected primarily by two things, the mechanical presetability and end effects. The first determines the minimum or maximum capacity which can be preset to a desired accuracy; this limiting factor seems to be the more important of the two and will be treated below. The end effect limits the minimum capacity and will be neglected here. Unfortunately, this effect is rather difficult to compute or to estimate. In neglecting it we favor the cylindrical case where this effect is more pronounced than in the other two cases. It will be shown that the conical capacitor has a considerably wider range even if the end effect is neglected.

Let us assume a certain given cylindrical electrically shielded space within which an adjustable capacitor is to be placed. The shield is usually grounded. In cylindrical geometry the capacitance is directly proportional to the length of the meshed sections. If we are to be certain that all preset capacities are accurate to, say, ± 0.2 percent we must make sure that the position of the traveling electrode is always reproduced at least to 0.2 percent; the critical position will, of course, be at the minimum capacity. For a micrometer having a maximum travel of 2 in. and a resetability of ± 0.1 mil everywhere along this travel, the smallest meshed section will have to be 50 mils. The ratio of maximum to minimum capacity will therefore be 40 to 1.

On the other hand, for practical purposes, a disk-type capacitor ceases to behave like a normal capacitor approximately at separations exceeding the value of the radius of the disks. At higher separations these disks placed inside a shield have relatively high shunt capacities to the shield. Let us consider in all cases 1 in. as the diameter of the available cylindrical space; the shield may be 1½ or 2 in. in diameter. The critical position of the micrometer in the case of disks will be at the maximum capacity, namely at a disk separation of 50 mils. The range will therefore be fixed approximately by the ratio of one-half in. to 50 mils or 10 to 1. With conical electrodes one can realize a range many times that of a cylindrical or disk capacitor.

2. Conical Capacitor

Consider a capacitor formed by two right frustums as shown in figure 1. The cross section shows the essential dimensional elements of this capacitor. Let the sections of the conical electrode surfaces indicated by the length l be referred to as the "meshed" surfaces. Let also:

2θ = angle of the cones.
D = adjustable distance between the apexes of the cones. As D increases the capacitance decreases, because the distances between the conical surfaces increase and the length of meshed surfaces is reduced.
h = the height of the inside cone (A) from its apex to the base of its effective meshed surface.

[1] J. C. Balsbaugh and P. H. Moon, A bridge for precision power-factor measurements on small oil samples, Trans. AIEE **52,** 528 (June 1933).
[2] M. C. Selby, Analysis of coaxial conical capacitor (publication pending).

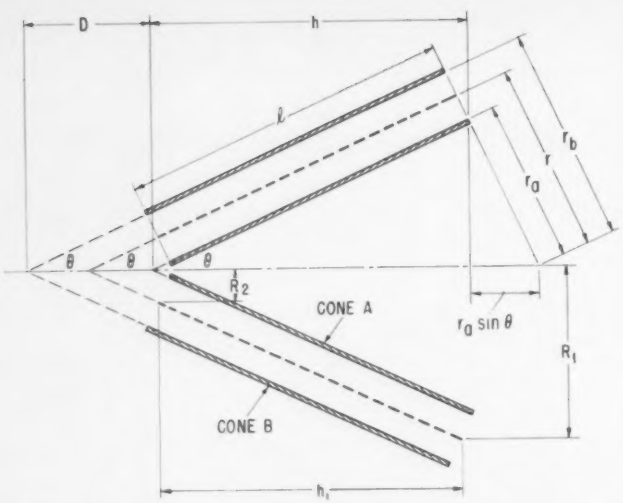

FIGURE 1. *Cross-sectional dimensions of conical capacitor.*

Solid lines indicate the conducting surfaces of frustums A and B, respectively. Heavy dashed lines indicate a surface of a frustum taken at random parallel to the two conducting surfaces. The thin dashed lines indicate the geometric extention of the 3 surfaces to the apexes of the cones.

A rigorous analytical solution for the conical case seems, unfortunately, unobtainable at this time. The classical approach and existing limitations to the particular boundary value problem were investigated and the results (not shown here) were discouraging. In order to develop more confidence in an approximate solution, one of the field construction methods, the graphical, was employed to justify the basic introductory assumption that the charge distribution over the conical surfaces is essentially uniform. A physical visualization of two closely-spaced parallel conducting closed surfaces of any shape may be of further assistance in this respect. Assuming a certain potential of the inner conductor and zero potential on the outer, the charge distribution over the inner will be a normal function of the contour when the spacing between these conductors is infinity. As this spacing is reduced to zero the surface charges will be redistributed and will approach uniformity. At certain finite, and particularly at relatively small spacings, uniform charge distribution may be assumed with fairly good accuracy. The potential gradient is therefore perpendicular to the two metal surfaces nearly everywhere in the space between them. Since the conical conducting surfaces are parallel and coaxial, it follows that the electric lines in the dielectric space (assumed to be air) are everywhere normal to both surfaces. Moreover, since the electrodes are equipotential surfaces, it follows also that everywhere over these surfaces and over any other surface parallel to and located between these conducting surfaces

$$\mathbf{E}\cdot\boldsymbol{\eta}=\mathbf{E}=-\frac{dV}{dn} \tag{1}$$

where $\mathbf{E}$ is the potential gradient or the electric field intensity, $\boldsymbol{\eta}$ is unit vector normal to the surfaces, and V is the potential at any point.

When relative positions and distances between the cones increase and begin to approach the order of magnitude of the height of the frustums, the well-known condition is being approached when σ is a maximum near the apex of the inside cone and a minimum near the inside apex of the enclosing cone.

Referring to figure 1 and taking the surface S_f of any other coaxial frustum of half angle θ located between the two conical electrodes and applying Gauss' law to this surface, the total enclosed charge Q is given by

$$\int_S \mathbf{D}\cdot d\mathbf{S}=\epsilon E S_f=Q. \tag{2}$$

The dielectric constant of the interelectrode space is ϵ, and the integral is applied only to the conical surface because the surfaces of the bases of the frustum by assumption do not contribute any electric flux.

From the geometry of the figure and the well-known interrelations of $C=Q/V$

$$V=-\int_{r_b}^{r_a} E dr=-\frac{Q}{\epsilon\pi l}\int_{r_b}^{r_a}\frac{dr}{(2r\cos\theta-l\sin\theta)}$$

$$=\frac{Q}{2\epsilon\pi l\cos\theta}\ln\frac{(2r_b\cos\theta-l\sin\theta)}{(2r_a\cos\theta-l\sin\theta)}. \tag{3}$$

Expressing r_a and r_b in terms of h and D we have

$$C=\frac{2\pi\epsilon l\cos\theta}{\ln\left[1+\dfrac{2D\cos^2\theta}{2h-l\cos\theta}\right]}. \tag{4}$$

The values of r, r_a, and r_b are defined in figure 1.

When the internal electrode is a cone, it may be considered a frustum having a negligible small top section and an altitude $h=l\cos\theta$. Then

$$C=\frac{2\pi\epsilon h}{\ln[1+2(D/h)\cos^2\theta]}. \tag{5}$$

Using the absolute rationalized practical system of units, h is in meters, and $\epsilon\cong 8.854\times10^{-12}$ farads per meter (in vacuum and approximately in air) and

$$C=55.6h\frac{1}{\ln[1+2(D/h)\cos^2\theta]}\,pf. \tag{6}$$

3. Computed and Measured Values

Figure 2 compares experimental data with calculations based on eq (6). $\theta=10°\,34'$, $(D+h)=2.845''$, height of enclosing cone$=2.845''$, and the maximum displacement was 2 in.

In order to compare the range of the conical capacitor with others, one must do so within the same mechanical precision limits, e.g., one must find the minimum value of D consistent with a reproducibility

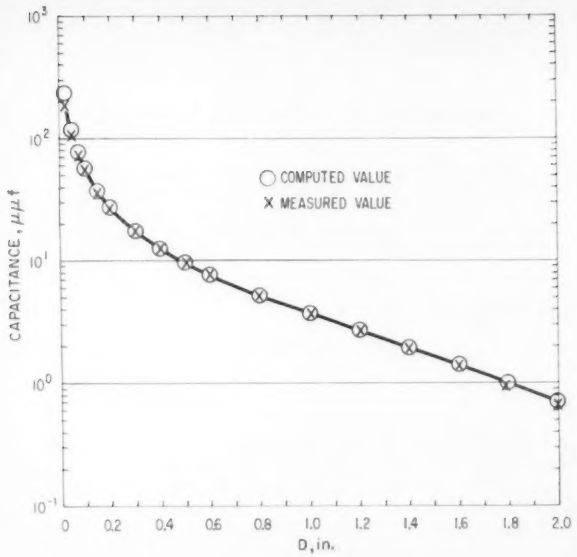

FIGURE 2. *Capacitance values of right-cone continuously adjustable capacitor versus displacement.*

of, say, 0.2 percent in capacitance, which is the precision considered above in the hypothetical cylindrical example. The derivative of C with respect to D or h will yield the necessary information.

$$\frac{dC}{C}=\frac{dh}{h}[1+F(h)]$$

where

$$F(h)=\frac{2(D+h)\cos^2\theta}{(h+2D\cos^2\theta)\left[\ln\left(1+2\frac{D}{h}\cos^2\theta\right)\right]}. \quad (7)$$

The error in the capacitance is thus larger than that in h by an additional factor $F(h)$, a function of h.

It is readily seen that $F(h)$ is a pure numeric and that h may be used in any units. The table below gives one computed value of $F(h)$ and expected error for the capacitor of figure 2 for

$$\frac{\Delta h}{h}\cong\frac{1}{3}\times 10^{-4}.$$

TABLE 1.

D''	h''	$F(h)$	$\Delta C/C$	C max.	C min.	$\frac{C\text{ max.}}{C\text{ min.}}$
0.050	2.795	56	0.2%	116.1	0.69	168

It appears, therefore, that for the same resetability of h as for the cylindrical and disk cases of 0.1 mil, a reproducibility of capacitance values to 0.2 percent, and a maximum displacement of 2 in., the range of the conical capacitor of the above dimensions would be about 168 to 1, as against 40 to 1 for the cylindrical and 10 to 1 for the disk type. The conical type capacitor recently found practical application at the National Bureau of Standards in an attenuator-thermoelectric (AT) type r-f voltmeter for voltages from an average of 5 to 1000 v at frequencies of 1 to 10 Mc.[3]

Figure 2 shows satisfactory agreement between computed and measured capacitance values of an experimental conical capacitor. Validity of formula (6) was also established for $\theta=20°$ and 45° with good agreement between computed and measured values.

Several female and male conical conductors may be combined to form a single capacitor. Such a capacitor having three pairs of conductors is shown in figure 3. Capacitance ranges 2 to 300 or 3 to 450,

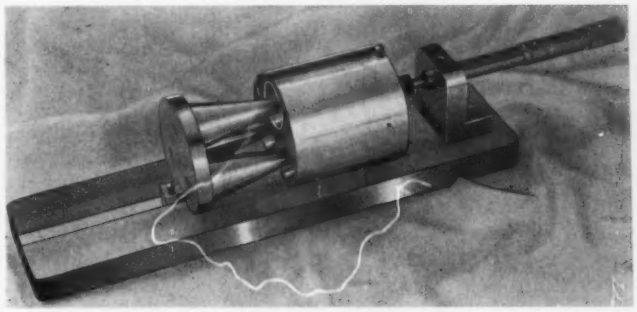

FIGURE 3. *Conical coaxial capacitor employing three pairs of cones.*

etc., pf may thus be obtained within practical space limitations. Moreover, longitudinal displacements of high accuracy at large values of D are relatively easy to obtain; this enables the realization of still larger capacitance ranges by reducing say, the 3-pf minimum capacitance to 1 pf. It is evident that one can obtain different curves of capacitance versus displacement by changing the cross-sectional contour of one or both surfaces of the electrodes from conical to other suitable shapes. One should also be able to increase the range further by making use of additional ring-flanges at the bases of the cones; the cross-sectional contours of these rings may in turn be shaped to produce a certain desired function of capacitance versus displacement.

[3] These types of voltmeters were announced and briefly described in NBS Tech. News Bull. **40**- 29 (1956).

BOULDER, COLO. (Paper 63C2–10)

Journal of Research of the National Bureau of Standards—C. Engineering and Instrumentation

Vol. 63C, No. 2, October–December 1959

A Photoelectric Followup and Recording System, and its Application to Remote Observations of the Beam in High-Precision Balances

H. A. Bowman and L. B. Macurdy

(July 22, 1959)

A device is described which permits a significant increase in the frequency of the oscillations of the beam of a balance, thereby shortening the interval during which upsetting ambient conditions can act. The device is a servo-driven photoelectric followup system responding to the position-modulated light signal reflected from a mirror attached to the balance 12 ft away from the photocell. Reproducibility in observing the position of the light beam is 0.001 in. or less.

1. Introduction

For the past 10 years the NBS Mass Unit has been studying the causes of uncertainties in high-precision mass determinations. These studies have demonstrated that causes of major uncertainties are due to variations in ambient conditions occurring during the experimental interval. Exclusive of the time required by the preparations for a mass-determination experiment, such as cleaning weights, and exclusive of computation time, about one-third of the experimental interval is required for manipulating the weights and the balance, and about two-thirds for the actual swinging of the beam. The virtues of a radically decreased beam period are that the interval during which ambient changes can act is reduced; the adjustments required to control the period of oscillation of the beam are simple. The reason why short periods are conventionally rejected is that the square of the period, to a good approximation, is proportional to the balance sensitivity (deflection/change of mass). This must not be confused with the weighing precision that can be achieved. For assessing the latter, a short period presents an important advantage in that the on-scale range of the balance is increased, thereby permitting the use of larger (and hence more accurate) sensitivity weights.

The most serious disadvantage of a fast-swinging beam is the difficulty of maintaining the accuracy of the turning-point observations. If the overall experimental precision is to be maintained, turning point data must be more accurate with a fast-swinging beam than with a slow one due to the fact that the balance sensitivity is less for a fast-swinging beam. These comments on beam period and observational accuracy are general and apply to all equal arm balances.

The desirability of an improved method of observing the motion of the balance beam has long been recognized. Photoelectric methods [1] have previously been used; however, a survey of existing instrumentation of this type did not reveal devices capable of operating directly in mass-determination work where precision of the very highest order was required.

Design requirements for an instrument considered suitable for NBS Mass Laboratory studies are as follows:

a. The device should be capable of defining the position of a light beam to a few ten thousandths of an inch at the end of a 12-ft optical lever.

b. It should have freedom from zero drift over long periods (of several days) from either thermal or electrical causes; or, if such drift exists, it should be capable of being measured by independent means.

c. The data must be available in numerical form for computation or in a form suitable as an input for a strip chart recorder.

d. There should be a surplus of mechanical power, directly related to beam motion, for the operation of automatic computation or data-handling devices or for manipulation of various balance-control mechanisms.

e. The device should be capable of operating in normal fluorescent illumination.

f. The design should use, insofar as practicable, commercially available assemblies or subassemblies.

g. The design configuration should be sufficiently flexible to permit its use in several different applications required in mass-laboratory studies.

A photoelectric device was fabricated which acceptably meets the above requirements. Completed about a year ago, it has been a principal tool in a series of design studies preliminary to the construction of a high-speed automatic weighing system of

[1] V. E. Birgel, Installation for the experimental investigation of precision balances, Techniques of Measurement, No. 1, p. 43 (Jan. 1956); C. Norman Cochran, Automatic recording vacuum microbalance, Rev. Sci. Instr. **29**, No. 12 (Dec. 1958).

the highest attainable precision. At the completion of these studies the device, with modifications, will become a permanent part of this proposed weighing system.

2. Description of the Instrument

This automatic observing device may be assembled in several different forms, the essential features of one of which are shown in figure 1. The photoelectric light source is a single tungsten-filament bulb excited by a well regulated and filtered d-c power supply. The light from this bulb is reflected from an off-axis mounted mirror on the shaft of a 3,600-rpm synchronous motor driven from the 60-cycle commercial power line, through a high-quality achromatic condenser lens to a mirror mounted on the beam of the balance under observation. The balance-beam mirror reflects this light to a photoelectric cell carried to and fro on a lead screw driven by a two-phase motor through a rubber-tire and friction-disk assembly. The image of the tungsten filament, brought to focus by the condenser in the photocathode plane, is oriented vertically by appropriate positioning of the bulb. The 3,600-rpm synchronous motor imparts a small amount of 60-cps nutation to the light beam which manifests itself as an apparent small side-to-side motion of the light beam across the face of the photocathode parallel to the length of the lead screw. When the photocell lies in the center of this nutation it is illuminated 120 times per second, and the resulting 120-cps output is dissipated in a 60-cps filter immediately following. If, however, the photocell is off-center in the nutation its output contains a 60-cycle component, the phase and magnitude of which are functions of the direction and amount of this offcenter displacement. This component is amplified and applied to the control winding of the two-phase motor. When the phase of the nutation is properly adjusted with respect to the 60-cycle power line, the motor rotates the lead screw in the direction necessary to re-center the photocell in the light beam. When the balance beam swings, the nutating light beam moves back and forth along the length of the lead screw, and the motion of the balance beam is determined from observations on the angular position of the lead screw.

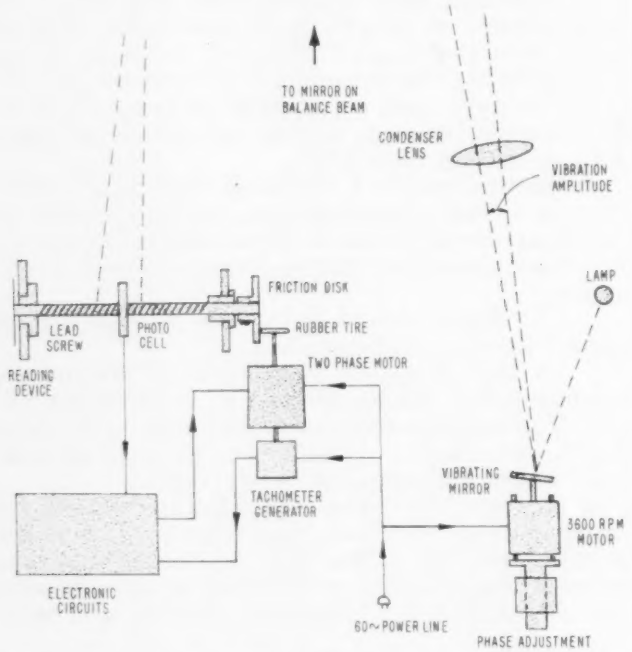

FIGURE 1. *Schematic diagram of the essential elements of the balance observing device (when assembled to provide turning point data).*

2.1. Optical System

In any measuring system in which the smallest readable unit is evaluated in terms of the quantity measured by observations widely separated on the scale, great care must be taken to assure that the various optical elements in the system do not distort the relative lengths of the scale units. In weighing, sensitivity weights are added to the major loads on the pans to permit balance indications to be converted into mass units. Distortion arises from parallax in eyepieces and from the various windows and mirrors which are not perfectly flat. As the magnification of the observing system increases, distortion increases. In the NBS system all mirrors are made by evaporating aluminum films on optical flats. Windows are polished flat and the two surfaces are maintained parallel. They are coated with magnesium fluoride to reduce reflection losses. There is only one lens in the system, which is an f/5 achromatic objective of 25 in. in focal length.

Requirements for maximum-displacement sensitivity are equality in the image plane of the width of the image of the tungsten filament, of the width of the photocathode, and of the peak amplitude of the nutation. The width of the photocathode is slightly less than $\frac{1}{16}$ in. The condenser lens magnifies the image of the 0.005-in. diameter filament to about $\frac{1}{16}$ in. at the extremity of the 310-in. image distance. The amplitude of the nutation is adjustable by varying the amount of off-axis displacement of the mirror on the 3,600-rpm synchronous motor, as shown on figure 2.

The photosensitive unit is a cadmium selenide photoconductive cell, the peak response of which lies in the red region. This photocell used with a tungsten-filament light source makes an excellent combination for use in a room which is illuminated with fluorescent lighting (largely blue response). The collimator in front of the cell is merely a ½-in. diameter tube 3-in. long with a blackened inner wall. Some experiments indicate that the predominately red light from the tungsten filament may be thermally upsetting to the balance. Additional disadvantages of the red-sensitive system currently in use are the low frequency response of the cadmium selenide cell,[2] and the sensitivity of this cell to

[2] The time constant at 0.01-fc illumination is 0.3 sec, at 0.1 fc it is 0.07 sec, and at 1.0 it is 0.017 sec. From trade data published by the Clairex Corp., New York, N. Y.

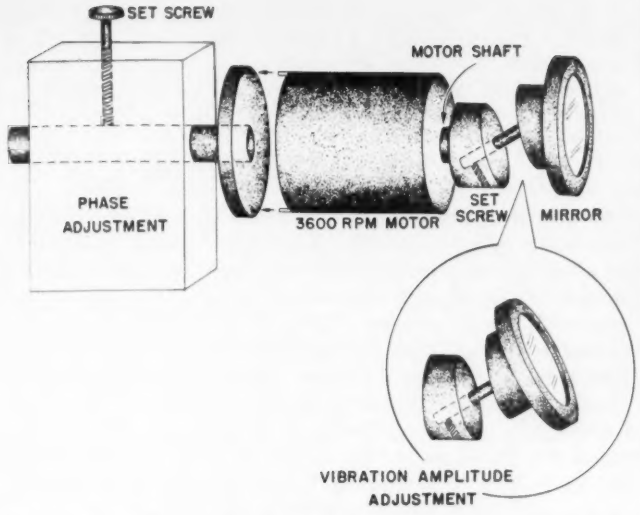

FIGURE 2. *The synchronous motor-supporting assembly which provides both amplitude and phase control of the nutation of the light beam.*

temperature changes. Experiments with blue sensitive systems (high-frequency vacuum photodiodes) were successful and the present system could be so modified.

Light beam nutation is presently achieved by the rotating mirror shown in figure 2. For applications requiring that the light source be rigidly attached to the balance case an alternative method of nutating the light beam must be used, since the vibration associated with the 3,600-rpm motor is greater than could be tolerated in a high precision balance. There are two satisfactory methods of obtaining a carrier signal, both of which are vibration free. One method requires (a-c) excitation of the tungsten filament in a suitably-oriented magnetic field. Under these conditions the tungsten filament vibrates back and forth at an amplitude controlled by the magnitude of the field. A variation of this method is d-c filament excitation in the presence of a-c magnetic field. The effect of the vibration of the lamp filament is vanishingly small when related to balance operation; however, a different method of attaining a carrier was successfully tried over short optical paths. A neon pilot lamp, excited by the power line, provided illumination in the pass band of the photocell. The image of the two electrodes was brought to focus in the plane of the photocathode, and the action of the servosystem immediately centered the photocell in the dark space between the two electrode images.

2.2. Mechanical System

The heart of the mechanical system is the lead screw, figure 1, which replaces the engraved scales used in high-quality telescope-observing systems. Its threaded length is 20 in. with a 1½ in. shank at each end. The major diameter of the thread is ½ in. and of the shanks ¼ in. It was ground from SAE No. 6150 chrome vanadium steel. Threads were lapped and polished until the lead error was well distributed along the entire threaded length. This lead error distribution was measured by the NBS Engineering Metrology Section to be a total of 0,0004 in. in 20 in. It has a "2 start, 10 pitch thread" (20 lands and 20 grooves per inch) with a 60° profile.

The driven member is a bronze half nut with straight milled ridges meshing with the top surface of the lead screw. These ridges are relieved at both the crests and troughs, thereby assuring that driving contact is maintained with the polished 60° thread surfaces. This bronze member is attached (at the appropriate angle) to the carriage of the photocell. The photocell carriage is supported at three points—two ball bushings around a rod mounted parallel to the lead screw and the bronze driven-member riding on the lead screw itself.

The lead-screw shanks ride in bronze bushings mounted in heavy-brass end plates which are, in turn, rigidly attached to a lathe bed obtained for the purpose. At one end of the lead screw a friction disk is mounted whose bore has been reamed to match the diameter of the shank. The friction surface (on which the rubber-tire drive wheel bears) was turned normal to this reamed bore, and faces away from the threaded portion of the lead screw. The portion of the back surface of this disk which bears against the collar of the supporting-bronze bushing (see fig. 1) is also turned normal to the bore. The drive wheel then holds the friction disk in constant contact with this thrust collar and the reverse surface of the friction disk defines the reference surface from which all displacement measurements on the photocell are made. The shank at the opposite end of the lead screw is free to move in its bushing either longitudinally (under thermal forces on the lead screw) or rotationally.

The shaft of the two-phase motor is extended and is fitted with a rubber-tire wheel which can drive the friction disk at any desired radius. This radius is selected to provide gear reduction between the two-phase motor and the photocell carriage sufficient to insure that the motor will operate near the upper limit of its speed, and will, of course, depend upon the amplitude and peak velocity of the gross motion of the photocell carriage. A bronze radial bushing can be slid to any position on the extended shaft of the two-phase motor to take up the radial load necessarily applied to the shaft by the friction drive. This bushing is not shown in figure 1, however, its necessity is obvious.

2.3. Observing-Recording System

One of the system design requirements, stated in the introduction, was that data be furnished in numerical form as well as in a form suitable for a strip-chart recorder. Numerical data on the angular position of the lead screw at the instant of the balance turning point are observed on a dial directly coupled to the lead screw. However, the motion of the lead screw is sufficiently rapid (even when going through a turning point), that an operator would experience

great difficulty in estimating the extreme position of the dial attached to the end of the lead screw in the process.

In order to provide the operator sufficient time to observe and make an accurate estimate of this extreme angular position, there is one turn or 0.1 in. of free play between the lead screw and this dial. The dial is therefore motionless during the interval that the lead screw makes a complete revolution after the turning point is reached. This dial is engraved with 100 index marks spaced about ⅛ in. apart, each interval representing 0.001 in. of linear motion of the photocell carriage. When this dial is stopped with turning-point data showing, the operator is able to make an unhurried estimate to one or two ten-thousandths of an inch of the true position of the turning point. Turning-point data in inches and tenths of an inch are observed on a second dial geared down by a ratio of 20 from the lead screw. Thus, data to six significant figures are obtained, three figures on each of two dials.

There are on the market several data-taking disk systems designed to be driven by lead screws or other rotating members. Such systems automatically type turning-point data or record corresponding binary or decade information on magnetic tape or IBM punch cards. The drive mechanism for the lead screw was designed with the possibility in mind of later installing one of these automatic data-taking devices, hence there is available sufficient torque to drive any of the numerous types currently available.

When it is desired to obtain a continuous record of balance-beam motion on a strip chart recorder, a high-linearity multiple-turn servo-type potentiometer is coupled to the lead screw. A d-c voltage is then impressed across this potentiometer and with two wire-wound resistors a Wheatstone bridge circuit is formed, with the recorder occupying the position of the galvanometer.

2.4. Electronic System

The electronic system is divided into two groups. The first group contains the d-c power supplies and the power amplifying circuitry. There are many vacuum tubes associated with these functions, as well as power resistors and transformers, all of which generate large quantities of heat. Accordingly, the first group of electronics is located remotely from the lead screw and balances and is coupled to the second group by a shielded cable.

The second group of electronic circuits is mounted in a small chassis next to the lead screw. There are only two small electrometer tubes in this chassis which together dissipate only about 3 w. One tube is an amplifier with the high impedance cadmium selenide cell in the grid circuit, and the other is a cathode follower which provides a low impedance signal to the long cable connected with the power amplifying circuits located remotely from the lead screw. The chassis at the lead screw also contains the necessary switches, adjustable resistors, etc., to phase properly the various error signals, feedback voltages, etc.

Most of the major electronic components are high quality commercially available units. Every effort was made to keep signal lines shielded to guard against hum pickup, and manufacturer's recommendations as to grounding were carefully followed.

2.5. Thermal Considerations

Undesired thermal effects exist in almost all high-precision measuring systems. By careful placement of system components they are largely under control in the NBS balance observing device. In this apparatus, the main source of heat is the electronic power circuits, and as explained above, this group is located away from the lead screw. The two phase motor dissipates rather large quantities of heat, and, unfortunately, it must be located in fairly close proximity to the screw. In order to protect the screw, the motor is surrounded by a copper tube cooling jacket, through which water is circulated.

It was previously stated that photocell displacement measurements along the lead screw are made with respect to the thrust plane of the bronze thrust bearing at the drive end of the lead screw. The opposite end of the lead screw is free to slide in its radial bearing under thermal forces. In the same manner, the lathe bed upon which the lead screw is mounted is bolted to the marble pier only at the thrust bearing end, the opposite end being free to move under whatever forces may operate. A fused silica (quartz) rod was mounted alongside the lead screw to monitor any thermal expansion. In use, it is rigidly attached to the end plate containing the lead-screw thrust bearing with a micrometer device for measuring changes in length of the lead screw with respect to its own nearly invariant length. In the original installation of this system, difficulties were traced by means of this rod to heat from the power electronics and the servomotor.

On a number of occasions the balance under observation has been left undisturbed and the position of the light beam recorded over intervals of two or three days. Under such circumstances the position of the beam is seen to move to and fro at an amplitude of several thousandths of an inch, as illustrated in figure 3. The period of this motion is roughly diurnal due to motion of the building (probably caused by solar heating.)

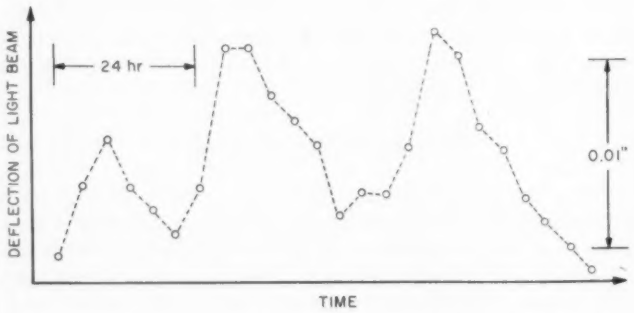

FIGURE 3. *The motion of the light beam reflected from the mirror on the balance over a three-day interval.*

The only remaining troublesome heat source is the assembly (shown in fig. 2) comprising the 3,600-rpm synchronous motor and the tungsten-filament light source. This motor is kept running 24 hr per day; however, the light source is turned down at night to a level sufficient only to maintain the photocell in the light beam under the loop action. When the lamp voltage is raised in the morning the recorder indicates a drift of about 0.003 in. in less than 1 hr. Thereafter there is no observable drift from this source. This drift may be a nonsymmetrical heating effect in the balance itself caused by the increased light level. Observations of this type resulted in the decision to use a heat filter and a multiplier phototube when this device is permanently fitted into an automatic high-speed weighing system. Consideration has been given to the use of a fused-silica lead screw; however, the reproducibility of existing balances does not now warrant this refinement.

3. Use of the Instrument

This device has been in use for about 1 yr in its present form during a study of the causes of uncertainties in balance operation. Data from these studies is not appropriate here; a few examples of the data presentation made by this device will be shown only to illustrate its operation. Figure 4a illustrates the improvement in readability achieved when the photoelectric device is substituted for the conventional telescope system. The dotted curve is a plot of the left-hand turning points as recorded by an experienced observer through a high quality telescope system of 3-in. aperture. The solid line is a plot of the same turning points but based upon photoelectrically taken data. Only the left-hand turning points are illustrated. When these left-hand turning points were combined with the associated right-hand turning points (not shown), the computed balance indications were plotted and shown in figure 4b. The gentle downward drift of the balance indications computed from automatic data is ascribed to slowly changing thermal conditions in the balance case. During this experiment the period of the balance beam was about 20 sec.

Figure 5 shows two examples of balance indications computed from data by means of the device taken during experiments on various types of mechanical assemblies associated with high-precision balances.

Figure 6 shows a plot of balance-beam motion made on the strip-chart recorder when air turbulence

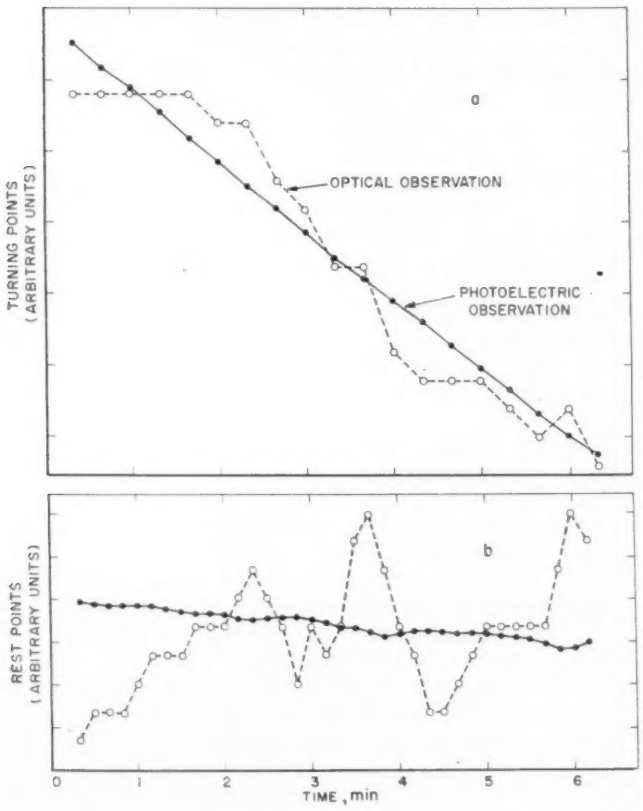

FIGURE 4. *Comparison of photoelectric and telescopic observation of the balance beam motion.*

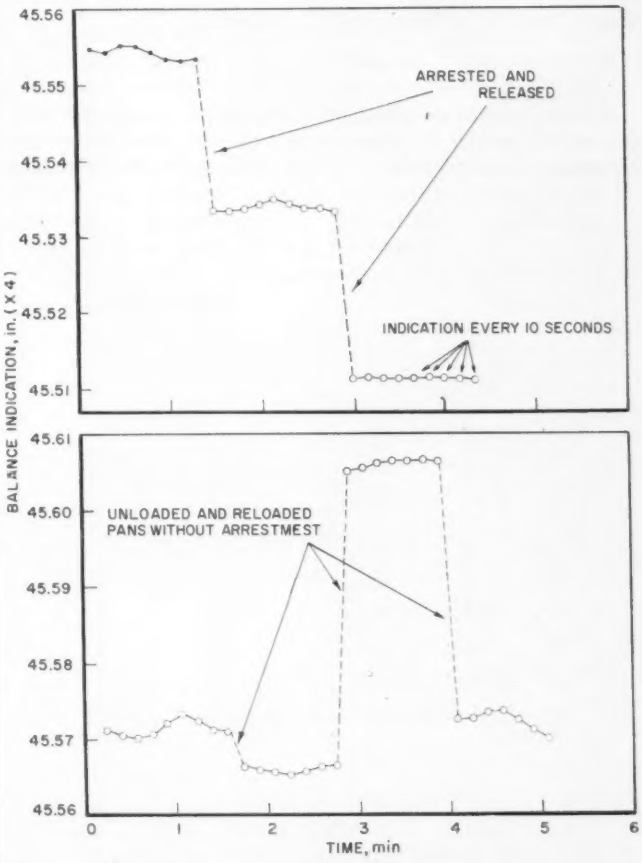

FIGURE 5. *Illustrating mechanical errors in balance response: (above) arrestment error, (below) loading error.*

Balance indication, plotted vertically, is numerically equal to 4 times the rest point.

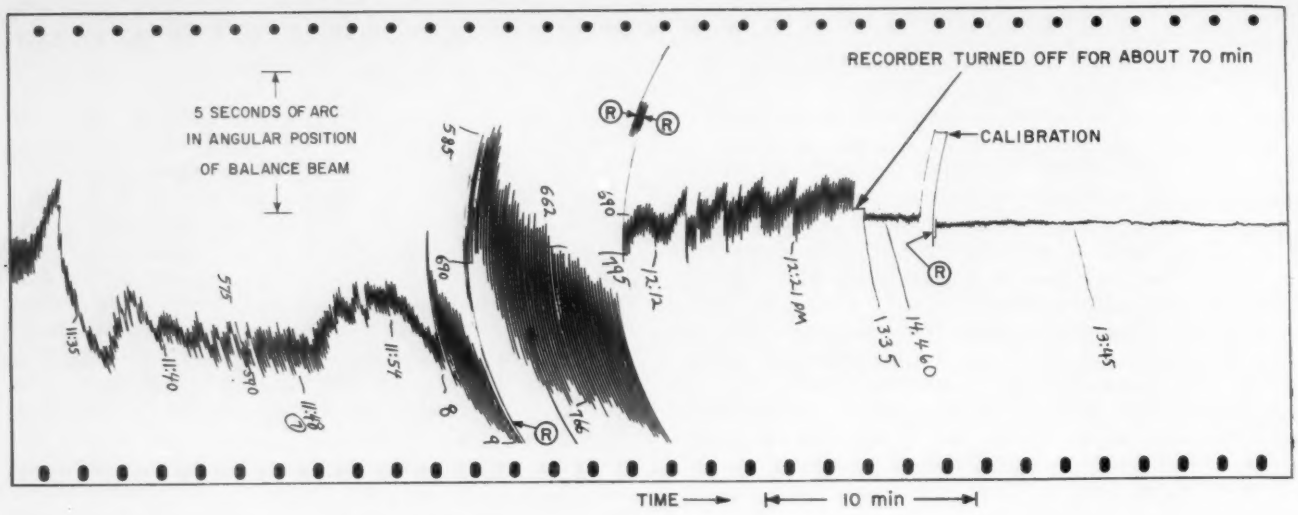

FIGURE 6. *Balance response due to turbulent air in balance case.*

The encircled R indicates that the pen was manually recentered.

existed in the balance case because of unfavorable thermal conditions. In the latter portion of the chart, the turbulence had subsided.

Consultation on electronic and servo problems was provided by M. L. Greenough of the Electronic Instrumentation Section. T. R. Young of the Optical Instrument Section consulted on optical problems. The high precision mechanical work was performed by C. H. Hochgesang in the NBS Instrument Shop, under the direction of N. C. Pines.

WASHINGTON, D.C. (Paper 63C2–11)

Journal of Research of the National Bureau of Standards—C. Engineering and Instrumentation

Vol. 63C, No. 2, October–December 1959

A Stroboscopic Vibration Analyzer

S. Edelman, R. Brooks, S. Saito, E. Jones, and E. R. Smith

(July 15, 1959)

An instrument for studying the amplitude and phase relations which exist in complex periodic processes is described in this paper. The process treated here is vibration of complicated bodies. The motion at each point of interest is detected by a vibration pickup. The signal from each pickup is heterodyned with a common signal that differs from the vibration frequency by a small amount to produce a set of signals at the difference frequency. The desired relations are exhibited at the difference frequency which is low enough to give a slow motion effect. The output circuitry allows scope for ingenuity to choose a presentation suited to a particular problem.

1. Introduction

Stroboscopic instruments have been used for the visualization and analysis of periodic motion for many years. The simple stroboscope, consisting of a light flashing at an adjustable rate, has long been used for studying rotating machinery and low frequency vibrations in the laboratories and industrial plants. More sophisticated designs such as the Chadwick-Helmuth Slip Sync, the Winkler Strobo-Sync, or the International Research and Development Corporation Vibration Analyzer, permit more detailed analysis of the motion by synchronizing the flash of light with the motion being studied, and the first two provide a means of slowly shifting the phase of the flash so that the entire cycle of the motion is visible. In addition to these commercial instruments there are laboratory instruments [1, 2, 3, 4, 5, 6, 7, 8] [1] having the same ability to slow as well as to stop apparent motion at any portion of the cycle and also the ability to observe motion of microscopic amplitude. In all these instruments the vibrating object must be observed directly or through some optical system. Where the field of view is large the allowable magnification of the motion is small.

The "strobolyzer" described here carries stroboscopic vibration analysis further by allowing observation of vibrating bodies of any size and complexity as well as motions whose amplitudes may range from submicroscopic to directly visible, and whose frequencies may range from subsonic to ultrasonic.

This improvement is accomplished by observing the pattern of motion depicted by the response of a number of vibration pickups to the vibration, in place of observing the vibrating body itself. The signals from the pickups are processed in such a way that stroboscopic effects such as apparent slow motion or stopped motion at any phase of the vibration cycle can be obtained.

[1] Figures in brackets indicate the literature references at the end of this paper.

2. General Construction

The basic operation of the strobolyzer is shown schematically in figure 1. A number of vibration pickups are used to detect the motion of the vibrating body. If the body vibrates at some frequency, (f cps) the signal from each pickup will be at f cps, but, in general, will differ from the signals of the other pickups in amplitude and phase. The number and location of the pickups are chosen so that all significant aspects of the motion are observed. This choice may be made on the basis of an a priori estimate of the vibration pattern and an originally arbitrary distribution may be modified in the light of increasing knowledge as the study progresses. The signal from each pickup is mixed with a reference signal at (f-Δ) cps where Δ is usually about 1 cps but can be varied.

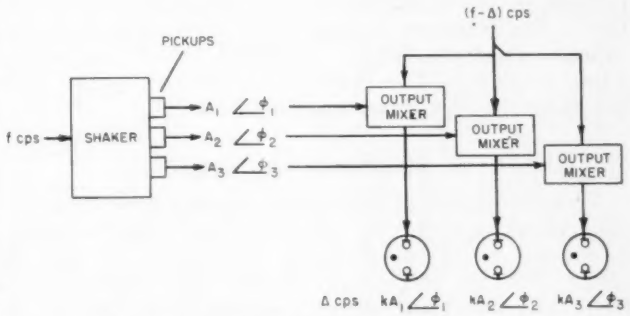

FIGURE 1. *Block diagram of strobolyzer.*

If the signal from pickup i is $A_i \sin(\omega t+\phi_i)$ and the signal which is mixed with each of the pickup signals is $B \sin(\omega t-2\pi\Delta t)$, then the signal from the output mixer, M_i, is the sum of these:

$$M_i=A_i \sin(\omega t+\phi_i)+B \sin(\omega t-\delta t),$$

where $\delta=2\pi\Delta$,

$$M_i=\sqrt{A_i^2+B^2+2A_iB\cos(\delta t+\phi_i)}\sin(\omega t+\Psi_i)$$

where $\Psi_i=\tan^{-1}(A_i\sin\phi_i-B\sin\delta t)/(A_i\cos\phi_i+B\cos\delta t)$. This is a sine wave at the vibration frequency whose amplitude varies with time according to the expression under the radical sign. This expression can be rewritten as:

$$B\sqrt{1+r_i^2}\left\{1+2\frac{r_i}{1+r_i^2}\cos(\delta t+\phi_i)\right\}^{1/2}$$

where $r_i=A_i/B$. Expanding by means of the binomial theorem:

$$M_i=B\sqrt{1+r_i^2}\left\{1+\frac{r_i}{1+r_i^2}\cos(\delta t+\phi_i)\right.$$
$$\left.-1/2\left(\frac{r_i}{1+r_i^2}\right)^2\cos^2(\delta t+\phi_i)+\ldots\right\}$$

The higher order powers of $\cos(\delta t+\phi_i)$ can be expressed as harmonics of $\delta/2\pi$ but if $B>>A_i$, r_i will be small and terms containing powers of r_i greater than the first are negligible. Since the first term is constant, the time varying part of the amplitude consists of a sine wave whose frequency is Δ. This equation is well known in the theory of heterodyning and is treated in textbooks on radio engineering. It is shown [9] that by making B large compared to A_i and by using a square law detector, a signal is obtained at a frequency of Δ cps whose amplitude is proportional to A_i for all practical purposes and whose phase is ϕ_i. A suitable output mixer circuit can be found in electronics texts, for example, Terman [9, p. 569, fig. 41]. The output signal from each mixer is applied to a suitable indicator, which follows the Δ cps signal. The group of indicators is arranged approximately in the arrangement of the pickups on the vibrating body. With a little practice the indications are interpreted as motions and the vibration pattern can be visualized. A system somewhat similar to the one treated in this paper was described by Goldman and Richards [10].

3. Modified Oscillator

The generation of the signal which differs from the vibration frequency by Δ cps is shown schematically in figure 2. The vibration frequency (f cps) is obtained from a General Radio Type 913C beat frequency oscillator which consists of a fixed oscillator whose signal is always 186,000 cps, a variable oscillator whose signal differs from 186,000 cps according to the setting of the tuning dial, a mixer which combines the two signals, and an output section which amplifies the difference of the two signals. In the modification for the strobolyzer a second mixer and output section were placed in parallel with the original sections and a phase shifter was inserted between the fixed oscillator and the new mixer.

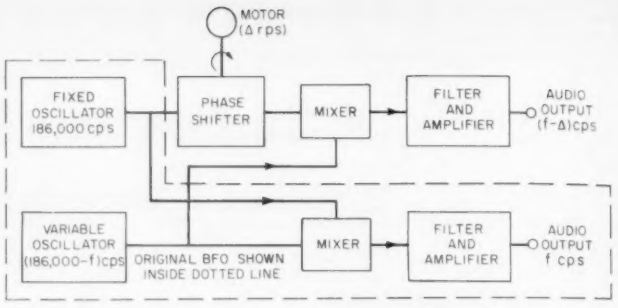

FIGURE 2. *Modified beat frequency oscillator.*

The phase shifter used in the modified oscillator is the capacitive type described in Terman's Handbook [9, p. 949, fig. 56e]. When the phase splitting input circuit is properly tuned, the phase shift is equal to the rotation of the shaft in corresponding units and there is no change of amplitude with phase. Since the phase shifter is in the fixed oscillator circuit there is no need to retune the phase splitting circuit for any output frequency of the beat frequency oscillator. If the output of the fixed oscillator is $A_F\sin(\omega_F t)$ where $\omega_F=2\pi\times186{,}000$ radians per second, the output of the phase shifter will be $C_\phi A_F\sin(\omega_F t+\theta_\phi)$ where C_ϕ comprises the changes in amplitude caused by the insertion of the phase shifter and its associated circuitry while θ_ϕ comprises the corresponding phase shifts including the shift due to the initial setting of the phase shifter. C_ϕ can be made unity by inserting an amplifier ahead of the phase shifter. Constant rotation of the phase shifter at Δ rps adds to θ_ϕ a phase angle which is a linear function of time: $\theta_\phi-2\pi\Delta t$ and the signal to the mixer is

$$A_F\sin(\omega_F t+\Theta\phi-2\pi\Delta t)=A_F\sin\{2\pi(F-\Delta)t+\Theta_\phi\}$$

where 186,000 is written as F for convenience. In the original GR mixer, the signal from the fixed oscillator at F cps is mixed with the signal from the variable oscillator at $(F-f)$ cps and the output is the audiofrequency (f cps). In the added mixer the signal from the phase shifter at $(F-\Delta)$ cps is mixed with the signal from the variable oscillator at $(F-f)$ cps and the output differs from f cps by the frequency of rotation of the phase shifter, Δ cps.

If the phase shifter is not rotated the two outputs will be at the same frequency and the phase difference between them can be set at any value by setting the phase shifter. Thus, if the motor is stopped the indicators of the strobolyzer present the amplitude and phase relations at a particular phase of the vibration cycle. This "freezing" of the vibration pattern corresponds to the stroboscopic "freezing" of the motion when a flashing light is synchronized with the vibration frequency.

If the phase shifter dial is turned slowly by hand, the entire vibration cycle is traversed and can be studied at leisure. Differences in the phase of the motion at different points can be measured by noting the amount of rotation of the phase shifter dial required to move the indicators to corresponding positions.

If the phase shifter dial is rotated by the motor at Δ rps the entire vibration cycle is traversed repeatedly at Δ cps and the indicators show the phase and amplitude relations in slow motion.

4. Output Presentation

In the course of developing the strobolyzer a number of methods of output presentation were tried such as blinking neon bulbs and a-c voltmeters. As the number of channels increases it becomes difficult to read or follow a large number of meters or bulbs.

As an alternative a 10 channel bar graph presentation was developed for use with an oscilloscope; this instrument is called the multichannel electronic switch. The basic system samples each channel in succession at a rate sufficiently rapid to accommodate the retentivity of the eye and oscilloscope phosphor.

A Sylvania 6910 decade counter tube provides the sequencing function and counts the output of a 1,500 cps oscillator, shown in figure 3. Tubes V1 and V2 are used to sequence the counter tube.

The output pulses from the counter tube operate the gates for each channel; QIB is the gate transistor for a typical channel. A negative pulse is required to operate the gate, therefore transistor QIA is used to invert the positive pulses from the counter tube.

Since it is desirable to have a d-c or bar-type presentation instead of a sine wave from the vibration pickups, transistor QIC is used as an emitter follower and d-c rectifier. Transistor Q_o is the output transistor which also serves to invert the negative signals to give them a positive sense.

The oscilloscope Y axis input is connected to the output of Q_0. The X axis signal is the normal sweep of the oscilloscope itself and is synchronized or triggered from output No. 1 of the counter tube.

In order to accommodate large signals in the order of 40 v rms a divider is used to divide the signal by a factor of 20.

Occasionally the strobolyzer is used for investigations in which the original display methods are more useful, for example, cases where flashing lights can be arranged to give three dimensional effects. Neon bulbs can be connected to the output channels in such cases, either in conjunction with the oscilloscope display or in place of it.

The output channels also can be connected to recorders. As pointed out by Fred Mintz of Lockheed Aircraft Corp., the fact that the output frequency is always Δ cps makes it possible to record the significant phase and amplitude relations of vibratory motion at any vibration frequency with recorders of limited dynamic response since Δ can be chosen to suit the recorder.

Usually the relative amplitudes and phases constitute the desired information. If the absolute value of the motion is desired, the signal from any pickup can be fed into a voltmeter from a T connector at the input to its mixer channel.

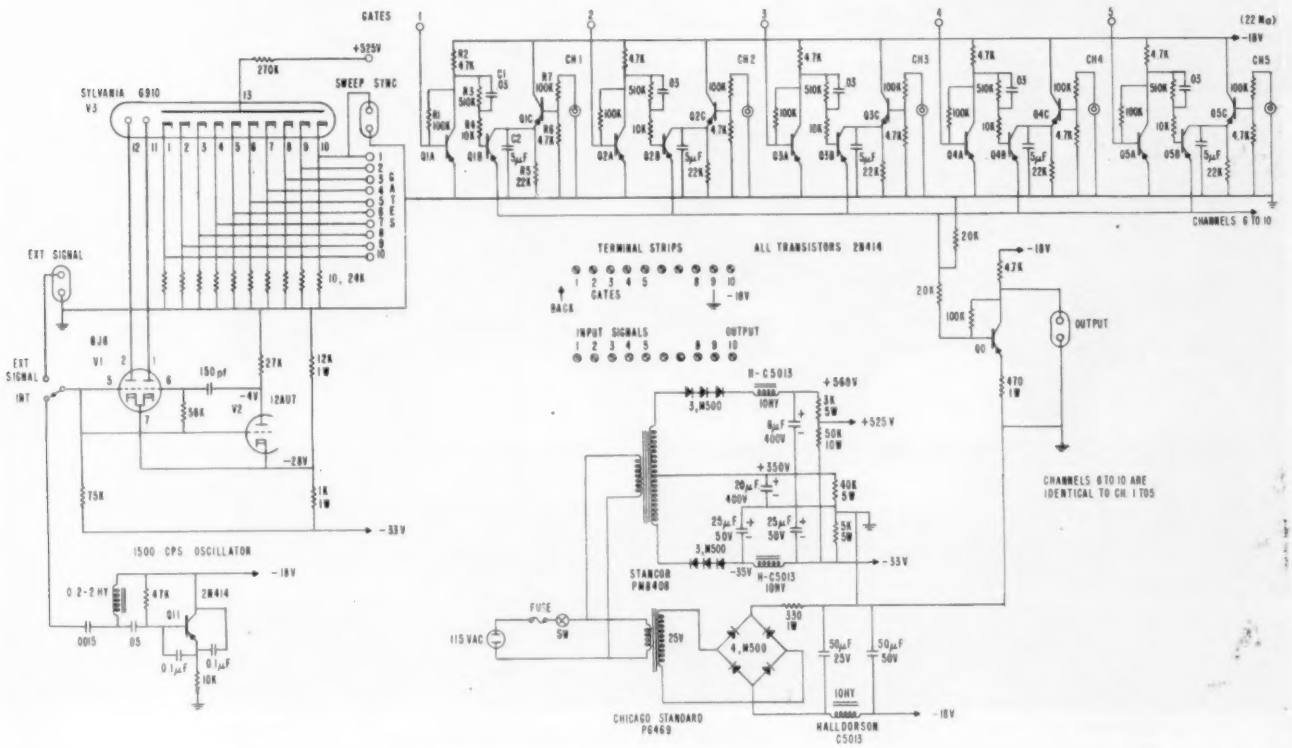

FIGURE 3. *Multichannel electronic switch.*

5. Uses

The strobolyzer was devised as a tool to aid improvement of vibration exciters for use in calibration of vibration pickups.

The accuracy of such a calibration depends greatly on the use of undistorted uniaxial sinusoidal motion. As techniques of vibration measurement improved it became apparent that a significant amount of distorted motion occurred in the shakers at some frequencies. In order to achieve accurate calibration at these frequencies it was necessary to determine the cause of the unwanted components of the motion; e.g., the excitation of a transverse or flexural mode of some part of the structure. By cementing a number of small, light vibration pickups to all parts of the shaker and by using the strobolyzer to determine the phase and amplitude of motion at each point relative to the other points it was possible to identify the origin of the unwanted motion. A chang of design to minimize such motion usually was no too difficult after the motion was known.

Figure 4a was contrived to illustrate the use of the strobolyzer to study the vibration of a bar excited near the middle by the loudspeaker pot in the foreground. The acceleration was detected by barium titanate pickups, the relative phase of the acceleration at each point being indicated by its corresponding d-c meter. Acceleration phases at four intervals separated by 90° are shown in figure 4b.

Figure 5 shows the use of the strobolyzer in studying the pattern of motion at the resonant frequencies of a thin-walled cylinder rigidly fastened at the base. The cylinder walls were too thin to allow mechanical driving or detection of the motion. The vibration was generated acoustically by the loudspeaker which is shown lifted several inches above its usual position in driving the structure. The mo-

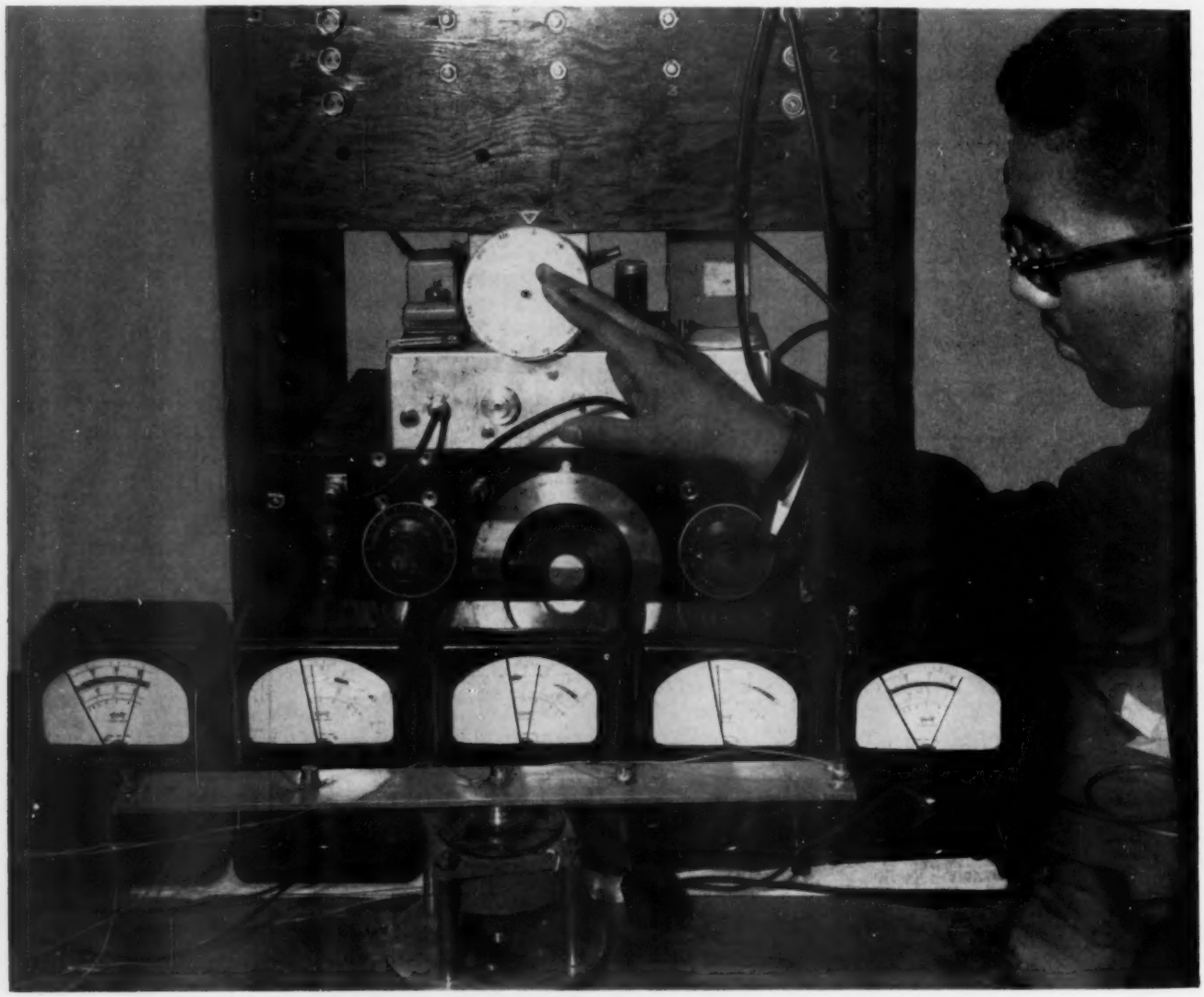

FIGURE 4a. *Acceleration of a bar driven at the center.*

Meter scales have been masked to show limits of indicator excursion as phase shifter is turned through 360°. Unmasked scale angle is proportional to peak acceleration.

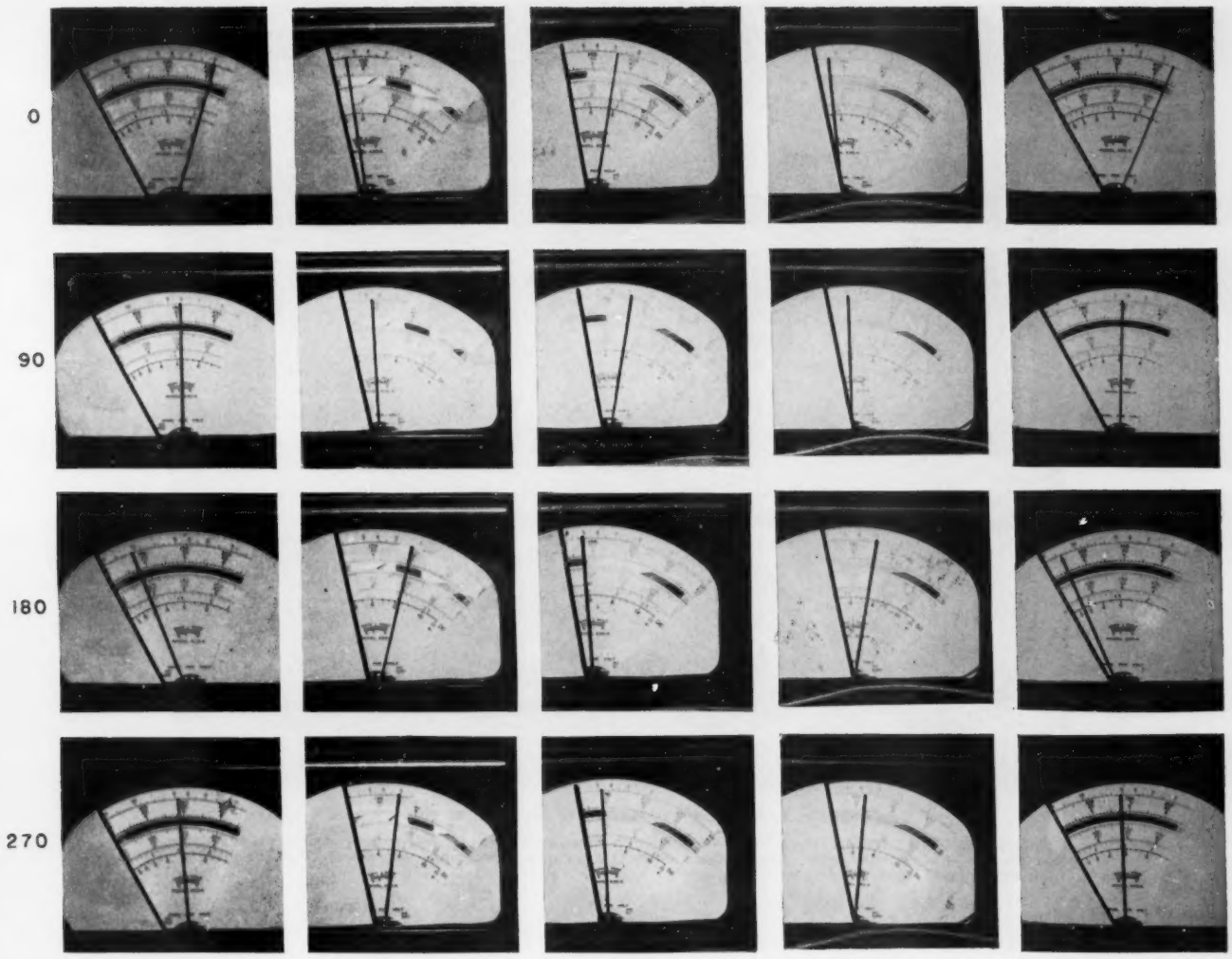

FIGURE 4b. *Acceleration of a bar driven at the center.*

Indicator positions give relative phase of acceleration at each pickup position for phase of vibration cycle shown on phase shifter dial.

tion of the cylinder walls was detected by noncontacting capacitive vibration pickups whose design was adapted from that described by Shafer and Plunkett [11]. The bases of the pickup supports were constructed so that the spacing between the cylinder wall and the pickup did not change as the pickup was moved around the periphery. Two of the pickup supports carried two pickups each to detect standing waves in the axial direction. Since the top of the cylinder was always a loop and the bottom always a node of displacement, a small spread in the position of the lower pickup sufficed to determine the presence of axial waves. The circumferential standing wave pattern was determined by moving the single pickup around the cylinder, noting the drop in amplitude and change in phase as a node was passed. Two barium titanate vibration pickups were cemented to the base to detect any motion which would be contrary to the assumption that the base support was rigid. A microphone monitored the sound output to detect any shifts in the pattern of standing waves of sound in the room. In preliminary experiments with the loudspeaker at a considerable distance above the cylinder it was found that movements of reflecting surfaces in the room, such as a change in the position of the observer might shift the whole vibration pattern along the periphery of the cylinder. This was annoying when it occurred part way through the determination of the vibration pattern at a particular frequency. The microphone was introduced to warn of such shifts. Later, it was found that the recurrence of such shifts was reduced by lowering the loudspeaker until it nearly touched the cylinder but they still occurred frequently enough to warrant continued use of the microphone.

The relationships existing among the different signals were displayed on the oscilloscope. The output signals at intervals of approximately 90° are shown below the picture. The signal indicated

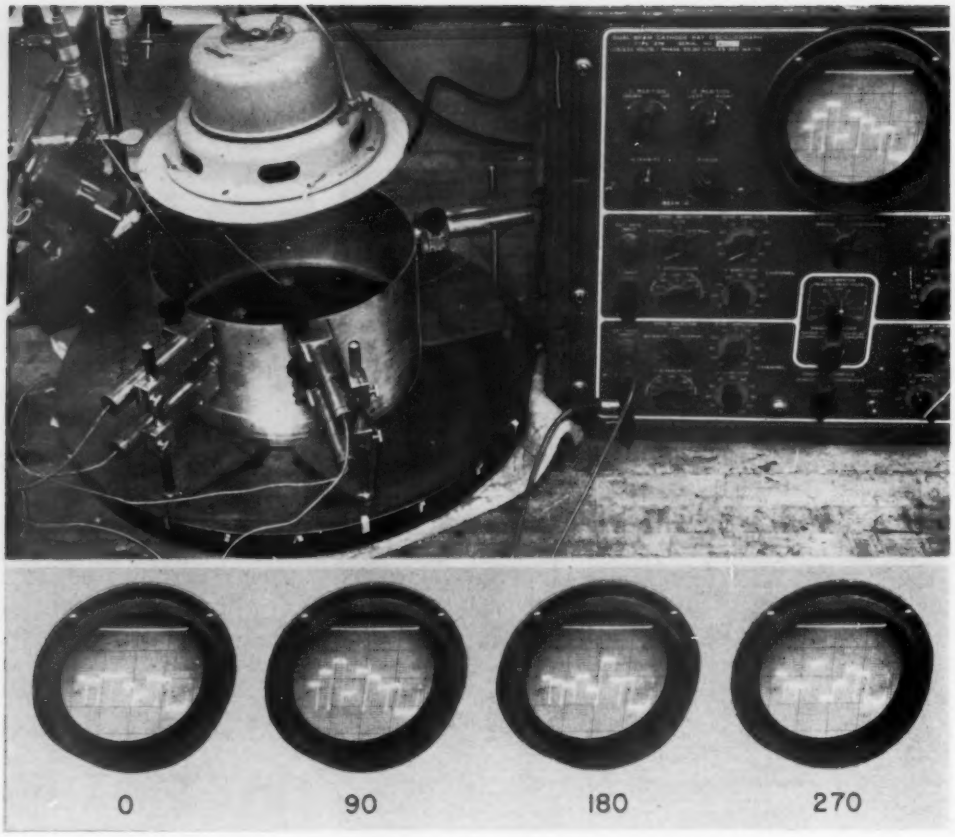

FIGURE 5. *Study of resonances of thin walled cylinder.*

Height of each bar of the oscilloscope trace gives relative phase and amplitude of corresponding pickup signal at a particular phase of the vibration cycle. The relations among the pickup signals at phase intervals of 90° of the vibration cycle are displayed below the picture.

by each bar is given in the list below with the bars numbered from left to right.

Signals Indicated by Oscilloscope Display

Bar	*Signal from pickup*
1	left lower capacitive pickup
2	right lower capacitive pickup
3	left upper capacitive pickup
4	right upper capacitive pickup
5	mobile capacitive pickup
6	loudspeaker signal used as a reference for phase measurement
7	microphone signal
8	piezoelectric pickup attached to base

As the examples described above indicate, the strobolyzer is more useful as an exploratory tool than as a routine measuring device. If the information of interest is the amplitude of vibration at a number of points for the purpose of estimating damage or malfunction, the strobolyzer has no advantage over conventional methods. However, if the problem is to visualize the varied details of the motion of a complex structure or to determine interactions among various motions, the strobolyzer provides unique assistance.

Since it is a new instrument, its effectiveness in probing problems depends to some extent on the ingenuity of the user in taking full advantage of its flexibility. For example, the motion to be studied need not be excited by the modified beat frequency oscillator shown in figure 2 and may not be under the control of the experimenter. In this case, the signal from one of the pickups is taken as the reference. The reference signal is applied through the phase shifter to each of the inner channels as shown in figure 6 so that the output of each mixer channel is at Δ cps. When the strobolyzer is used in this way it is necessary to tune the phase shifter to each audiofrequency which is used. One convenient way to do the tuning is to use ganged wafer switches to connect matched pairs of resistors and capacitors for selected frequencies which are used frequently and to use trimmer capacitors for intermediate frequencies. Considerable information can be obtained by proper filtering of the pickup signals.

The strobolyzer is flexible in the wide variety of transducers which may be used to supply the input signals, and therefore also in the wide variety of periodic phenomena which may be studied.

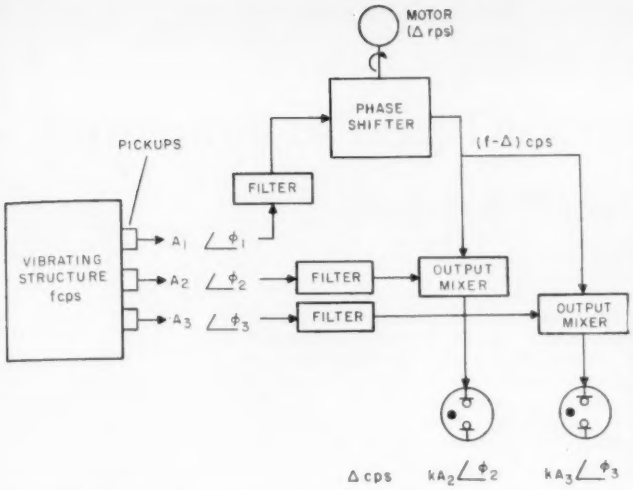

FIGURE 6. *Use of strobolyzer to study externally excited motion.*

Sidney Kohrn of the Bureau staff helped considerably in the development and early use of the instrument described here.

In the course of several stimulating discussions, G. F. Sheets, Jr. of the White Sands Proving Ground contributed to the development of the output circuit.

6. References

[1] Paul Paasche, Z. tech. Physik. **9,** 411 (1928).
[2] W. D. Dye, Proc. Roy. Soc. (London) **A138,** 1 (1932).
[3] G. F. Hull, Rev. Sci. Instr. **15,** 340 (1944).
[4] Bruce, Macinante, and Kelly, Nature **167,** 520 (Mar. 31, 1951).
[5] S. Tolansky and W. Bardsley, Proc. Phys. Soc. (London) **B64,** 224 (1951).
[6] Bruce, Macinante, and Kelly Australian J. App. Sci. **4,** 28 (1953).
[7] E. A. G. Shaw, J. Acoust. Soc. Am. **28,** 38 (1956).
[8] E. R. Smith, S. Edelman, E. Jones, and V. A. Schmidt, J. Acoust. Soc. Am. **30,** 867 (1958).
[9] F. E. Terman, Radio Engineers Handbook, McGraw-Hill Book Co., Inc., p. 567, (1943).
[10] D. E. Goldman and J. R. Richards, Measurement of High Frequency Sound Velocity in Mammalian Soft Tissues, J. Acoust. Soc. Am. **26,** p. 981, (Nov. 1954).
[11] S. N. Shafer and R. Plunkett, Proc. Soc. Exp. Stress Anal., XIII, No. 1, p. 123 (1955).

WASHINGTON, D.C. (Paper 63C2–12)

Journal of Research of the National Bureau of Standards—C. Engineering and Instrumentation

Vol. 63C, No. 2, October–December 1959

Evaluation of Lens Distortion by the Inverse Nodal Slide

Francis E. Washer and Walter R. Darling

(June 4, 1959)

The evaluation of lens distortion by means of the inverse nodal slide method is discussed. The sources of error inherent in the method are investigated. Emphasis is given to the effect of asymmetric use of apertures. Measurements are reported on the same lens for which distortion values were measured by the direct nodal slide and photographic methods. A comparison of results obtained by the three different methods is given. It is concluded that accurate values of the distortion of a lens can be obtained by the inverse nodal slide method and that the precision of measurement is comparable to that of the two other methods mentioned when proper attention to sources of error is given.

1. Introduction

In the course of an extended investigation into the factors affecting the accuracy of measurements of lens distortion, a variety of ways were employed to facilitate the location of possible sources of error. In a previous paper, the values of distortion for a single lens by two different methods were reported [1].[1] These were designated methods A and B; A is photographic employing the precision lens testing camera [2], while B is visual employing the nodal slide bench [3]. It was established that results comparable in accuracy and in good agreement could be obtained by either process provided proper consideration is given to various potential sources of error.

In this paper, a third manner of evaluating distortion is presented. This is a visual method that is essentially the reverse of the nodal slide method B. For that reason it is designated the inverse nodal slide method and is hereinafter referred to as method D. While this cannot be regarded as a new method, it is sufficiently different from A and B that it can be regarded as independent and so serve as a valuable check on the reliability of the values of distortion obtained by methods A and B. In addition, it provides a process for determining quantitatively the effect of asymmetric use of apertures upon the measured values of distortion. This is an especially valuable feature as it is probable that errors from this source can and do occur in some of the diverse methods presently employed for the measurement of distortion.

To facilitate the comparison of the reliability of method D with methods A and B, the values of distortion obtained by method D for wide angle lens No. 3 are contained in this article together with the results obtained on the same lens by A and B. This lens has a nominal focal length of 150 mm, maximum aperture of $f/6.3$, and a half-field angle of 45°.

It should also be mentioned for purposes of clarity that a method C was also developed and used in the course of this study. This differed from method D in that a larger aperture (4 in.) viewing telescope was used; and while fully as reliable as D, it was not as convenient to use in studying the effects of asymmetric use of apertures. For this reason detailed discussion of results obtained by method C is not reported.

[1] Figures in brackets indicate the literature references at the end of this paper.

2. Inverse Nodal Slide Method

In the direct nodal slide method, transverse linear displacements of the image formed in the image plane of the lens under test of an illuminated target located in the focal plane of the collimator are measured with the aid of a viewing microscope. In the inverse method, transverse angular displacements of the parallel beam of light emergent from the lens under test having a point source of light located in its focal plane are measured with the aid of a viewing telescope.

2.1. Description of the Apparatus

The optical T-bench (figs. 1 and 2) which is described in some detail in an earlier paper [4] is well suited to the measurement of distortion by the inverse nodal slide method. The lens under test is mounted in the nodal slide with its front facing the viewing telescope as shown in the figures. The illuminated target is mounted on a separate movable slide behind the lens. The viewing telescope has a full aperture of 40 mm and is mounted on a flexure plate fixture that permits precise pointing of the telescope at the target as seen through the lens. Micrometers on the flexure plate mounting permit the measurement of changes in the direction of pointing of the telescope.

2.2. Method of Measurement

In the inverse nodal slide method, a point source of light, or a properly illuminated reticle bearing well-defined cross lines, is initially placed at the focal point of the lens under test as shown in figure 1.

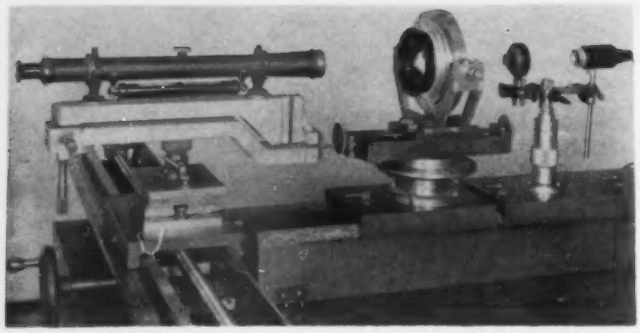

FIGURE 1. *Photograph showing test equipment for method D (axial condition).*

The lens under test is shown mounted on the nodal slide in the center of the photograph. The illuminating system and target reticle are shown at the right behind the lens. The viewing telescope is shown at the left. It is equipped with micrometer adjustments to change its pointing and the whole assembly can move transversely on the ways forming the upper part of the T.

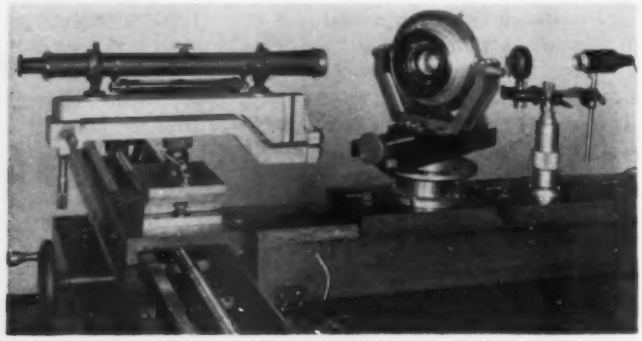

FIGURE 2. *Photographs showing test equipment for method D (off-axis condition).*

The same equipment appearing in figure 1 is shown with the lens rotated about the vertical axis and the reticle displaced to maintain proper focus condition for extra-axial measurements.

This target is viewed through the front of the lens with a telescope focused for infinity. The lens is properly mounted in the nodal slide and so adjusted that small rotations of the lens about its vertical axis do not produce noticeable deviations of the emergent beam. (In the present work, if the point source of light is imaged on the crosshair of the viewing telescope and the image does not move when the lens is rotated about its vertical axis by amounts not exceeding ± 2 deg, the adjustment is satisfactory.) When this condition is present, the rear nodal point of the lens lies in the vertical axis of rotation of the nodal slide and the test may begin. To determine the distortion at angle β, the target reticle is moved away from the lens until the distance separating the rear nodal point of the lens and the point source is $f \sec \beta$. The lens is now rotated by an amount $+\beta$, and the pointing of the viewing telescope is changed by a micrometer until coincidence of its crosshairs with the image is achieved. The setting of the micrometer in scale divisions is read and recorded as R. The lens is now rotated through zero to $-\beta$ and similar pointings made with the reading recorded as L.

The values of radial distortion, D_β, for a given lens when determined by method A are fairly simply obtained from the following relation

$$D_\beta = r - f \tan \beta,$$

where r is the measured distance on the negative from the axial point to the image of an infinitely distant object point lying in the direction marking angle β with the axis of the objective and f is the equivalent focal length of the objective. In the evaluation of distortion by method D, the value of the radial distortion D_β is given by the equation

$$D_\beta = \frac{-k(R-L)f}{2 \cos^2 \beta}, \qquad (1)$$

where f is the equivalent focal length of the lens under test and k is the constant of the micrometer in radians/scale division. The value of k is known from previous calibrations to be 2.8323×10^{-5} radians or 5.8421 sec of arc per scale division. The terms R and L in eq (1) are the readings of the angle measuring micrometer in scale divisions. The values of R and L are measured with respect to an arbitrary zero which is the same for both; it is customary to select this arbitrary zero in such a manner that the values of R and L are approximately equal in magnitude but opposite in sign for comparable conditions of $+\beta$ and $-\beta$.

2.3. Discussion

When distortion is measured directly on the usual type of optical bench, the infinite object is provided by a large collimator that is well corrected for longitudinal spherical aberration. Consequently, there is usually no occasion to be concerned about whether or not the portion of the collimator aperture from which the parallel beam emerges is concentric with the axis of the collimator or displaced laterally therefrom. However, under the condition described in 2.2, it is evident that the beam of collimated light emergent from the lens under test will usually be incident upon the objective of the viewing telescope in such a manner that asymmetric use of the telescope aperture will result. This belief was borne out by the first set of measurements from which were derived values of distortion so different from those obtained with the same lens by methods A and B that they were initially believed to be valueless. This was particularly true for the larger values of β where the clipping of both telescope and lens apertures was most pronounced. It therefore seemed worthwhile to make a study of these effects.

3. Effect of Aperture on the Measured Values of Distortion

It has long been known that asymmetric use of apertures can cause errors in telescope pointing [5]. Most of the discussion of this subject has been in the field of proper centering of small prisms on

spectrometer tables, etc. In other fields, it has been customary to warn against asymmetric use of apertures when doing work of highest accuracy. There is, however, a dearth of publications dealing with the probable magnitudes of error from this source likely to be introduced when evaluating lens distortion. Accordingly, a series of careful measurements have been made which are herein reported.

3.1. Method of Measurement of Aperture Effect

As mentioned in section 2.1, method D is used on the T-bench. The lens and source are on the vertical arm of the T and the viewing telescope is mounted on the crossbench. The telescope is pointed at right angles to the bench ways and the whole telescope assembly can be moved transversely across the emergent beam of the lens. The bench ways are quite straight so the pointing of the telescope is not affected by the transverse displacement. In making a set of measurements, such as shown in table 1, the lens is rotated by amount $+\beta$, the telescope slide is moved to the left along its ways until no light from the target is seen through the telescope. The telescope slide is then moved slowly while viewing through it until the first faint image is seen. The reading of the bench scale for this point is recorded and noted as first image (F.I.). The telescope is then moved transversely along the bench until the image begins to disappear; this bench scale reading is recorded and noted as last image (L.I.). The midpoint of these two bench scale readings is assumed to be the proper setting for centered apertures of lens and telescope. The telescope is then set successively at 5-mm intervals above and below this central reading of the bench scale (this center point is underlined in table 1) until the whole range for which the image can be seen is covered. Pointings of the telescope are read and recorded for each of these settings. The readings of the pointing micrometer are recorded under R for $+\beta$ and under L for $-\beta$. The same procedure is repeated with the telescope aperture reduced to 8 mm. In order to give a clear picture of how the portions of the apertures are being used, the drawings shown in figure 3 and 4 were prepared. Figure 3 shows the relation of the cross section of the emergent beam from the lens and the telescope aperture for successive 5-mm displacements of the telescope assembly along its ways. This drawing is based on the displacements shown in table 1 for $\beta=+5°$. It is to be noted that the cross section of the emergent beam from the lens is assumed to be still circular and that it remains stationary while the telescope aperture moves across it. The departure from a true circle is not significant at 5°,

TABLE 1. *Variation of distortion for $\beta=5°$ with relative location of measuring aperture in the emergent beam for wide angle lens No. 3*

The column, headed bench scale, gives the successive positions of the angle measuring telescope as its aperture is moved transversely across the beam emergent from the test lens. The difference in telescope pointing is given in scale divisions, R for $\beta=+5°$ and L for $\beta=-5°$ (1 scale division = 5.8421 sec). D_R and D_L are the corresponding values of distortion, D_β is the average value. The location of the center of the emergent beam is indicated by the underlined value of the bench scale. Part (a) shows the values of distortion with the telescope aperture set at 40 mm and part (b) shows similar information for the telescope aperture set at 8 mm. Values of distortion are given in microns.

Bench scale	R scale divisions	D_R	Bench scale	L scale divisions	D_L	D_β
(a) Telescope of 40-mm aperture						
mm			*mm*			
−0.7	F. I.	-------	−1.7	F. I.	-------	-------
5	0.3	−1	3.4	1.4	+6	2
10	−1.1	5	8.4	1.1	+5	5
15	−2.4	10	13.4	1.5	+6	8
20	−2.6	11	18.4	1.7	+7	9
25	−2.6	11	23.4	2.4	+10	11
30	−2.6	11	28.4	2.6	+11	11
35	−2.2	10	33.4	2.6	+11	10
40	−2.2	10	38.4	2.9	+13	11
45	−2.2	10	43.4	3.8	+16	13
50	−2.2	10	48.4	2.6	+11	10
55	−1.3	6	53.4	3.9	+17	11
60.7	L. I.	-------	58.8	L. I.	-------	-------
(b) Telescope of 8-mm aperture						
15.2	F. I.	-------	13.6	F. I.	-------	-------
20	0.4	−2	18.4	2.4	+10	4
25	−2.0	9	23.4	0.7	+3	6
30	−2.4	10	28.4	2.4	+10	10
35	−3.3	14	33.4	2.5	+11	13
40	−1.3	6	38.4	2.9	+13	9
44.8	L. I.	-------	43.2	L. I.	-------	-------

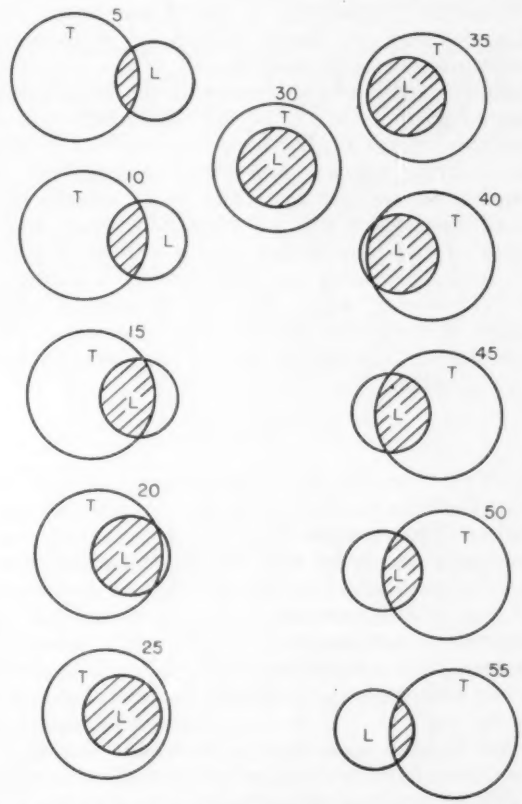

FIGURE 3. *Sketches showing the relation of the cross section of the beam, L, emergent from the lens under test and the aperture, T, of the viewing telescope.*

The shaded areas show the portion of the 40-mm telescope aperture being used. The numbers correspond to successive positions occupied by the telescope assembly and are the bench scale readings shown in table 1 (a) when determining D_R.

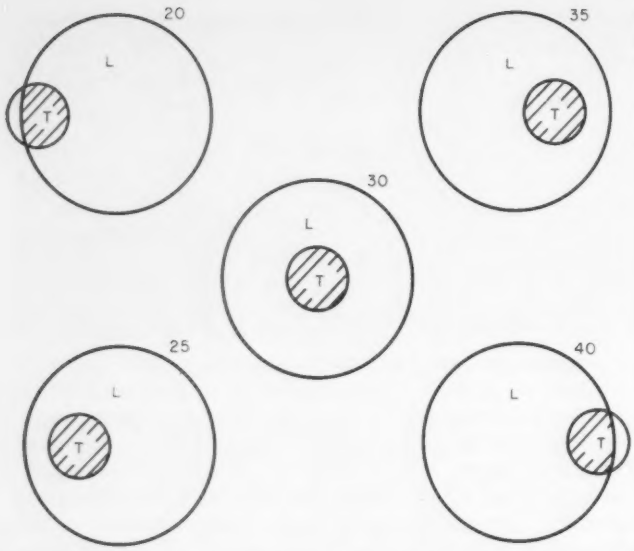

FIGURE 4. *Sketches showing the relation of the cross section of the beam, L, emergent from the lens under test and the aperture, T, of the viewing telescope.*

The shaded areas show the portion of the 8-mm telescope aperture being used and its relation to the total emergent beam from the lens. The numbers correspond to the bench scale readings in table 1(b) in the determination of D_R.

but at the larger angles of β the transverse diameter is reduced in proportion to cos β and may be still further reduced at large values of β because of vignetting by the lens mount.

While the value of the distortion D_β is customarily computed with the aid of eq (1), this method of computing the values of D_β does not lend itself readily to the determination of the effect of aperture. It is reasonable to assume that the most nearly correct value of distortion will be obtained when the exit aperture of the lens under test is centered with respect to the entrance aperture of the viewing telescope. However, when the lens is turned through the angle β about its vertical axis, the center of the exit aperture of the lens is moved transversely by the amount x_β where

$$x_\beta = N_p \sin \beta, \tag{2}$$

where N_p is the distance separating the rear nodal point of the lens under test and the center of its exit aperture. This means that the telescope must be moved transversely by amount $2x_\beta$ from the position properly occupied when measurements are made at angle $+\beta$ to the position properly occupied when measurements are made at angle $-\beta$. Even when this is done, it is possible for R_β to differ in magnitude from $-L_\beta$ although the value of D_β is still given correctly by eq (1). This condition does not necessarily reduce the reliability of the final values of D_β as this dissimilarity of values of R_β and $-L_\beta$ usually results from small misalinements of the viewing telescope or small transverse maladjustment of the rear nodal point of the lens with respect to the axis of rotation of the nodal slide. It can be shown that the presence of these maladjustments does not produce error in the accepted values of D_β.

However, for convenience in computations and graphing of results, it was decided to establish the zero of the micrometer at a point such that $R_\beta = -L_\beta$ for the condition of optimum reliability even though the telescope was moved transversely between the two determinations. With the zero so established it was then possible to evaluate the partial distortions D_R and D_L in a convenient manner.

The values of the partial distortions D_R and D_L are computed with the aid of the following relations:

$$D_R = \frac{-kRf}{\cos^2 \beta} \tag{3}$$

and

$$D_L = \frac{+kLf}{\cos^2 \beta} \tag{4}$$

and the final value D_β is obtained from the relation

$$D_\beta = \frac{D_R + D_L}{2}, \tag{5}$$

which is equivalent to the expression shown in eq (1). In table 1, values of D_R are shown for $\beta = 5°$ for each successive setting of the bench scale; the values of D_R are also plotted in figure 5. It is clear that the magnitude of D_R varies with position of the viewing telescope along the bench scale. It is also clear that different portions of the apertures of lens and telescope are being used for each position. For the telescope of 40-mm aperture, the value of D_R (shown in box A of fig. 5) remains fairly constant during the middle part of the run but dips sharply at the extremes. It is probable that this effect arises from spherical aberration in the lens and telescope objective with the lens making the greater contribution. That the contribution of the lens is the greater is evident from consideration of the curve showing the values of D_R (shown in box B of fig. 5) obtained when the telescope aperture is reduced to 8 mm. The relation of the cross section of the emergent beam from the lens and the telescope aperture is shown in figure 4. In this instance, the telescope aperture is so small that it is unlikely that spherical aberration in the telescope objective can produce appreciable error in pointing. Nonetheless, a comparable rise and fall of D_R is evident at the start and finish of the traverse of the telescope aperture across the lens aperture.

While figures, comparable to figures 3 and 4 showing the relation of apertures in determining D_L, are not included in this report, it is obvious that they would look very similar to figures 3 and 4. The values of D_L are determined in the manner already described for D_R. The values of D_L are shown in table 1 and are plotted in figure 5. Two methods are used in determining D_β. The first and preferred method is to average D_R and D_L with the aid of eq (5) for comparable relative positions of the aperture. Values of D_β by this method are shown in table 1. A second, but less sound method, is to average for identical settings of the bench scale.

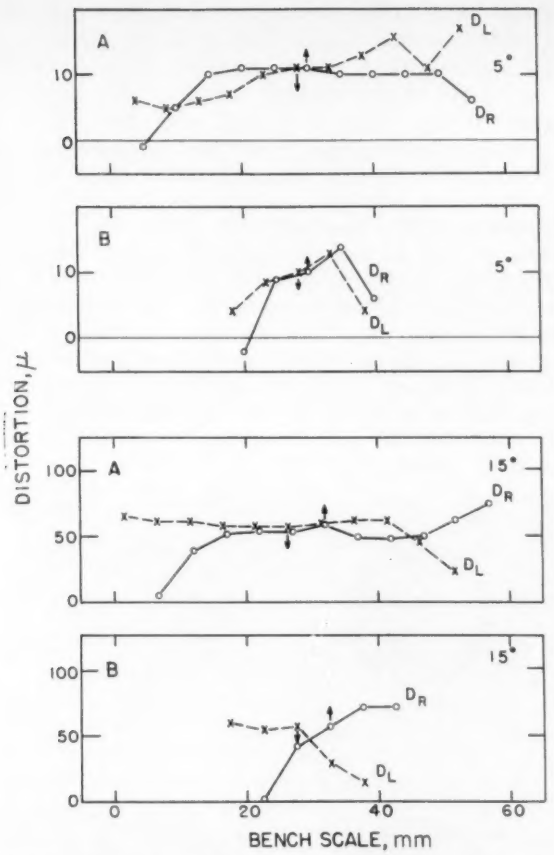

FIGURE 5. *Variation of distortion, D_R and D_L as a function of transverse displacement of the viewing telescope with respect to the aperture of the lens under test.*

The boxes designated A show values of D_R and D_L obtained with the viewing telescope of 40-mm aperture for $\beta=5°$ and 15°. The upward pointing arrows attached to the circles mark the positions of centered apertures for the positive values of β; the downward pointing arrows attached to the crosses mark the positions of centered apertures for the minus values of β. The boxes designated B give like information obtained with the viewing telescope of 8-mm aperture for $\beta=5°$ and 15°.

The foregoing procedures of determining D_R, D_L, and D_β were repeated at successive values of β ranging from 10° to 45° at 5° intervals, and the values for D_β for β ranging from 5° to 45° are shown in table 2. The values of D_R and D_L, obtained for $\beta=15°$, 30°, and 45° are shown graphically in figures 5 and 6. It is evident throughout this array that values of the distortion remain fairly constant in the center portions of the run and vary sharply at the extremes for the telescope with the 40-mm aperture. On the other hand, the results obtained with the 8-mm aperture vary throughout the range of bench settings used. The center points for the various values of β varied in location with respect to the bench scale as indicated by eq (2). For the four values of β for which values of D_R and D_L are plotted, the short arrows in the figures mark the accepted center point for each run. It may be noted that their separations increase with increasing β. The values of the separations of aperture centers are shown under the heading $2x_\beta$ in table 3 and are plotted as a function of sin β in figure 7. It is evi-

TABLE 2. *Variation of values of distortion in microns, D_β with relative location of the measuring aperture in the emergent beam for wide angle lens No. 3 for a series of values of β*

Part (a) shows the variation of D_β with separation, h, of the center of the measuring aperture with respect to the center of the emergent beam from the lens for a viewing telescope of 40-mm aperture. Part (b) shows the results for similar measurements when the telescope aperture is reduced to 8 mm.

h	Variation of D_β with h for β =							
	10°	15°	20°	25°	30°	35°	40°	45°
(a) Telescope of 40-mm aperture								
mm								
−25	15	35	66	106	161	212	----	--
−20	24	50	77	140	183	232	227	92
−15	27	56	92	146	198	240	234	96
−10	29	56	96	148	199	241	235	96
− 5	28	55	96	149	200	242	235	94
0	30	58	99	149	201	240	235	91
5	30	55	98	149	199	240	234	89
10	29	55	97	146	198	243	234	94
15	27	56	98	150	201	245	236	91
20	25	55	90	138	206	251	244	91
25	24	49	82	135	197	281	----	--
(b) Telescope of 8-mm aperture								
−10	13	31	59	103	162	232	----	--
− 5	20	47	88	136	192	252	226	93
0	29	56	98	150	207	252	241	91
5	27	50	87	142	208	253	240	98
10	25	42	78	131	201	----	----	--

TABLE 3. *Displacement of centers of apertures $2x_\beta$, determined with telescope at 40-mm aperture, of emergent beam from lens with rotation of lens about its rear nodal point as a function of angular separation from the axis*

Angular separation from axis	Bench scale		Displacement $2x_\beta$
	Right	Left	
deg	*mm*	*mm*	*mm*
0	29.2	29.2	0.0
5	30.0	28.4	1.6
10	31.1	27.5	3.6
15	32.0	26.5	5.5
20	33.4	26.1	7.3
25	33.7	25.3	8.4
30	34.9	24.4	10.5
35	36.0	24.2	11.8
40	37.8	23.4	14.4
45	40.6	21.5	19.1

dent from the maximum value of $2x_\beta$, that if the telescope were to remain permanently located at the position of optimum centering of lens and telescope apertures for $\beta=0$, the maximum aperture of the viewing telescope should be not less than the sum of $2x_\beta$ and $d \cos_\beta$ where d is the effective aperture of the lens under test. For the lens used in this experiment, the minimum acceptable aperture of the viewing telescope is 36.2 mm.

This separation of the aperture centers as the lens is rotated about the vertical axis passing through the rear nodal point from $+\beta$ to $-\beta$ arises from the fact that there is an appreciable axial distance separating the rear nodal point and the plane of the entrance pupil of the lens. Consequently, the lens aperture moves from side to side and the light proceeding from it is incident upon the objective of the viewing

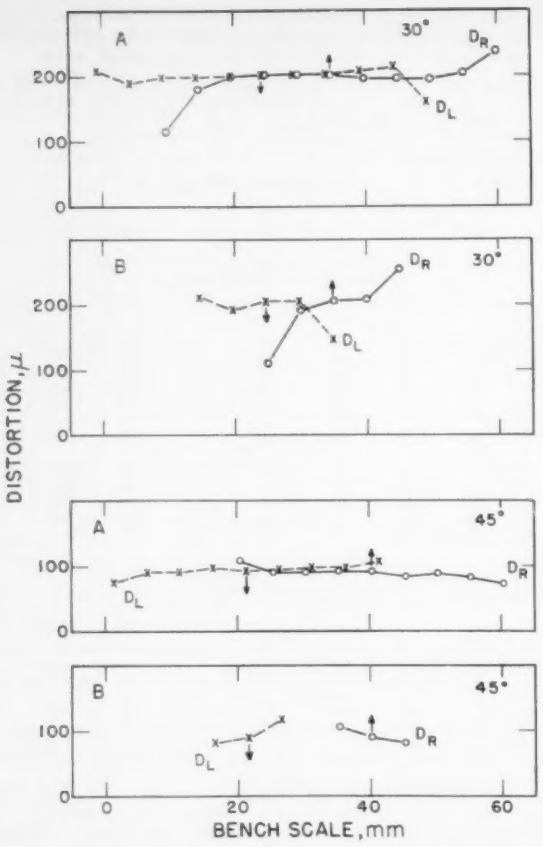

FIGURE 6. *Variation of partial distortions* D_R *and* D_L *as a function of transverse displacement of the viewing telescope with respect to the aperture of the lens under test.*

The boxes, designated A, show values of D_R and D_L obtained with the viewing telescope of 40-mm aperture for $\beta=30°$ and 45°. The upward pointing arrows attached to the circles mark the positions of centered apertures for the positive values of β; the downward pointing arrows mark the positions of centered apertures for the minus values of β. The boxes designated B give like information obtained with the viewing telescope of 8-mm aperture for $\beta=30°$ and 45°.

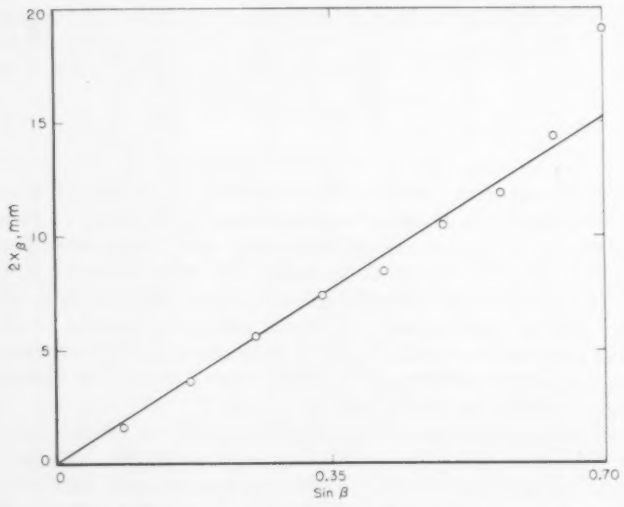

FIGURE 7. *Measured separation of right and left aperture centers* $2x_\beta$ *as a function of sin* β.

For a rotation of the lens under test about a vertical axis passing through the rear nodal point, the position of the aperture center of the emergent beam for the setting $+\beta$ is separated from the position occupied by the same aperture center for the setting $-\beta$ by amount $2x_\beta=N_p \sin \beta$, eq (2).

telescope in a different region for each value of β. This effect is seen more clearly in figure 8 which shows a photograph of the lens aperture as seen in the exit pupil of the viewing telescope for successive settings of the lens $\beta=\pm30°$ and $\beta=\pm45°$. In making this photograph, the viewing telescope was made coaxial with the lens at $\beta=0$ so that the two apertures were centered with respect to each other. The viewing telescope was left fixed and the lens rotated to $+\beta$ and a photograph made. Without changing any adjustment of the camera or viewing telescope, the lens was rotated to $-\beta$ and a second exposure on the same camera film was made. Consequently, the figure shows the relative portions of the telescope aperture used under the two conditions. Unless the correction of the viewing telescope is

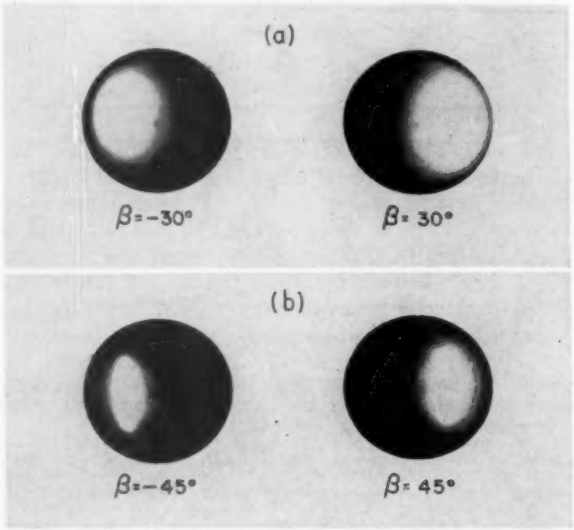

FIGURE 8. *Photographs showing the appearance of the aperture of the lens under tests as seen in the exit pupil of the viewing telescope for two successive settings of the lens at* (*a*) $\beta=+30°$ *and* $\beta=-30°$ *and* (*b*) $\beta=+45°$ *and* $\beta=-45°$.

The apertures of the lens and viewing telescope were centered initially at $\beta=0°$. The position of the telescope remained fixed while the lens was rotated to the successive positions. The dark circular area shows the exit pupil of the telescope while the light area shows the aperture of the lens under test.

excellent, it is evident that differing performance for the two areas can produce differences in the measured characteristics of the lens. In addition, it is also apparent that the lens aperture can be so far displaced with respect to the telescope aperture that partial obscuration can occur thus permitting the aberrations of the lens itself to make differing contributions with resultant errors in the final average values of distortion. To minimize the effect of unsymmetrical use of apertures, it is desirable that the aperture of the viewing telescope be sufficiently large that the cross section of the emergent beam from the lens shall at all times be within the boundaries of the aperture of the viewing telescope. Moreover, the objective of the viewing telescope should be excellently corrected over its entire area. In the present

instance, the diameter of excellent correction should be not less than 37 mm. It is questionable if this condition is satisfied by the objective of the viewing telescope used in this work for a diameter greater than 25 mm.

3.2. Effect of Incorrect Use of Aperture on Distortion Values

In section 3.1, it was shown that appreciable variation in the values of D_R and D_L can be produced by the relative location of the cross section of the emergent beam from the lens within the aperture of the viewing telescope. It is of interest to determine the probable magnitude of the differences in the final values of the distortion that can be produced by the asymmetrical use of apertures. To determine this the maximum value of D_R was paired with the maximum value of D_L for each value of β and a maximum value of D_β for each value of β was determined. These maximum values of D_β are shown in table 4 under the heading D_E. In a similar manner, minimum values of D_R and D_L are paired to determine a minimum value of D_β for each value of β. Finally, the centered values of D_R and D_L are paired to determine the most probable value of D. All of these combinations are listed in table 4 under the appropriate value of D_E (the distortion referred to the equivalent focal length). The proper adjusting term to convert D_E to distortion referred to the calibrated focal length D_C is shown under the heading ΔD. The results are also shown graphically in figure 9 where the various values of distortion,

TABLE 4. *Extreme values of distortion in microns obtainable by possible combinations of the partial values of distortion, D_R and D_L*

The normal values for centered apertures are also shown. The value of distortion referred to the equivalent focal length is D_E; the value of distortion referred to the calibrated focal length is D_C; and $\Delta D = \Delta F \tan \beta$, is the adjusting factor. Part (a) shows the values of the distortion with the telescope aperture set at 40 mm and part (b) shows similar information for the telescope aperture set at 8 mm.

Angular separation from axis	Maximum			Minimum			Normal		
	D_E	ΔD	D_C	D_E	ΔD	D_C	D_E	ΔD	D_C
	(a) Values of distortion with measuring aperture of 40 mm								
deg									
0	0	0	0	0	0	0	0	0	0
5	14	20	−6	2	15	−13	11	17	−6
10	33	40	−7	6	29	−23	30	34	−4
15	70	62	−8	14	44	−30	58	52	6
20	114	83	31	35	60	−25	99	71	28
25	166	107	59	75	77	−2	149	91	58
30	223	132	91	137	95	42	201	112	89
35	281	160	121	205	116	90	240	136	104
40	259	192	67	212	139	73	235	163	72
45	108	229	−121	75	165	−90	91	195	−104
	(b) Values of distortion with measuring aperture of 8 mm								
0	0	0	0	0	0	0	0	0	0
5	14	20	−6	1	15	−14	11	18	−7
10	37	39	−2	1	29	−28	29	36	−7
15	66	59	7	7	44	−37	56	54	2
20	117	81	36	20	60	−040	98	73	25
25	170	103	67	63	77	−14	150	94	56
30	234	128	106	129	96	33	206	116	90
35	266	155	111	201	116	85	252	141	111
40	252	186	66	215	139	76	241	169	72
45	111	222	−111	81	166	−85	91	202	−111

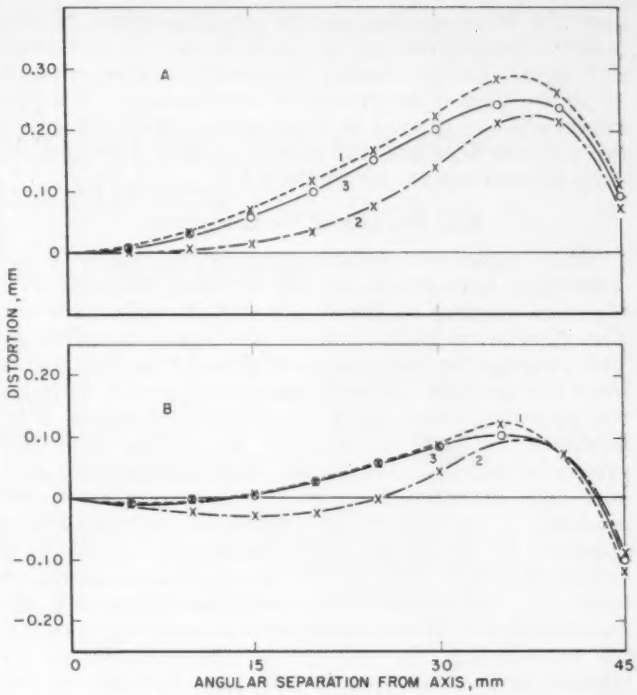

FIGURE 9. *Variation of distortion for incorrect and correct relative locations of the lens aperture with respect to the aperture of the viewing telescope as a function of angular separation β from the axis.*

The values of the distortion, D_E, referred to the equivalent focal length are shown in box A; the values of the distortion, D_C, referred to the calibrated focal length are shown in box B. The curves marked 1 show the maximum incorrect values obtained; the curves marked 2 show the minimum incorrect values; while the curves, marked 3, show the normal or correct values of the distortion.

D_E, are shown in box A and similar values of D_C are shown in box B. The results for the 40-mm measuring aperture alone are shown in the graph.

It is evident that strikingly large differences exist between the maximum and minimum values of distortion ranging as high as 90μ for D_E and 60μ for D_C. It is, of course, unlikely that one would arrange the conditions of measurement to produce the values shown in curve 1 or 2 throughout the entire range but it is not unlikely that experimental conditions are frequently such that the experimenter obtains values nearer to those shown by curves 1 and 2 than those shown by curve 3. The magnitude of the differences show how important it is that the relative positioning of test and measuring apertures be such as to minimize the possibility of errors arising from unsymmetrical use of apertures. It must be mentioned that while this study was made by the inverse nodal slide method, similar results could be obtained by improper use of the direct nodal slide method or any other method where asymmetrical use of apertures could occur.

4. Evaluation of Distortion by Method D

4.1. Preliminary Remarks

In the foregoing section, an important potential source of error in the measured values is described

and the analysis leading to an evaluation of the possible magnitude of its contribution is discussed at length. On the basis of this study, the importance of well-centered apertures is emphasized. We are now ready to proceed to the evaluation of distortion for a given lens and to determine the precision of such measurements by method D.

4.2. Results of Measurement

Seven separate determinations of the values of the distortion were made on lens 3 using the centered aperture reading as far as possible in each instance. The results of measurement are listed in table 5. The average for each value of β and the departures from the average for each run are shown. Finally, the probable error for a single determination, PE_s is shown for each value of β. It is clear that the precision indices in each case are satisfactorily low and compare favorably with values obtained by methods A and B. The values of the distortion obtained by method D also compare favorably with values obtained by methods A and B as is shown in table 6. The values of distortion obtained by methods A and B are taken from an earlier paper [1]. On considering the values of distortion listed in table 6, it is clear that in only one instance is the difference between the values obtained by any of the three methods and the average as great as 5μ. The average departure does not exceed $\pm 3\mu$.

5. Conclusion

It is evident from the information contained in the foregoing section that the inverse nodal slide method is satisfactory for use in the evaluation of distortion provided that care is taken to insure the symmetric use of apertures. Further experiments were also made using a larger telescope having a clear aperture of 4 in. and an objective well corrected for spherical aberration. With this larger telescope, it was not necessary to traverse the telescope mount sidewise to center the aperture. The values of distortion obtained with this larger telescope were essentially the same as those obtained with the 40-mm centered telescope and so are not herein reported.

TABLE 5. *Measured values of the distortion in microns, referred to the calibrated focal length, obtained for wide angle lens No. 3 by method D (visual inverse nodal slide method)*

Seven separate determinations, their average, the departures from the average, and the probable error of a single determination (PE_s) are shown.

Angular separation from axis	(a) Values of distortion obtained from calibration							Average for seven
	1	2	3	4	5	6	7	
0	0	0	0	0	0	0	0	0
5	−6	−6	−5	−5	−6	−5	−5	−5
10	−4	−7	−7	−6	−7	−7	−6	−6
15	6	5	1	4	5	2	3	4
20	28	26	25	26	24	26	28	26
25	58	59	57	61	58	57	58	58
30	89	94	87	93	87	90	91	90
35	104	103	108	113	109	112	109	108
40	72	78	78	80	78	76	76	77
45	−104	−103	−108	−113	−109	−112	−109	−108
	(b) Departures from the average for calibration							PE_s
	1	2	3	4	5	6	7	
0	0	0	0	0	0	0	0	±0
5	−1	−1	0	0	−1	0	0	0
10	2	−1	−1	0	−1	−1	0	1
15	2	1	−3	0	1	−2	−1	1
20	2	0	−1	0	−2	0	2	1
25	0	1	−1	3	0	−1	0	1
30	−1	4	−3	3	−3	0	1	2
35	−4	−5	0	5	1	4	1	3
40	−5	1	1	3	1	−1	−1	2
45	4	5	0	−5	−1	−4	−1	3

TABLE 6. *Comparison of the values of distortion D_D obtained by the inverse nodal slide method with values of distortion D_A and D_B for the same lens obtained by the precision lens testing camera and the direct nodal slide*

Part (a) shows the measured values of the distortion obtained by methods A B, and D and their average. Part (b) shows the departures from the average for each method and the average departure for any of the three methods. All values are given in microns.

Angular separation from axis	(a) Values of distortion obtained by method			Average for the three
	A	B	D	
deg				
0	0	0	0	0
5	−5	−7	−5	−6
10	−5	−8	−6	−6
15	4	1	4	3
20	21	21	26	23
25	49	52	58	53
30	82	87	90	86
35	113	106	108	109
40	79	79	77	78
45	−113	−106	−108	−109
	(b) Departures from the average for method			
	A	B	D	
0	0	0	0	
5	1	−1	1	
10	1	−2	0	
15	1	−2	1	
20	−2	−2	3	
25	−4	−1	5	
30	−4	1	4	
35	4	−3	−1	
40	1	1	−1	
45	−4	3	1	

The authors express their appreciation to Mr. E. C. Watts who made the drawings that appear in this article.

6. References

[1] F. E. Washer, W. P. Tayman, and W. R. Darling, Evaluation of lens distortion by visual and photographic methods, J. Research NBS **61,** 509 (1958) RP2920.

[2] I. C. Gardner and F. A. Case, Precision camera for testing lenses, J. Research NBS **18,** 449 (1937) RP984.

[3] A. H. Bennett, The distortion of some typical photographic objectives, J. Opt. Soc. Am. and Rev. Sci. Instr. **14,** 245 (1927).

[4] F. E. Washer, Optical T-bench method of measuring longitudinal spherical aberration, J. Research NBS **61,** 31 (1958) RP2880.

[5] L. W. Tilton, Permissible curvature of prism surfaces and inaccuracy of collimation in precise minimum-deviation refractometry, J. Research NBS **11,** 25 (1933) RP575.

WASHINGTON, D.C. (Paper 63C2–13)

Journal of Research of the National Bureau of Standards—C. Engineering and Instrumentation

Vol. 63C, No. 2, October–December 1959

Evaluation of Lens Distortion by the Modified Goniometric Method

Francis E. Washer and Walter R. Darling

(August 3, 1959)

This is the third of a series of papers dealing with factors affecting the accuracy of measurment of lens distortion by varicus visual and photographic processes. This paper presents the results of a study of the visual modified goniometric method which employs a viewing theodolite and accurate linear scale. Sources of error are investigated and discussed. Measurements are reported on the same lens that was used in the analysis of two visual and one photographic distortion measuring processes. A comparison of results by the four different methods is given. It is concluded that accurate values of lens distortion can be obtained by the modified goniometric method provided care is taker to use centered apertures and to preserve known angular relationships between telescope pointings and successive locations.

1. Introduction

The accurate evaluation of radial distortion in the focal plane of airplane camera lenses has been of prime importance since the advent of mapping programs that make extensive use of photographs made with airplane cameras. Radial distortion, as herein used, is the linear displacement of an imaged point from the point where it would have been imaged if the lens were perfectly orthoscopic. This displacement is measured in the image plane of the lens along a radius drawn from the intersection point of lens axis and image plane. The presence of distortion impairs the usefulness of the photographs in precision mapping. For this reason, specifications have been generally established which set limits on the magnitude of the permissible distortion for lenses used in various types of aerial photography. To determine compliance with these specifications, the values of the distortion are measured for each lens. Various methods have been developed for making these measurements and it is important that these produce reliable results.

A study of several methods commonly used in the evaluation of lens distortion has been in progress at this Bureau for some time. The methods investigated thus far are:

A. Photographic-precision lens testing camera.

B. Visual—nodal slide optical bench with collimator.

D. Visual—inverse nodal slide bench with point or line target in rear focal plane of lens.

F. Visual—modified goniometric with linear scale in rear focal plane of lens.

In this study, measurements were made on the same lens by all four methods; the results were compared and attempts were made to locate the sources of error most likely to impair the reliability of results obtained by each method. The results of these investigations have been reported for methods A, B, and D;[1,2] the present paper gives the results for method F.

A comparison of the values of the distortion obtained by methods A, B, D, and F are given in table 1 and figure 1. The values shown for A, B, and D are the final accepted values for these methods after all known sources of error have been eliminated or minimized; the values shown for F are the results of a single determination before any attempt was made to reduce or eliminate nonobvious sources of error.

Examination of the values of distortion shown in part (a) of table 1 shows that while there is good agreement among corresponding values obtained by A, B, and D, the values obtained by method F depart markedly from those yielded by the other three. This is shown more clearly in part (b) of table 1 where the departures for each method from the average of values $\bar{D}_3$, obtained by A, B, and D are given. The values for F were not included in the average as it was believed that this set of values was affected by errors markedly in excess of the random errors of the order of $\pm 2\mu$ that affected the others. This is further justified by considering the values of the departures from the average. Here the maximum departure of any value from the average

[1] F. E. Washer, W. P. Tayman, and W. R. Darling, Evaluation of lens distortion by visual and photographic methods, J. Research NBS **61**, 509 (1958) RP2920.

[2] F. E. Washer and W. R. Darling, Evaluation of lens distortion by the inverse-nodal slide, J. Research NBS **63C**, 105 (1959).

TABLE 1. *Measured values of the distortion in microns, referred to the calibrated focal length for wide angle lens No. 3 by four different methods.*

The values for A, B, and D in part (a) are final accepted values while those for F are for a single preliminary determination. The nominal focal length of the lens is 152 mm. Departures from the average, $\Delta D = \overline{D}_3 - D_A$, $\overline{D}_3 - D_B$, etc., are shown in part (b).

Angular separation from axis	(a) Values of distortion obtained by method				Average $\overline{D}_3$ for methods
β	A	B	D	F	A, B, & D
deg					
0	0	0	0	0	0
5	−5	−7	−5	−1	−6
10	−5	−8	−6	−15	−6
15	4	1	4	−21	3
20	21	21	26	6	23
25	49	52	58	52	53
30	82	87	90	57	86
35	113	106	108	92	109
40	79	79	77	67	78
45	−113	−106	−108	−92	−109
	(b) Departures ΔD from the average for method				
	A	B	D	F	
0	0	0	0	0	
5	1	−1	1	5	
10	1	−2	0	−9	
15	1	−2	1	−24	
20	−2	−2	3	−17	
25	−4	−1	5	−1	
30	−4	1	4	−29	
35	4	−3	−1	−17	
40	1	1	−1	−11	
45	−4	3	1	17	

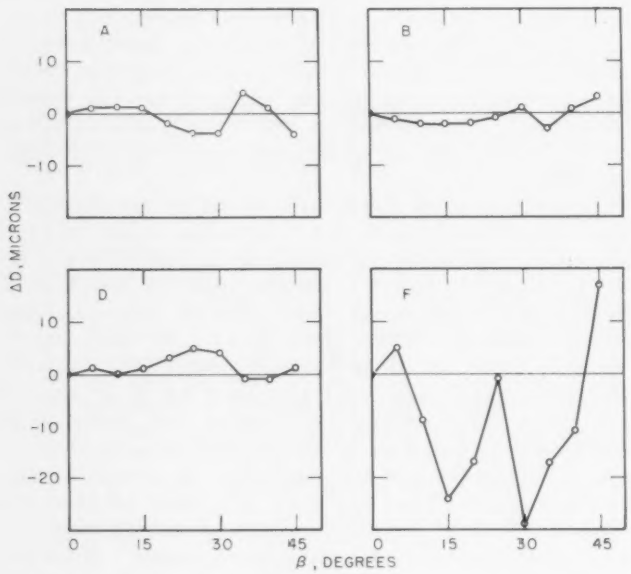

FIGURE 1. *Variation of the departures, ΔD, from the average value of distortion, $\overline{D}_3$, with angular separation β from the axis.*

The variation for each of the four methods are shown in the frames designated A, B, D and F.

is $\pm 5\mu$ for A, B, and D, while departures ranging from -29 to $+17\mu$ are present for method F. This is shown still more strikingly in figure 1, where it is clear that any random or systematic errors do not cause the values for A, B, and D to depart more than $\pm 5\mu$ from the average and such departures as exist are for the most part negligible; it is also clear from figure 1, that the values obtained by method F are affected by large errors somewhat cyclic in nature.

Because of the wide variance shown in the preliminary analysis, it appeared worthwhile to make a careful study of method F to determine the causes of these discrepancies.

2. Study of the Modified Goniometric Method (Method F)

2.1. Theory

In the usual goniometric method a device similar to a large spectrometer is used. The lens in its camera is so mounted that its front nodal point lies in the axis of rotation of the observing telescope. A scale in the focal plane of the camera is observed through the telescope and settings made on successive scale lines having known separations. For each such setting, the circular scale of the spectrometer is read in terms of angle. From the known separation of successive scale lines and the corresponding angular observations, it is possible to determine the focal length of the lens and the values of the distortion at selected points.

The modified goniometric method, as here used, is similar to the method described by Merritt.[3] The relations from which values of the focal length and distortion are obtained are the same for both the usual and modified goniometric methods. If a graduated scale is located in the focal plane of the lens, and the separations of successive scale divisions from the central division assumed to be located on the lens axis are designated as $a_1, a_2, \ldots a_n$, and the angular separations of the corresponding divisions as viewed through the front of the lens be designated as $\beta_1, \beta_2 \ldots \beta_n$, then

$$f_1 = a_1 \cot \beta_1. \tag{1}$$

where f_1 is the equivalent focal length of the lens. Using this value of f and known values of β_1 the distances to the other scale divisions are computed and the distortion, D, is given by the relation

$$D_n = a_n - f_1 \tan \beta_n. \tag{2}$$

2.2. Description of the Apparatus

The arrangement of the apparatus is shown in figures 2 and 3. The lens is mounted in the nodal slide located on one leg of the T-bench. The scale, a calibrated meter bar, is placed in the focal plane of the

[3] E. L. Merritt, Methods of field camera calibration, Photogrammetric Eng. XVII, 610 (1951).

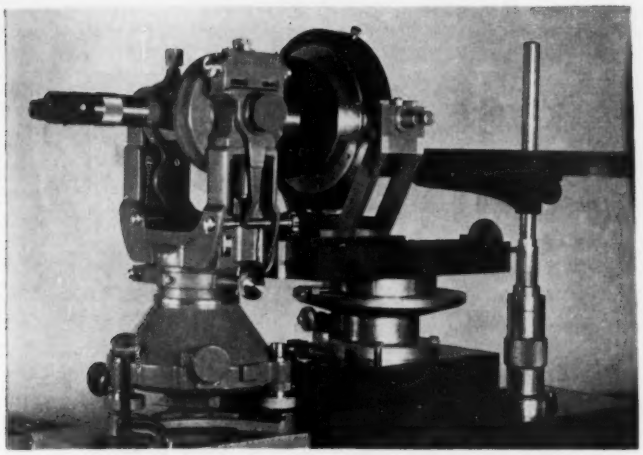

FIGURE 2. *Arrangement of apparatus for method F, the modified goniometric method.*

The scale at the right is located in the focal plane of the lens mounted on the nodal slide in the center of the picture. The theodolite on the left faces the front of the lens under test. For the position shown, settings can be made over the range $\beta = +11$ to -11 degrees.

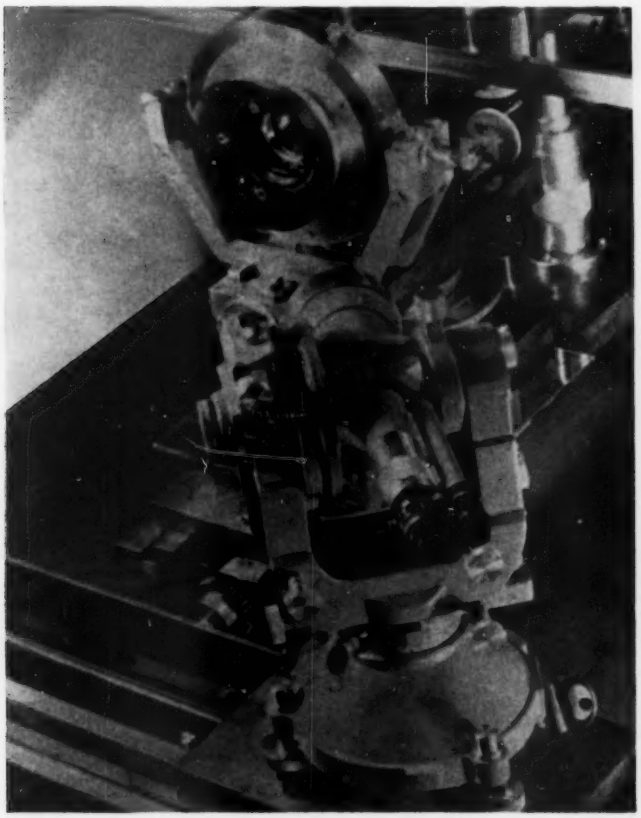

FIGURE 3. *Same as figure 1 except theodolite has been displaced along the bench for making measurements in an extra axial region.*

lens and placed as nearly normal as possible to the lens axis which is initially made parallel to the bench ways. The Wild theodolite is mounted on a saddle located on the cross arm of the T-bench. It is so placed that its objective is as near as feasible to the front of the lens under test. For this particular arrangement, settings can be made from +30 to −30 mm on the scale. For wide angles the arrangement shown in figure 3 is used. The appearance of the scale of the meter bar as seen through the observing telescope is shown in figure 4 for three angles of viewing.

2.3. Results of Measurement

It is obvious that an entire diameter of the picture area of the lens cannot be investigated for any one position of the theodolite. In order to cover all points along a single diameter, the theodolite must be traversed along the bench in a series of steps. This gives rise to alternate possibilities. The theodolite may be held in a single position with respect to the bench while a series of observations are made at selected points along the scale and then moved for successive series or it may be moved between each setting. The first process seemed easier in the early part of the work and was used. The results of measurement taken by this process are shown in the following section in table 2.

The center of rotation of the observing telescope is separated by a very appreciable amount from a vertical line passing through the front nodal point

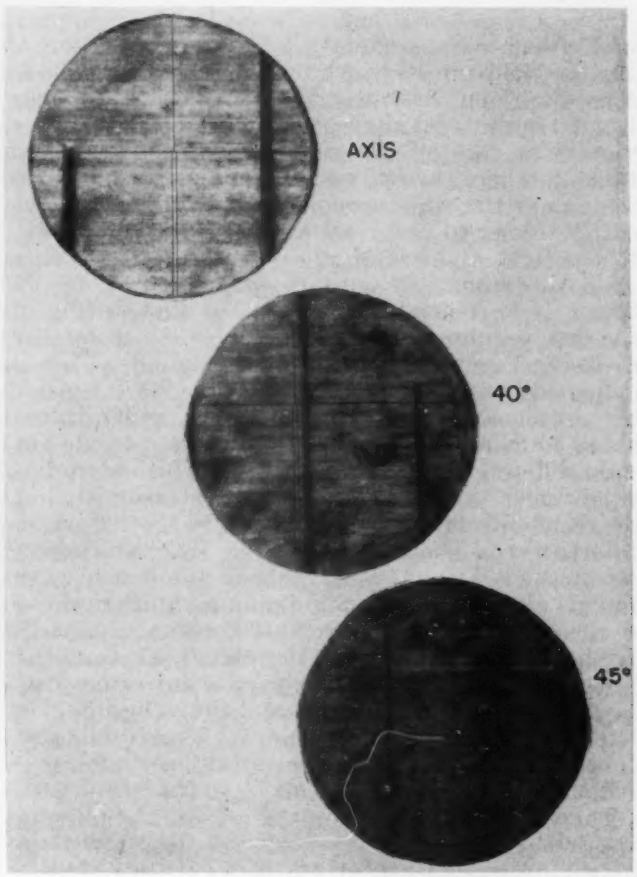

FIGURE 4. *Scale of the meter bar as seen through the viewing telescope.*

TABLE 2. *Measured values in the object space of the angular separation, β, from the axis corresponding to the 10 mm intervals of a standard scale located in the focal plane of wide angle lens No. 3*

Values are shown for corresponding positions along the same diameter to the right and left of axis. The position of the theodolite for each series of settings is indicated by the bench scale readings. The change in the value of β that occurs on shifting of the theodolite position is shown under $\Delta\beta$.

Right				Left			
Bench scale	Meter bar	Angular separation, β, from axis	$\Delta\beta$	Bench scale	Meter bar	Angular separation, β, from axis	$\Delta\beta$
mm	*mm*	*deg*	*deg*	*mm*	*mm*	*deg*	*deg*
569.0	0	0.0000		569.0	0	0.0000	
	10	3.7523			10	3.7535	
	20	7.4585			20	7.4829	
	30	11.1039			30	11.1729	
			0.0019				−0.0280
498.5	30	11.1058		639.0	30	11.1449	
	40	14.6558			40	14.7417	
	50	18.0686			50	18.2166	
	60	21.3551			60	21.5645	
	70	24.4945			70	24.7641	
	80	27.4799			80	27.8161	
	90	30.3061			90	30.7400	
			0.0208				−0.0381
427.3	90	30.3269		708.0	90	30.7019	
	100	32.9835			100	33.4457	
	110	35.4940			110	36.0266	
	120	37.8604			120	38.4541	
	130	40.0879			130	40.7390	
			0.0185				−0.0106
378.4	130	40.1064		754.4	130	40.7284	
	140	42.1921			140	42.8877	
	150	44.1553			150	44.8924	
	160	45.9564			160	46.7749	

of the lens. Consequently for a single location of the theodolite on its bench it is possible to make settings on a comparatively few divisions of the scale located in the focal plane of the lens under test before vignetting cuts off the view. This is indicated in table 2, where the successive readings of the bench scale show that the theodolite occupied seven different positions to cover an angular range of $\beta=46°$ to the right and left of axis. When the theodolite is moved from one position to another along its bench, it is customary to make the first setting of the new position on the same line of the meter bar as the last setting of the former position. This is indicated in table 2 by the double entries for meter bar divisions 30, 90, and 130. The angular values obtained for these double entries do not coincide but show differences of varying amounts which are tabulated under the caption $\Delta\beta$. If it is assumed that the theodolite always is moved parallel to itself, these differences $\Delta\beta$ should equal zero. The alternative explanations are: (1) Curvature of the bench ways and (2) aberrations arising from an asymmetrical use of aperture. If the second cause is regarded as negligible, then subtracting the decrement, $\Delta\beta$, from the observed values of β should eliminate any errors arising from (1). This was done and the values of β so determined are given in table 3. This table also shows the values of equivalent focal length and distortion, D_R, to right of axis and D_L to the left of axis.

The values of distortion in table 3 are not directly comparable in the form shown to those given in table 1. Consequently it was necessary to evaluate D_R and D_L for values of β at 5° intervals. This was done by linear interpolation and the values are

TABLE 3. *Values of the distortion,* D_R *and* D_L*, referred to the equivalent focal length* (f=152.518 mm)*, based on the measurements shown in table 2*

Values of β are adjusted by adding the measured values of $\Delta\beta$ to the measured values of β for each bench setting.

Right				Left			
Meter bar	β	$f\tan\beta$	D_R	Meter bar	β	$f\tan\beta$	D_L
mm	*deg*	*mm*	*mm*	*mm*	*deg*	*mm*	*mm*
0	0.0000	0.000	0.000	0	0.0000	0.000	0.000
10	3.7523	10.003	−.003	10	3.7535	10.006	−.006
20	7.4585	19.967	.003	20	7.4829	20.033	−.033
30	11.1039	29.933	.067	30	11.1729	30.124	−.124
40	14.6539	39.881	.119	40	14.7697	40.210	−.210
50	18.0667	49.752	.248	50	18.2446	50.277	−.277
60	21.3532	59.627	.373	60	21.5925	60.363	−.363
70	24.4926	69.482	.518	70	24.7921	70.447	−.447
80	27.4780	79.321	.679	80	27.8441	80.563	−.563
90	30.3042	89.139	.861	90	30.7680	90.803	−.803
100	32.9608	98.897	1.103	100	33.5118	100.994	−.994
110	35.4713	108.674	1.326	110	36.0927	111.188	−1.188
120	37.8377	118.465	1.535	120	38.5202	121.405	−1.405
130	40.0652	128.273	1.727	130	40.8051	131.673	−1.673
140	42.1509	138.056	1.944	140	42.9644	142.047	−2.047
150	44.1141	147.872	2.128	150	44.9691	152.353	−2.353
160	45.9152	157.469	2.531	160	46.8516	162.707	−2.707

TABLE 4. *Values of the distortion,* D_E *and* D_C *for wide angle lens No. 3 for values of* β *varying in 5° steps*

These values are derived from table 3.

β	D_R	D_L	D_E	$\Delta f\tan\beta$	D'_C	ΔD_T	D_C
deg	*mm*	*mm*	*mm*	*mm*	*mm*	*mm*	
0	0.000	0.000	0.000	0.000	0.000	0.000	0.000
5	.009	−.015	−.003	.004	−.007	−.003	−.004
10	.057	−.095	−.019	.008	−.027	−.005	−.022
15	.132	−.214	−.041	.012	−.053	−.007	−.046
20	.322	−.322	.000	.016	−.016	−.009	−.007
25	.545	−.455	.045	.020	.025	−.010	.035
30	.841	−.740	.050	.025	.025	−.010	.035
35	1.284	−1.106	.089	.030	.059	−.007	.066
40	1.721	−1.579	.071	.036	.035	.003	.032
45	2.326	−2.359	−.016	.043	−.059	.007	−.066

shown in table 4. The asymmetry of the distortion pattern results from a small tilting of the scalebar with respect to the focal plane of the lens. This effect can be readily compensated at the proper stage by computation.[4] The value of the distortion, D_E, referred to the equivalent focal length is given by the relation

$$D_E=\frac{D_R+D_L}{2}. \tag{3}$$

Values of D'_C, the distortion referred to the calibrated focal length are derived from D_E in the usual manner. Finally these values are corrected with the aid of the equation

$$D_C=D'_C-\Delta D_T, \tag{4}$$

where ΔD_T is the correction for the tilt of the scale bar and D_C is the value of the distortion referred to

[4] F. E. Washer, Sources of error in various methods of airplane camer calibration, Photogrammetric Eng., XXII, 727 (1956).

the calibrated focal length which is accepted as the best value obtainable by this method of analysis. Comparison of the values of D_C shown in table 4 with the values of the average $\overline{D_3}$ for methods A, B, and D given in table 1 shows marked disagreement. The disparity between corresponding values is so great that it is apparent that the measurements are being affected by some uncompensated source of error.

It seems probable that the aberrations arising from asymmetrical use of apertures contribute heavily to the observed disparities. With this in mind it seemed worthwhile to neglect errors arising from bench curvature and to attempt to reduce the aberration effects by averaging the value of β in the double-entry regions of table 3 on the hypothesis that the two separate values were obtained for opposite conditions of vignetting and that the average might approximate the value obtained for centered apertures. This was accordingly done and the values of β so determined are listed in table 5. No adjustment was made for those values of β at the nontransition points. The values of distortion are computed and are shown in table 5. D_R and D_L are evaluated at 5° intervals and are tabulated in table 6, together with D_E and D_C. The values of D_C obtained in this manner are nearer to the values shown in table 1 than are the values given in table 4 which indicates that this method of reducing the data is superior to the method used in deriving table 4. The disparities that remain are due in part to some noncompensated bench curvature and in part to observation arising from unsymmetrical use of apertures. On making an adjustment, ΔD, for the error arising from the measured departure of the bench from straightness, the value D_F represents a value free from error arising from bench curvature. This value, D_F, is still somewhat different from the average given in table 1 showing that the aperture error is appreciable.

TABLE 5. *Values of the distortion,* D_R *and* D_L, *referred to the equivalent focal length* (f=152.518 mm) *based on the measurements shown in table 2*

No adjustment if made for the values of β except to average the two values of β at each transition point.

Right				Left			
Meter bar	Angular separation from axis	$f \tan \beta$	D_R	Meter bar	Angular separation from axis	$f \tan \beta$	D_L
mm	*deg*	*mm*	*mm*	*mm*	*deg*	*mm*	*mm*
0	0.0000	0.000	0.000	0	0.0000	0.000	0.000
10	3.7523	10.003	−.003	10	3.7535	10.006	−.006
20	7.4585	19.967	+.033	29	7.4829	20.033	−.033
30	11.1048	29.936	+.064	30	11.1589	30.086	−.086
40	14.6558	39.887	.113	49	14.7417	40.131	−.131
50	18.0686	49.758	.242	50	18.2166	50.194	−.194
60	21.3551	59.633	.367	60	21.5645	60.277	−.277
70	24.4945	69.489	.511	70	24.7641	70.357	−.357
80	27.4799	79.328	.672	80	27.8161	80.468	−.468
90	30.3165	89.183	.817	90	30.7210	90.634	−.634
100	32.9835	98.984	1.016	100	33.4457	100.742	−.742
110	35.4940	108.766	1.234	110	36.0266	110.919	−.919
120	37.8604	118.563	1.437	120	38.4541	121.162	−1.162
130	40.0972	128.419	1.581	130	40.7337	131.342	−1.342
140	42.1921	138.257	1.743	140	42.8878	141.668	−1.668
150	44.1553	148.086	1.914	150	44.8924	151.945	−1.945
160	45.9564	157.697	2.303	160	46.7749	162.272	−2.272

TABLE 6. *Values of the distortion,* D_R *and* D_L *for wide angle lens No. 3 for values of* β *varying in 5° steps*

The values of D_E (distortion referred to the equivalent focal length) and D_C (distortion referred to the calibrated focal length) are also given together with the adjustment of pointing error ΔD_E and the final value of distortion for the method, D_F. These values are derived from table 5.

β	D_R	D_L	D_E	$\Delta f \tan \beta$	D_C	ΔD_E	D_F
deg	*mm*	*mm*	*mm*	*mm*	*mm*	*mm*	*mm*
0	0.000	0.000	0.000	0.000	0.000	0.000	0.000
5	.010	−.015	−.002	−.009	−.011	.003	−.008
10	.055	−.069	−.007	−.019	−.026	.005	−.021
15	.126	−.136	−.005	−.029	−.034	.007	−.027
20	.316	−.238	.039	−.039	.000	.010	.010
25	.538	−.366	.086	−.050	.036	.010	.046
30	.801	−.608	.096	−.062	.034	.010	.044
35	1.191	−.849	.171	−.076	.095	.006	.101
40	1.575	−1.284	.146	−.091	.055	−.002	.053
45	1.988	−1.964	.012	−.108	−.096	−.006	−.102

2.4. Errors Arising From Asymmetric Apertures

In an earlier paper (see footnote 3), an extended discussion of the effect of asymmetrical apertures is given. It is evident from a consideration of the arrangement of apparatus used in the modified goniometer method that the apertures are being used asymmetrically for most settings. To show that this is so, a series of photographs of the effective aperture of the lens under test as seen in the exit pupil of the viewing telescope was made. Some of these photographs are reproduced in figure 5. The dark circles indicate the exit pupil of the telescope; the light circles or ovals show the effective aperture of the lens under test as seen in the exit pupil; and the irregular light areas are caused by random reflections of stray light hitting the interior walls of the telescope tube. The principal interest in these photographs is to note the different relative positions of the lens aperture as seen in the exit pupil. Referring to table 1, it may be noted that for bench scale reading 569 mm, and for meter bar reading of 30 mm, the aperture is at the right side of the pupil and partially obscured while for the second entry of 30 mm at bench scale reading of 639 mm, the aperture is at the left of the pupil and cut even more. The difference in β for these settings is 0.0280°. Similar conditions exist for meter bar readings of 90 and 130. It is obvious that in proceeding from meter bar reading +30 to −30 the lens aperture is centered for only one setting at 0 mm, and an asymmetric condition exists at all other positions in the range from +30 to −30. One would expect that values of the distortion obtained under these conditions would show large random variations from the true value. This is indicated in table 7 which shows a comparison between values of $\overline{D_3}$ from table 1 and method F from table 6.

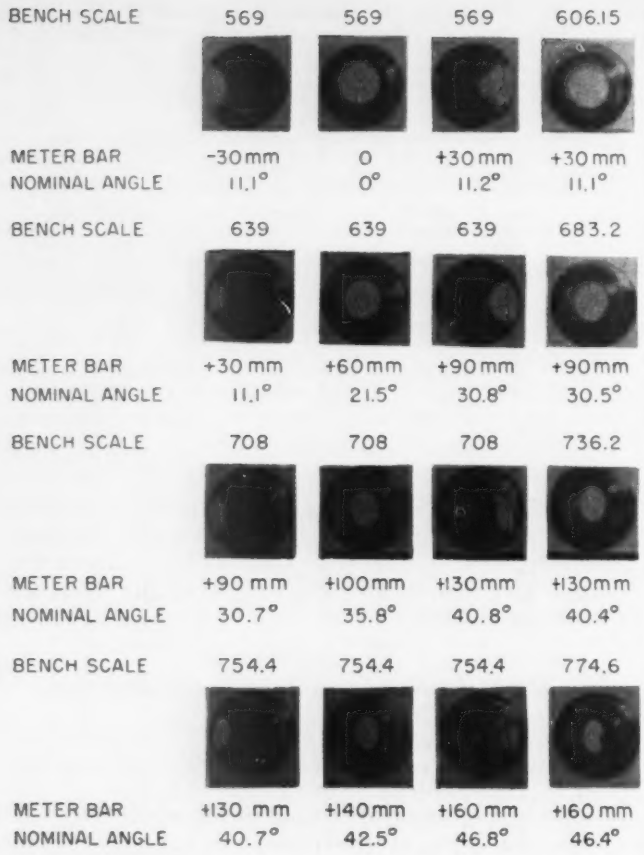

FIGURE 5. *Photographs showing the relative position of the effective aperture of the lens under test in the exit pupil of the measuring telescope for a series of bench and meter bar readings.*

TABLE 7. *Comparison of the values of distortion* D_F *obtained by method F from table 6 with the average values* $\overline{D}_3$ *from table 1*

For these values of D_F, the exit apertures of the lens and entrance aperture of the telescope are centered for values of β near 0°, 23°, 36°, and 44°. All values are in microns.

β	$\overline{D}_3$	D_F	$\Delta D=\overline{D}_3-D_F$
deg			
0	0	0	0
5	−6	−8	2
10	−6	−21	15
15	3	−27	30
20	23	10	13
25	53	46	7
30	86	44	42
35	109	101	8
40	78	53	25
45	−109	−102	−7

2.5. Method of Eliminating Effect of Unsymmetrical Apertures

The improvement in reliability of results shown in table 6 over those shown in table 4 appeared to warrant additional measurements using a method calculated to minimize any effects arising from unsymmetrical use of apertures. Accordingly new measurements were made which are given in table 8. In these measurements, it is assumed that the movement along the crossbench does not alter the reliability of the angle measurements, so the theodolite was displaced for each setting in such a manner that the exit aperture of the lens under test appeared centered in the exit pupil of the telescope. The appearance of the exit pupil is shown in the right hand column for a few cases in figure 5. Each setting was repeated 5 times so as to determine the probable error of the mean for each value of β. The probable error of the mean for the values of β was found to be approximately ± 2 seconds which corresponds to a maximum error in the distortion values of ± 0.003 mm.

The values of the distortion, D_R and D_L, were determined from the measured values of β corresponding to the scale divisions of the meter bar and are given in table 8. These values were used to determine the values of D_E (distortion referred to the equivalent focal length) at 5° intervals which are given in table 9. This table also shows the values of D_C (distortion referred to the calibrated focal length). While the error arising from bench curvature was assumed to be negligible, it is known that this is not quite true. However, the magnitude of this error has been measured for each position occupied by the theodolite and an appropriate correction is made under the caption ΔD_E (compensation for pointing error). Finally the value of D_F is shown in the last column.

Comparison of the values of D'_F from table 9 with that of $\overline{D}_3$ from table 1 is shown in table 10 together with the difference $\overline{D}_3-D'_F$. Consideration of the values of $\overline{D}_3-D'_F$ leads to the belief that systematic error of some sort is still present. A possible source is curvature of the meter bar.

TABLE 8. *Measured values in the object space of the angular separation,* β*, from the axis corresponding to 10 mm intervals of a standard scale located in the focal plane of wide angle lens No. 3*

Conditions the same as for table 2, except apertures are centered for each setting. Each value of β is the average of 5 settings; the average probable error of the mean is $\pm 0.0056°$ or 2.0 seconds which corresponds to a maximum distortion error of ± 0.003 mm. The values of the distortion are also shown.

Right				Left			
Bench scale	Meter bar	β	D_R	Bench scale	Meter bar	β	D_L
mm	*mm*	*deg*	*mm*	*mm*	*mm*	*deg*	*mm*
569.8	0	0.0000	0.000	569.8	0	0.0000	0.000
556.6	10	3.7523	−.002	581.2	10	3.7498	.004
544.4	20	7.4715	−.001	594.3	20	7.4706	.001
531.8	30	11.1260	.007	606.2	30	11.1265	.005
519.1	40	14.6887	.022	619.9	40	14.6912	.015
505.6	50	18.1375	.041	633.2	50	18.1414	.030
495.2	60	21.4549	.053	645.6	60	21.4586	.052
480.8	70	24.6261	.091	658.2	70	24.6313	.074
469.1	80	27.6430	.123	669.9	80	27.6492	.102
456.8	90	30.5027	.154	683.2	90	30.5093	.131
443.3	100	33.2041	.184	697.0	100	33.2108	.159
431.4	110	35.7521	.199	709.4	110	35.7582	.175
418.5	120	38.1506	.198	724.0	120	38.1544	.182
406.5	130	40.4028	.190	736.2	130	40.4095	.159
393.4	140	42.5212	.146	751.5	140	42.5304	.100
380.0	150	44.5066	.093	763.4	150	44.5245	.000
367.7	160	46.3712	.009	774.6	160	46.3968	−.134

TABLE 9. *Values of the distortion* D_R, D_L, *and* D_E *derived from table 8*

The values of D_C, the distortion referred to the calibrated focal length and the values of D'_F derived from D_C after compensation for pointing error ΔD_E are also shown. All values are in microns.

β	D_R	D_L	$\frac{D_R+D_L}{2}$	$\Delta f \tan B$	D_C	ΔD_E	D'_F
deg							
0	0	0	0	0	0	0	0
5	−2	3	0	10	−10	3	−7
10	5	4	4	21	−17	5	−12
15	24	16	20	32	−12	7	−5
20	53	42	48	43	5	10	15
25	95	77	86	55	31	10	41
30	149	126	138	68	70	10	80
35	195	170	182	83	99	6	105
40	191	163	177	99	78	−2	76
45	71	−34	18	118	−100	−6	−106

TABLE 10.—*Comparison of the values of* D'_F *from table 9 with* $\overline{D}_3$ *from table 1*

The magnitude of the correction D_C required to compensate assumed curvature of target scale (sagitta=22 μ) and final accepted value D_F for method F are also shown. All values are in microns.

β	$\overline{D}_3$	D'_F	$\overline{D}_3 - D'_F$	ΔD_C	$D_F = D'_F + D_C$
deg					
0	0	0	0	0	0
5	−6	−7	1	2	−5
10	−6	−12	6	3	−9
15	3	−5	8	4	−1
20	23	15	8	5	20
25	53	41	12	6	47
30	86	80	6	6	86
35	109	105	4	5	110
40	78	76	2	2	78
45	−109	−106	−3	−5	−111

A computation was made, to determine the probable magnitude of the assumed curvature (see footnote 4). A value of 22μ for the sagitta of the curve seemed satisfactory and reasonable and is used to determine the values of ΔD_C. The value of D_F shows the effect of making this correction and is accepted as the best set of values of distortion obtained by method F.

2.6. Review of Results Obtained by Four Different Methods

In the course of this investigation, extended series of measurement of the values of radial distortion have been made on a single lens using four distinctly different methods designated A, B, D, and F. Table 11 shows, in section (a), the final value accepted for each method together with the average for the four. Part (b) of table 11 shows the departure from the average for each of the four methods together with the probable error of a single determination for a given method with respect to the average for all methods. The departure from the average for each of the four methods is also shown in figure 6. In the course of the investigation, it has been shown that the PE_s for values obtained by any one of the methods is approximately ± 3 μ. It is shown in table 11, that the departure of the

TABLE 11. *Measured values of the distortion in microns referred to the calibrated focal length for wide angle lens No. 3 for four different methods*

The values for A, B, D, and F in part A are the final accepted values obtained by each of the four methods. Departures from the average $\overline{D}$ for the four are shown in part (b) together with the value of PE_s, the probable error for values obtained by a single method.

Angular separation from axis β	(a) Values of distortion obtained by method				Average $\overline{D}$
	A	B	D	F	
0	0	0	0	0	0
5	−5	−7	−5	−5	−6
10	−5	−8	−6	−9	−7
15	4	1	4	−1	2
20	21	21	26	20	22
25	49	52	58	47	52
30	82	87	90	86	86
35	113	106	108	110	109
40	79	79	77	78	78
45	−113	−106	−108	−111	−109
	(b) Departures from the average for method				
	A	B	D	F	PE_s
0	0	0	0	0	±0
5	1	−1	1	1	1
10	2	−1	1	−2	1
15	2	−1	2	−3	2
20	−1	−1	4	−2	2
25	−3	0	6	−5	3
30	−4	1	4	0	2
35	4	−3	−1	1	2
40	1	1	−1	0	1
45	−4	3	1	−2	2

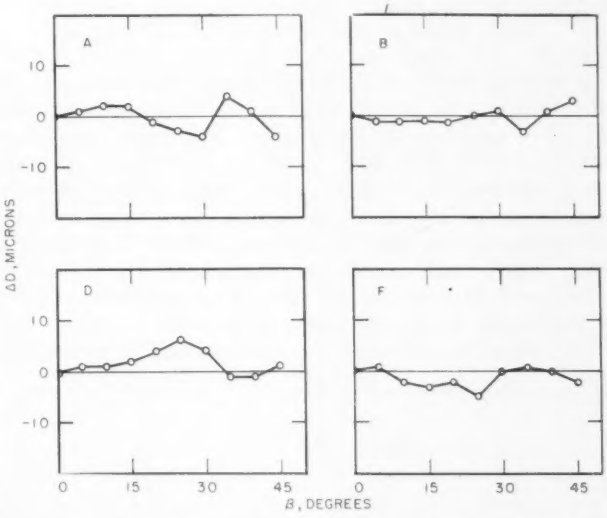

FIGURE 6. *Variation of the departures,* ΔD, *from the average value of distortion with angular separation* β *from the axis.*

The values of ΔD are computed with respect to the average value of D for the four methods A, B, D, and F using the final accepted values for method F.

values obtained by a single method from the grand average for four methods does not usually exceed ± 3 μ.

It can therefore be concluded that the results obtained by any one of these methods are likely to be as good as those obtained by any other of the remaining three methods, and moreover the errors in the values of distortion are unlikely to depart

by an amount in excess of $\pm 5\ \mu$ from the true value. This statement is made on the assumption that proper care is taken in measurements for any of the methods and that all conditions are equivalent.

3. Conclusions

While the equivalence of the four methods studied can be regarded as established as a result of these investigations, there are other factors that are worthy of mention in connection with them. It can be safely stated that method B is the easiest of the methods to use and requires the simplest apparatus, namely nodal slide, visual optical bench, and collimator. It is also relatively easy to understand. Method D is quite easy and simple but more difficult to comprehend because of the inverse manner of the use of the nodal slide. In addition, unusual care is required to insure proper centering of apertures unless a large diameter viewing telescope is used. Method F while reliable is the most difficult of all. There appear to be more sources of error likely to creep in than for method B and D, and in addition, it requires more extensive use of trigonometric tables and interpolation than any of the other three methods. Method A is possibly the easiest to understand. It does however, require complex equipment. It is slower than method B when there is only one lens to measure. However, as the number of lenses to be tested increases, it becomes more efficient as no time need be lost waiting for negatives to dry before measurement and it is possible to complete measurements on 10 lenses quicker by method A than by method B. Method A has, of course, the major advantage that it approximates more nearly conditions of use than any of the other methods.

WASHINGTON, D.C. (Paper 63C2–14)

Journal of Research of the National Bureau of Standards—C. Engineering and Instrumentation

Vol. 63C, No. 2, October–December 1959

Proposed Criteria for Defining Load Failure of Beams, Floors, and Roof Constructions During Fire Tests

J. V. Ryan and A. F. Robertson

(July 30, 1959)

A brief account is presented of procedures used in development of criteria for defining the point at which fire test specimens fail to sustain load during test. It is proposed that both a deflection of $L^2/800d$ and an hourly rate of deflection of $L^2/150d$ be taken as an indication of load failure. In these formulas, L is the span between supports of the member or element found to be critical under fire exposure, and d is the distance between upper and lower extreme fibers of the particular structural component or assembly.

1. Introduction

Recently an investigation was performed on the effect of variations in ceiling fabrication on the fire endurances of a number of floor constructions [1].[1] During initial tests of this study it became apparent that in many cases structural failure might be expected to occur before failure based on a defined temperature rise at the unexposed surface. Since the test procedure used [2] is not specific in defining methods for determining the point at which the specimen fails to "sustain the applied load," it appeared desirable to adopt laboratory procedures which would provide an objective method of determination of this end point. The first attempt at selection of a criterion of load failure, that of a critical deflection[2] of 3 in. [1], was selected for the particular type of floor construction used. It was chosen because it seemed to represent a significant indication of deflection and, in addition, the data then available, figure 1, example I, showed that the corresponding rate of deflection was so great that collapse of the construction might be expected to occur rather promptly.

It appears that a critical deflection method of specifying the time at which failure to carry the load occurs is not generally applicable to a wide variety of construction types. This brief paper outlines some considerations made in developing more general criteria of load failure for beam, floor, and roof constructions during fire endurance tests.

2. Load Failure Criteria

2.1. Deflection

The selection of a critical deflection for defining load failure, while possibly useful in specific cases, is not applicable to the general case because of differences in specimen construction, span, manner of support, and materials of construction used. It would be preferable to specify a deflection in terms of the construction design. This was considered, but it alone was found deficient in properly allowing for variations in longitudinal restraint at the ends of the load-carrying members of the construction.

2.2. Increase in Rate of Deflection

Tests performed in which heavy steel beams were incorporated as load carrying members showed the shortcomings of deflection alone as a criterion of load failure. In tests such as this it was not uncommon to find very large deflections develop without any indication of rapidly increasing rate of deflection with resultant impending collapse. Therefore, an analysis of some fire endurance data was made to determine the feasibility of using an increase in rate of deflection as an indication of load failure. Figure 1, example II, illustrates the method used. The initial nearly constant rate of deflection R_1 was determined and then the time of load failure was assumed to occur at a time when this initial rate had been exceeded by a fixed percentage. In the case illustrated $R_2=1.5R_1$. The difficulty with this procedure was largely that of determining the point on the curve at which R_1 was to be measured. Therefore it seemed desirable that the limiting rate of deflection be defined on some other basis, preferably dependent only on the structural features of the design. Also, it seemed apparent that rate of deflection alone was not an adequate criterion.

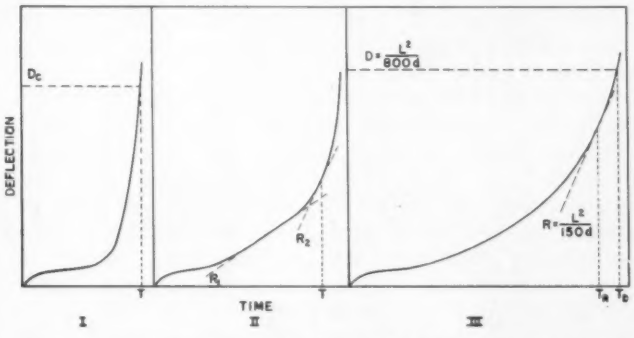

FIGURE 1. *Typical curves of observed deflection data illustrating determination of failure time.*

I, prechosen critical deflection D_c;
II, increase in rate of deflection by predetermined ratio, $R_2=KR_1$;
III, combination of rate and deflection, both determined by size and span of structural element (failure time T_r or T_d, whichever is later).

[1] Figures in brackets indicate the literature references at the end of this paper.

[2] Deflections for determination of load failure are those resulting from fire exposure under design load, in excess of initial deformation due to application of the load.

TABLE 1. *Effect of new criteria on previously determined failure times*

This table compares the times of failures, as determined by the testing personnel on the basis of the criteria listed in the second column, in tests of several types of floor constructions with the times derived by examination of the test data in accord with the proposed load failure criteria. The criteria define load failure time as the earliest time when a deflection $D = L^2/800d$ and hourly rate of deflection $R = L^2/150d$ have both been attained or surpassed. In these formulas, L=clear span, d=depth to most remote stressed fiber. Most of the data are from tests performed before these formulas were considered.

NOTE: Times in parentheses ( ), indicate no data after the given time, although given deflection or rate not attained, net changes in ( ) correspond to these times.

Construction	Failure criterion	Dimensions		Deflection at failure		Criteria		Time criteria reached		Time to failure		Net change of fire endurance	Time to temperature limit rises on unexposed surface	
		L	d	Deflection	Rate	$L^2/800d$	$L^2/150d$	$L^2/800d$	$L^2/150d$	Reported	New criteria		250° F av	325° F max
Floors, wood joist														
		ft:in.	*in.*	*in.*	*in./hr*	*in.*	*in./hr*	*hr:min*	*hr:min*	*hr:min*	*hr:min*	*min*	*hr:min*	*hr:min*
ML, GP	Load failure	12:10	9.75	14	310	3.04	16.2	0:47	0:47	0:51	0:47	−4	(0:50)	(0:50)
Do	do	12:10	9.75	8.3	123	3.04	16.2	1:08	1:06	1:12	1:08	−4	(1:10)	(1:10)
ML, PP	do	12:10	9.75	5.7	25.+	3.04	16.2	0:57	1:00	1:06	1:00	−6	(1:05)	(1:05)
ML, LP	Collapse	12:10	9.75	16.+	1,150.+	3.04	16.2	0:26	0:19	0:29½	0:26	−3½	(0:30)	(0:30)
GB	Surf. temp	12:10	9.75	9.1	468	3.04	16.2	0:40	0:37	0:38	0:40	0	(0:45)	0:38
GL, GP	Load failure	12:10	9.75	3	9.+	3.04	16.2	1:43	1:42	1:44	1:43	−1	(1:40)	(1:40)
ML, GP	do	12:10	9.75	3.3	6.0	3.04	16.2	1:57	(2:00)	2:05	(2:00)	(?)	(2:00)	(2:00)
Steel joists														
SJ103, GS, GL, GP	Rapid defl	12:10	10	2.5	33	3.0	16.0	1:50	1:46	1:48	1:50	+2	(1:50)	(1:50)
Do	do	12:10	10	1.2	30	3.0	16.0	1:44	1:39	1:40	1:44	+4	(1:45)	(1:45)
Do	3-in. defl	12:10	10	3.0	16.0	3.0	16.0	2:06	2:06	2:06	2:06	0	(2:30)	[b]2:26
SJ103, GPl, GL, GP	do	12:10	10	3.0	47	3.0	16.0	1:07	1:03	1:07	1:07	0	(1:10)	(1:10)
SJ103, CS, GL, GP	Surf. temp	12:10	10	3.0	12	3.0	16.0	6:40	6:42	4:25	6:42	0	4:25	4:46
Do	do	12:10	10	3.0	4.8	3.0	16.0	4:12	4:21	3:14	4:21	0	3:14	3:19
Do	3-in. defl	12:10	10	3.0	33	3.0	16.0	1:06	1:01	1:06	1:06	0	(1:10)	(1:10)
Do	Surf. temp	12:10	10	3.0	20	3.0	16.0	2:54	2:50	2:44	2:54	0	(3:00)	2:44
Do	3-in. defl	12:10	10	3.0	10.8	3.0	16.0	1:51	1:54	1:51	1:54	+3	2:01	1:59
SJ81, CS, GL, GP	Rapid defl	8:0	8	1.4	3.0	1.44	7.7	2:17	(2:17)	2:15	(2:17)	(+2)	2:48	2:40
SJ102, BR, ML, GP	3-in. defl	12:10	10	3.0	10.1	3.0	16.0	1:24	1:26	1:24	1:26	+2	(2:45)	2:38
Precast concrete joists														
CS, Joists embedded	Hole through	12:10	9.25	3.6	12	3.2	17.1	0:33	0:40	0:35	0:40	0	(0:35)	0:36
CS, Joists embedded, GB	Excess defl	12:10	9.25	4.9	18	3.2	17.1	0:53	0:52	0:57	0:53	−4	1:10	1:13
CS, Joists embedded	Surf. temp	12:10	9.0	5.9	15.6	3.3	17.6	0:39	0:38	0:48	0:39	−9	0:48	0:51
Slabs														
Tile & concrete	Collapse	18:0	7.0	Collapse		8.34	44.4	1:10	1:10	1:10	1:10	0	(1:05)	(1:05)
Tile & concrete, GP	Waste ign	12:10	4.375	3.2	2.2	6.78	36.1	3:23	(4:07)	2:27	(4:07)	0	3:08	2:58
CC	Rapid defl	12:10	5.25	5.1	14	5.65	30.1	0:47	0:51	0:45	0:51	+6	(1:00)	(1:00)
Steel decks														
Cell, c. w, CF	Surf. temp	9:6	5.1	2.4	1.2	3.2	16.9	(6:45)	(6:45)	4:45	(6:45)	0	4:45	4:53
Do	do	7:0	5.6	0.8	0.1	1.6	8.4	(6:47)	(6:47)	3:20	(6:47)	0	3:20	3:34
Do	Rapid defl	8:0	5.6	1.7	1.1	2.06	11.0	3:18	(3:25)	3:00	(3:25)	(+25)	(3:30)	3:30
Do	Surf. temp	8:0	5.6	0.8	0.1	2.06	11.0	(7:00)	(7:00)	5:03	(7:00)	0	5:03	5:06
Form, c, BR, GP	do	4:8	1.5	1.5	3.9	2.7	14.3	(2:10)	(2:10)	1:52	(2:10)	0	1:52	1:57
Do	Flame through	4:8	1.5	3.9	15.+	2.7	14.3	1:35	1:26	1:40	1:35	−5	(1:40)	(1:40)
Do	Surf. temp	4:8	1.5	1.6	5.2	2.7	14.3	2:04	1:49	1:56	2:04	0	(2:00)	1:56
Do	do	4:8	1.5	0.7	2.9	2.7	14.3	1:58	1:58	1:50	1:58	0	2:14	1:50
Do	do	4:8	1.5	0	0	2.7	14.3	(3:12)	(3:12)	2:36	(3:12)	0	2:36	2:57

Prestressed concrete beams

														Time to steel temperature	
														750° F av	
T-beam	Rapid defl	10:0	9.0	3.3	9.0	2.0	10.7	1:17	1:21	1:39	1:21	−8	(1:27)		
Do	Collapse	16:0	14.7	8.0	305	3.12	16.8	3:40	3:40	3:40	3:40	0	3:26		
Do	Steel exposed	16:0	14.7	5.+	90	3.12	16.8	2:35	2:35	2:36	2:35	−1	2:31		
Do	None	16:0	14.7	5.0	4.6	3.12	16.8	5:37	(6:00)	6:00	(6:00)	(+?)	(6:00)		
Rect. Sect	Collapse	16:0	9.9	a 2.6	a 34.8	4.66	24.8	1:56	1:54	1:56	1:56	0	2:00		
Do	do	16:0	9.9	a 4.9	a 36.0	4.66	24.8	4:39	4:37	4:40	4:39	−1	(4:40)		
Steel beam—part of floor specimen															
12I31.8, b	Imminent	13:5	12.0	0.8	0.64	2.70	14.4	(6:45)	(6:45)	6:53	(6:45)	(?)	6:29	6:23	6:36
8WF17, w	do	12:11½	8.0	2.1	1.04	3.77	20.2	(6:45)	(6:45)	6:53	(6:45)	(?)	6:23	6:08	5:52
10WF21.5	do	17:4	9.9	4.7	4.2	5.5	29.1	(6:45)	(6:45)	6:47	(6:45)	(?)	6:08	6:54	(6:45)
6I12.5, f	Excess defl	12:10	6.0	6.2	13.1	4.9	26.3	1:57	1:49	2:+	1:57	−3	1:54	(2:15)	(2:15)
Do	Exceeded jack extension.	12:10	6.0	10.0	127.5	4.9	26.3	1:28	1:25	1:33	1:28	−5	1:24	1:41	1:41
Do	Structural fail	12:10	6.0	8.6	30.0	4.9	26.3	1:49	1:42	2:01½	1:49	−12	1:58	(2:00)	(2:00)
Do	Load fail	12:10	6.0	3.75	12.7	4.9	26.3	(1:58)	(1:58)	1:58	(1:58)	(+?)	2:04	2:31	2:31
Do	Imminent fail	12:10	6.0	1.2	5.0	4.9	26.3	(3:12)	(3:12)	3:12	(3:12)	(+?)	3:11	(4:00)	(4:00)
12WF27, bp	Defl. curve shape	17:8	11.95	2.9	1.9	4.7	25.1	3:26	(3:30)	3:00	(3:30)	(+30)	2:18	1:58	1:58
Do	do	17:8	11.95	3.2	1.0	4.7	25.1	(7:00)	(7:00)	6:30	(7:00)	(+30)	5:26	6:28	6:28
Do	do	17:8	11.95	2.8	6.2	4.7	25.1	(2:15)	(2:15)	2:15	(2:15)	(+?)	2:04	1:59	1:59

[a] Within 1 min before collapse. [b] Cotton waste ignited.

Key to construction abbreviations:

b = bolted to furnace frame
bp = bolted to plates, standard connectors
BR = built-up roof
c = continuous over more than one span
CC = cellular concrete
Cell = cellular-steel deck units
CF = concrete fill
CS = concrete slab
f = freely supported
Form = formed-steel deck units
GB = gypsum boards
GL = gypsum lath
GP = gypsum plank
GP = gypsum plaster
GS = gypsum slab
LP = lime plaster
ML = metal lath
PP = portland cement plaster
rect. sect. = rectangular section beam
w = welded

2.3. Deflection and Rate of Deflection Method

Previous experience had shown that to be useful a criterion of load failure must be applicable to a variety of construction variables including various types of end restraint, loading, and construction dimensions and materials. The large number and complexity of these variables, not to mention the effects of thermal strains, seem to require a special analysis of each structure. This seemed impractical for the purposes intended and as a result a compromise method was developed. This involves the requirement that both a deflection and rate of deflection be exceeded as an indication of load failure. The requirement of both criteria is believed to provide a practical substitute for detailed analysis of each structure tested.

The deflection of a beam or a floor construction in a fire test is the result of several factors, including the deflection due to the flexural stresses produced by the loads, that resulting from changes in temperature, and that resulting from movements of moisture in the materials. Deflections due to shearing deformations usually are small in comparison to those caused by flexure; for our present purpose they will be neglected. The usual assumption will be made that all transverse planes remain plane after bending. Then following the reasoning of Maney [3], it can be shown that the maximum deflection of a beam or floor of constant flexural rigidity throughout its length is given by:

$$y_{max} = k(L^2/d)\ (e_1 - e_2), \qquad (1)$$

in which

k = numerical constant; the value of which depends upon the type of support and the methods of loading.

L = length of specimen between supports.

d = depth of specimen (strictly the distance, normal to the neutral plane, between the planes of e_1 and e_2).

$e_1 - e_2$ = algebraic difference between the strains in or near the two surfaces of the specimens, measured in the direction of the span, in planes separated by the distance d.

The equation applies for strains in the elastic range. On examination, it appears that the ratio L^2/d might be useful in expressing limitations on deflection even when plastic deformation occurs. The usefulness of L^2/d for such limitations is demonstrated by study of the data from a number of fire tests. All these tests, which did not include those from reference [1], had been performed, and the time of failure to "sustain the applied load" established, prior to our consideration of the use of the term L^2/d in the criteria for failure. In addition, the tests were selected as representative of constructions which were considered to have failed to sustain the load during the test. Various constants were considered prior to selection of both:

$$\text{a deflection of } D \geq L^2/800d$$

and

$$\text{an hourly deflection rate } R \geq L^2/150d$$

as representing the best fit between the empirically specified load failure time and that predicted in the form of the proposed criteria.

To investigate the effect of applying such criteria for identification of time of load failure of structures during a fire test, data of 50 experiments were analyzed. The results are presented in table 1. Two columns of data are presented under the main caption "Time to failure." The first of these entitled "Reported" lists the reported failure time for the construction. In some cases this was limited by load failure, in others by temperature rise or ignition of waste. The second subcaption entitled "New criteria" indicates the time at which load failure would be indicated by application of the criteria proposed. In cases where the defined limiting conditions of ignition of cotton waste or temperature rise due to heat transfer occurred at earlier times than determined by these criteria, such earlier limiting conditions would determine the fire endurance of the specimens. The column entitled "Net change of fire endurance" indicates the change which would occur on application of the proposed criteria. The entries here recognize the fact that in some cases termperature rise, etc., may limit endurance. In other respects, the table is believed to be self-explanatory.

Study of the table indicates that application of the criteria to the specimens listed would have the effects of increasing the endurance in 13 instances, reducing it in 14, and in 23 instances there would either be no change or it would be uncertain. It thus becomes evident that use of the criteria is quite successful in selection of load failure times which are reasonably consistent with behavior as analyzed by the operator in charge of the test. The requirement that both a given deflection and rate of deflection be achieved is believed to present a useful method of defining the point of load failure of beams, floors, and roof constructions tested on end supports but regardless of the type of restraint applied at these ends.

3. Conclusion

The investigation performed seems to justify use of the following criteria for defining the time at which a specimen should be considered as having failed to sustain the load during a fire test.

A beam, floor, or roof construction mounted on end supports and subjected to a fire endurance test under design load will be considered to fail to "sustain the applied load" at that time when both the maximum net deflection resulting from fire exposure has equaled or exceeded $L^2/800d$, and the hourly rate of deflection has equaled or exceeded $L^2/150d$.

In these formulas:

L is the span between supports of the structural component or assembly found critical under fire exposure;

d is the distance between the upper and lower extreme fibers of the structural component or assembly.

D, L, and d are all in the same units of length; R a rate of the same length unit per hour.

Mr. D. E. Parsons suggested the advantages to be gained by use of criteria of the type proposed.

4. References

[1] J. V. Ryan and E. W. Bender, Fire endurance of open-web steel-joist floors with concrete slabs and gypsum ceilings, NBS Building Materials and Structures Report 141 (1954).

[2] Standard methods of fire tests of building construction and materials, ASTM Designation E119, ASTM Standards.

[3] G. A. Maney, Relation between deformation and deflection in reinforced concrete beams, Am. Soc. Testing Materials Proc. 14, II, 310 (1914).

WASHINGTON, D.C. (Paper 63C2–15)

Journal of Research of the National Bureau of Standards—C. Engineering and Instrumentation

Vol. 63C, No. 2, October–December 1959

Conductive Flooring for Hospital Operating Rooms

Thomas H. Boone, Francis L. Hermach, Edgar H. MacArthur, and Rita C. McAuliff

(July 9, 1959)

Characteristics and performance of available types of conductive flooring materials were investigated in the laboratory. The study showed that the electrodes and instruments used to measure the floor greatly affected the measured resistance, but that the method specified by the National Fire Protection Association for measuring the electrical resistance reasonably simulated the conditions under which a floor functions in reducing electrostatic hazards. The physical, chemical, and serviceability characteristics of conductive floorings investigated showed results comparable with those of nonconductive flooring of the same type. Consequently, with some limitations, an architect may base his choice of a conductive flooring material on his knowledge of the behavior of similar nonconductive materials.

1. Introduction

Sparks which can result from the accumulation of static electricity constitute a very real hazard in locations where explosive vapors are present [1].[1]

The most effective of the several possible means of mitigating this hazard consists in keeping the electrical resistance between all objects in the hazardous locations so low that dangerous voltages are never attained [2]. General quantitative considerations indicate that a resistance of 30 to 50 million ohms between objects is low enough for this purpose, for any rate of separation of charges which can reasonably be expected to be attained by accidental electrostatic processes [1,3]. Most objects normally rest or move upon the floor and therefore can be electrically connected by way of the floor. Flooring of sufficiently low electrical resistance (conductive flooring) is thus of paramount importance in the elimination of electrostatic hazards. At the same time, however, the electrical resistance must be high enough to minimize the possibility of electric shock from faulty electrical wiring or equipment.

The specification and the measurement of the resistance of conductive flooring are greatly complicated by a number of factors, such as the kinds of electrodes and the characteristics of the instrument used. A method recommended by the National Fire Protection Association (NFPA) has had general, but not universal, acceptance for routine measurements of installed floors [4,5]. In this method the resistance is measured with a 500-v instrument connected to two similar electrodes placed on the floor.[2] With these electrodes, which simulate footwear and conductive rubber objects, the specified lower and upper limits of resistance are 25,000 and 1,000,000 ohms (0.025 to 1 meg).

At present there are quite a few specially compounded proprietary flooring materials which meet these upper and lower limits. However, as is shown in this report, not all of the conductive floors remain within these limits of resistance under all conditions of use.

2. Scope of Investigation

A conductive floor must provide a path of prescribed conductance for a reasonable life and should, in addition, possess the physical properties required of an ordinary nonconductive floor. This investigation was planned: (1) To measure by established methods the electrical resistance of each sample of flooring; (2) to determine the effect of all pertinent factors that might affect its resistance, such as wear, aging, moisture, and maintenance; (3) to evaluate the factors that influence the measurement of electrical resistance of conductive flooring, by determining the effect of variations in test conditions upon the measured resistance; (4) to check these results by direct tests in which the flooring serves to reunite electrostatic charges; (5) to compare the significant physical properties of each sample with those of nonconductive floors of the same type. In addition to the tests conducted in the laboratory on samples of flooring, field tests of five different types of conductive floors were made in the Washington area.

Although this investigation was carried out primarily to evaluate conductive floors for hospital operating rooms, many of the results obtained should apply equally well to floors for eliminating electrostatic hazards in other locations such as munitions plants and munitions storage depots.

The authors realize that an additional important property for floors, particularly in hospitals, is that they be made and kept reasonably germ-free. Tests to determine differences in this respect were beyond the scope of this study.

3. Description of Flooring Samples

The samples for this study were obtained from domestic suppliers of commercially available con-

[1] Figures in brackets indicate the literature references on page 139.

[2] These requirements and recommended methods of testing floors are reproduced in full in appendix A at the end of this report.

ductive flooring. By request, each manufacturer supplied five similar 18-in. by 18-in. floors on plywood panels. The thickness of the floor, bonding technique, and any reinforcement and conductive intercoupling were of the manufacturer's own practice. Thus, each sample received was assumed to be of the type and construction considered by the manufacturer or his trade association as most suitable for conductive flooring.

Preliminary tests of several types of floors with electrodes spaced 1, 2, and 3 ft apart, and an analysis of the effect of sample size and shape (see section 5.3), showed that the resistance is not greatly affected by electrode spacing. Therefore, convenient 18-in. by 18-in. samples, which permitted a 1-ft spacing between electrodes, could be used. The preliminary study showed that the results should be very close to those which would have been obtained had larger samples or even an entire floor been used, with the 3-ft electrode spacing specified in NFPA 56.

The electrical conductivity of each sample, except the oxychlorides and one make of ceramic tile, depends either completely or partially on the presence of acetylene black (carbon). This is a special form of carbon black produced by the thermal decomposition of acetylene gas under carefully controlled conditions. In the case of the ceramic, linoleum, rubber, and vinyl samples, the carbon black is finely dispersed in the material during manufacture, while in the case of latex, concrete terrazzo, and the setting bed cement for ceramic tile, the carbon black is uniformly dispersed in the dry powder mixes, placed in containers, and shipped for on-the-job composition. Oxychloride floors are made by combining an aqueous solution of magnesium chloride with powdered magnesium oxide. Various fibrous and mineral fillers are mixed with the resulting paste which sets to a hard mass. Marble chips may be added to the mix and the surface ground to produce a terrazzo floor.

Brief descriptions of the composition and installation techniques of each of the conductive floors tested follow:

Ceramic, Sample No. 1: This flooring consisted of an attractive "block random, sprinkle pattern." The design had been made with black conductive tiles, $1\frac{9}{16}$ in. square, $\frac{3}{4}$ in. square and $1\frac{9}{16}$ in. by $\frac{3}{4}$ in. oblong. A nonconductive green oblong tile, $1\frac{1}{32}$ in. by $\frac{3}{4}$ in., was also inserted. The $\frac{1}{4}$-in.-thick tiles were laid in a conductive mortar underbed containing 3 percent acetylene black (carbon). The joints were grouted with nonconductive cement mortar and were approximately $\frac{1}{16}$ in. in width.

Ceramic, Sample No. 2: This flooring of brown conductive tile, $1\frac{9}{16}$ in. square by $\frac{1}{4}$ in. thick, had been laid the same as sample No. 1. Samples were also submitted with the tile set in a conductive adhesive using nonconductive cement mortar joints.

Coating, Sample No. 3: This flooring had been made from a mixture of plastics, solvents, and conductive ingredients, the mixture having been applied by spray, brush, or trowel to a thickness of $\frac{1}{16}$ in. It was supplied in black.

Concrete, Sample No. 4: The sample was submitted as representative of conductive concrete terrazzo. Detailed specifications have been published by the National Terrazzo and Mosiac Association for laying carbon black conductive terrazzo floorings for operating suites of hospitals. The sample had been constructed according to these specifications, which included a concrete underbed containing 3 percent carbon black and a terrazzo top surface with 2 percent carbon black. The amount of carbon black was based on the weight of dry cement. The matrix had a dark gray color with stone chips of black and green. These floorings were treated with a recommended penetrating type sealing compound.

Latex, Sample No. 5: This sample was a mixture of a neoprene latex and cement binder with pink, green, and white chips. The material had been troweled $\frac{1}{2}$ in. thick and was intended for use over existing or new structurally sound underfloors. As carbon black was used as the conductive medium, only black was available as a matrix color. As in other terrazzo-design floorings, various color combinations can be achieved by use of different colored chips. Approximately 60 percent of the surface area was covered by nonconductive chips. The manufacturer had applied four coats of his recommended sealer.

Linoleum, Sample No. 6: This flooring was black and was available in 6-ft-wide strips, $\frac{1}{8}$ in. thick. The linoleum had a burlap backing and could be placed over a suitable underfloor by conventional methods of installing linoleum. The manufacturer prescribed brass seam connectors with projecting points for the purpose of electrical intercoupling between sheets. The manufacturer also stated that wax or protective coatings in any form should not be used, and recommended a dry machine brushing to produce a polished appearance.

Oxychloride, Sample No. 7: The conductive terrazzo flooring had been laid $\frac{1}{2}$ in. thick over suitable underfloor. A liquid synthetic resin bonding agent, over which coarse mineral grains were spread, provided the anchoring between the top terrazzo surface and the underfloor. The matrix was green and approximately 50 percent of the surface area was covered with black and white nonconductive chips.

Oxychloride, Sample No. 8: This sample had been installed in the same manner as sample 7 except that the top $\frac{1}{2}$-in. coating was a plain, dark red, trowel finish.

Oxychloride, Sample No. 9: The conductive terrazzo flooring had been laid $\frac{1}{2}$ in. thick over asphalt felt and wire mesh with a suitable underfloor. The matrix was white and approximately 53 percent of the surface area was covered with black and white nonconductive chips. The surface was coated with a sealer.

Oxychloride, Sample No. 10: The conductive terrazzo flooring had been laid $\frac{1}{2}$ in. thick over 2-in.-square wire mesh and a suitable underfloor. The matrices of the samples received were red, green, and gray, all with approximately 30 percent of the surface area covered with black and white nonconductive chips.

Oxychloride, Sample No. 11: The conductive terrazzo flooring had been laid ½ in. thick over suitable underfloor. The matrix of this sample was green with approximately 65 percent of the surface area covered with black, green, and white nonconductive chips.

Oxychloride, Sample No. 12: The plain, trowel-finished, conductive flooring had been applied ½ in. thick over a suitable bonding agent and a suitable underfloor. The sample received was red, but other colors are also available. This so-called cupric oxychloride material differed from the other oxychlorides in that it contained finely divided copper powder (5–10% by weight of dry mix), which was claimed to impart a number of desirable characteristics. The manufacturer stated that the flooring should not be waxed, and recommended the use of a special sealer.

Rubber, Sample No. 13: This flooring consisted of rubber, homogeneously compounded with acetylene carbon black. The material was black, ⅛ in. thick, with a cotton fabric backing. Adhesive was used to fasten the sheets to a suitable underfloor and intercouplings similar to those used with linoleum (sample no. 6) can be used to connect the sheets of rubber electrically.

Vinyl, Sample No. 14: This flooring consisted of 9-in. by 9-in. polyvinyl chloride-based tiles, ⅛ in. thick, with a black conductive field and a white and green marbleized design. Installation was effected with a special underlayment felt which carried its own pressure-sensitive adhesive on both sides, thus serving to bond the felt to the underfloor and the tile to the felt. Copper foil, ½ in. wide, was placed on the felt to provide an electrical intercoupling between tiles.

Vinyl, Sample No. 15: This flooring consisted of 9-in. by 9-in. polyvinyl chloride-based tiles, 3/16 in. thick, with a molded terrazzo design of either a white or gray field with a black "chiplike" effect. Installation was by troweling adhesive onto a suitable underfloor and placing 1-in. copper foil on the adhesive to provide an electrical intercoupling between tiles.

4. Factors Influencing the Electrical Resistance

The changes of electrical resistance of the sample floorings when subjected to a practical range of environmental conditions were determined. Based on previous knowledge of the behavior of some similar types of floorings, the following were selected as the most important factors: aging, moisture, and maintenance procedures.

All of the resistance measurements were made in accordance with section 6–2 of NFPA method No. 56 (see app. A) except for reduced spacing of electrodes. This established test method provided a good basis for comparison of these floors, and, as shown in subsequent sections, proved to be suitable and realistic.

4.1. Age

In order to determine what changes may occur in the electrical resistance of conductive flooring as it ages, resistance measurements were taken over a period of 30 months for all samples except sample 4, which was received much later than the others. During this time the samples were exposed to 50 ±2 percent relative humidity (rh) and a temperature of 22° ±1° C. At intervals four measurements were made at four different positions on each panel with the electrodes 10 in. apart. A template was used to assure that the electrodes were always placed on the same areas of each sample. The graphs (fig. 1) illustrate the electrical resistance of each sample as a function of time. As indicated in figure 1, aging did not significantly affect the resistance of the floors except for some oxychloride samples.

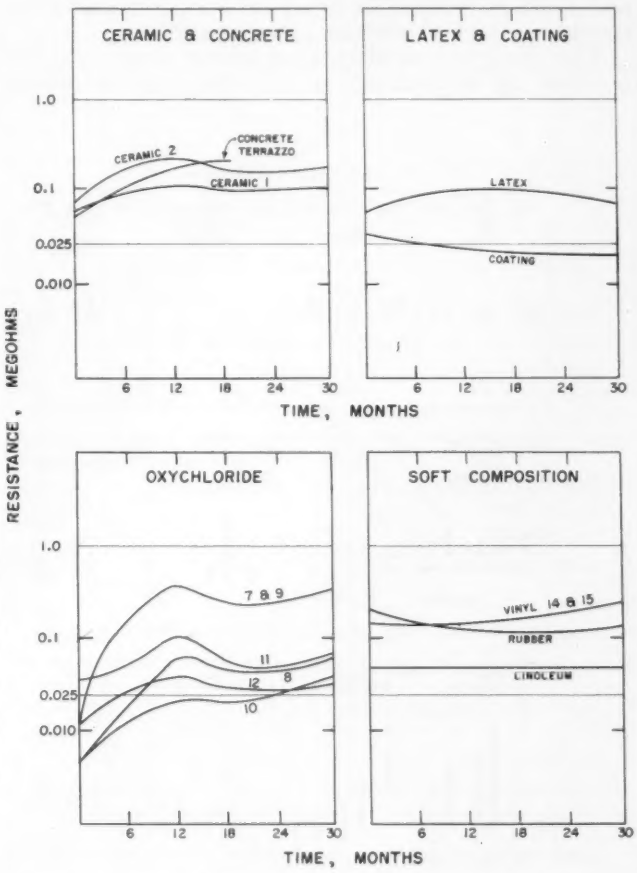

FIGURE 1. *Effect of aging on electrical resistance as measured by the NFPA method.*

Ambient temperature 22°±1°C, relative humidity 50 percent.

4.2. Humidity

Although the relative humidity in some hospital operating suites is controlled automatically by air conditioning equipment and thus can be maintained at any desired level, such equipment is still generally lacking, and most conductive floors are therefore

exposed to wide variations in relative humidity. Tests were conducted to determine the effect of extremes of relative humidity on the electrical resistance of the flooring samples. The samples were exposed to an atmosphere of 10 ±1 percent rh at 38° ±1°C for 3 weeks and to an atmosphere of 80 ±1 percent rh at 27°±1°C for 1 week. In the interval between the two tests they were stored at 22° ±1°C and 50-percent rh for 2 weeks. The electrical resistance was measured at the beginning and end of each of the two tests and for several days after the conclusion of each test. The results of these tests are shown by the solid lines in figure 2. As is evident from these graphs, only the oxychlorides were materially affected. It is evident that the electrical resistance of oxychloride flooring is dependent on its moisture content. As shown by the graphs, exposure of the oxychloride samples to 80-percent rh caused their resistance to fall below the 25,000-ohm minimum and exposure to 10-percent rh caused their resistance to go above the 1-meg maximum.

The effect of humidity on electrical resistance was pointed up secondarily in an investigation whose primary purpose was the study of the effect of alkali or lime content on the electrical resistance of various cement mixes. A few scattered measurements, made a number of years ago, had indicated that concretes made with high-alkali cements apparently had lower electrical resistance than those with low-alkali or high-lime content. Because conduction in concrete is electrolytic, this seemed to warrant further investigation, since ordinary concrete is not far above the present specification limit at moderate humidities. The results (table 1) verified that high alkali concrete does have somewhat lower resistance than the other types, but the difference is not marked and may be due to unknown factors. Table 1 also illustrates the effect of humidity on the electrical resistance of ordinary concrete (without carbon black).

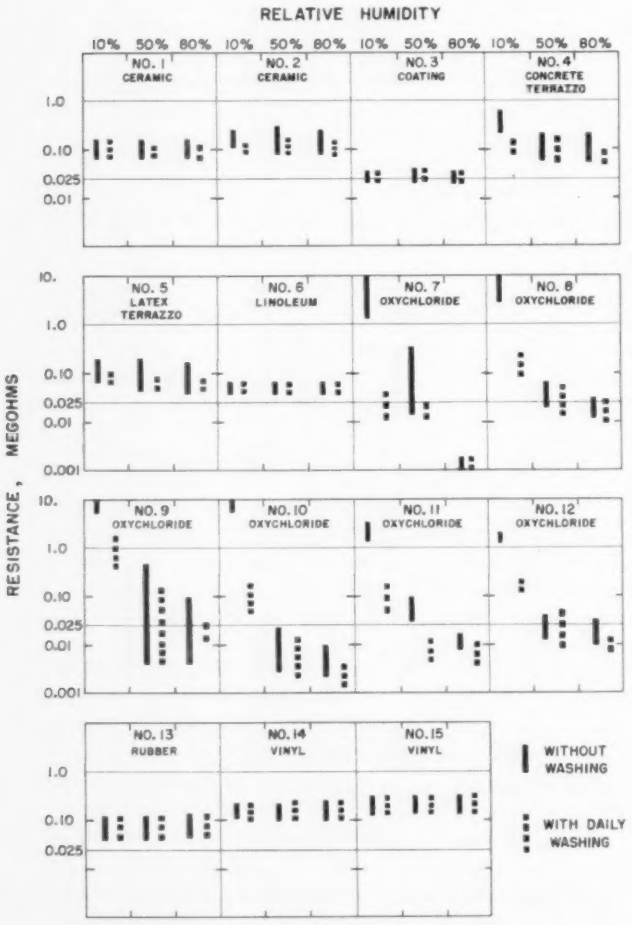

FIGURE 2. *Effect of ambient relative humidity and daily washing on electrical resistance as measured by the NFPA method.*

TABLE 1. *Electrical resistance of concrete specimens*

NBS No.	Alkali	CaO	Resistance	
			At 15% rh	At 50% rh
	%	%	*meg*	*meg*
1 HA	0.89		70	8
2 HA	.91		50	11
3 HA	.91		70	9
1 LA	.13		400	60
2 LA	.08		150	30
3 LA	.30		400	50
1 HC		65.0	440	80
2 HC		63.5	80	20
3 HC		63.3	90	15

NOTE: HA=High alkali cement; LA=Low alkali cement; HC=High lime cement. The samples were 1- by 1- by 11-in. concrete bars made with three different types of cement, each from a different supplier. All were of 1:1:2 mix (cement, fine, and coarse aggregate, respectively) with a cement-water ratio of about 36%. The samples were damp-cured and were then placed in a controlled humidity cabinet, first at 15% rh and then at 50% rh, at room temperature. The resistance of each was measured periodically with a 500-v d-c instrument between two resilient electrodes, one at each end of the same surface of the bar.

4.3. Surface Moisture

Since the floors of a hospital operating room are naturally kept as clean as possible, tests were conducted to determine the effect of routine maintenance (i.e., water mopping) on the electrical resistance of the samples. The samples were mopped at 9:00 a.m. daily for 1 week with a rubber sponge saturated with water, and any excess water was allowed to remain. The electrical resistance was measured daily at 1:00 p.m. Three series of such tests were run, one at 10 ±1-percent rh (38° C), one at 50 ±2-percent rh (22° C), and the third at 80 ±1-percent rh (27° C). The effect of these tests on the electrical resistance of the specimens is indicated by the dashed lines in figure 2. Again, the oxychlorides were the only samples that were materially affected, their resistance falling below the minimum permissible limit in all cases except in the test at 10-percent rh.

4.4. Service

In order to determine the degree of correlation between laboratory tests and tests of some conductive flooring in actual service, field tests were made

of floors in several hospitals in the Washington area. The results are shown in table 2. They indicate reasonably good correlation between the measured resistances of the samples and the installed floors under roughly comparable conditions.

TABLE 2. *Comparison of field and laboratory tests*

Type of floor	Similar to sample No.	Range of electrical resistance	
		Field	Laboratory (rh 10% to 80%)
		meg	*meg*
Ceramic	1	0.085 to 0.20	0.050 to 0.13
Concrete terrazzo	4	.12 to 1.5	.050 to .33
Concrete terrazzo	4	[a].80 to 9.0	.050 to .33
Linoleum	7	.025 to .045	.037 to .055
Oxychloride	9	[b]4.0 to 10 or more	.012 to 10 or more
Vinyl	15	.048 to .068	.17 to .26

[a] The installation method now specified by the National Terrazzo and Mosaic Association would probably eliminate this type of failure.
[b] This floor had been out of service for about three months and had not been washed regularly.

5. Factors Influencing the Determination of Resistance

The established method given in NFPA No. 56 (see appendix A) for measuring the electrical resistance of installed floors represents a series of compromises among several conflicting requirements. These have been necessary because, unlike metallic conductors, the resistance of the usual conductive flooring material depends upon how it is measured. It is greatly dependent upon such factors as voltage gradient, type and shape of electrode, and time and frequency of applied voltage. The large number of floors submitted in this program made it possible to evaluate these factors on a much better basis than heretofore.

The fundamental principle used in these studies was that a material whose properties depend upon the conditions of measurement should be measured by methods which simulate as closely as practicable the conditions under which the material is expected to function. The tests were intended to evaluate this similarity for each of the effects which prior experience had indicated were significant.

5.1. Applied Voltage

One of the most important of these effects is that of applied voltage. For most conductive flooring materials conduction is either by the migration of ions (electrolytic) or by complex chains of particles of carbon in a nonconducting matrix. In either mechanism it would be expected that the magnitude of the applied voltage would affect the measured resistance. To determine this a Wheatstone bridge [3] was used to apply a d-c voltage to each sample and to measure the corresponding resistance. The voltage was increased in steps of 50 v to the maximum output voltage obtainable (limit 500 v.).

The results for typical flooring materials are given in figure 3. They show that for most materials the resistance is approximately an exponential function of the applied voltage, described by an equation of the form $R=kV^n$. The exponent, n, ranged from 0 to -2.

Experiments have shown that a minimum voltage of about 400 v is required for an electrostatic spark in air at atmospheric pressure [2]. Thus the principle just mentioned indicates that a voltage near this should be used in evaluating floors for locations such as hospital operating rooms, in which ignition of flammable gases by sparks is the principal hazard. Such floors should not be measured by ordinary ohmmeters which apply only a few volts to the sample. Fortunately 500-v insulation-measuring instruments (direct or ratio ohmmeters) are readily available.

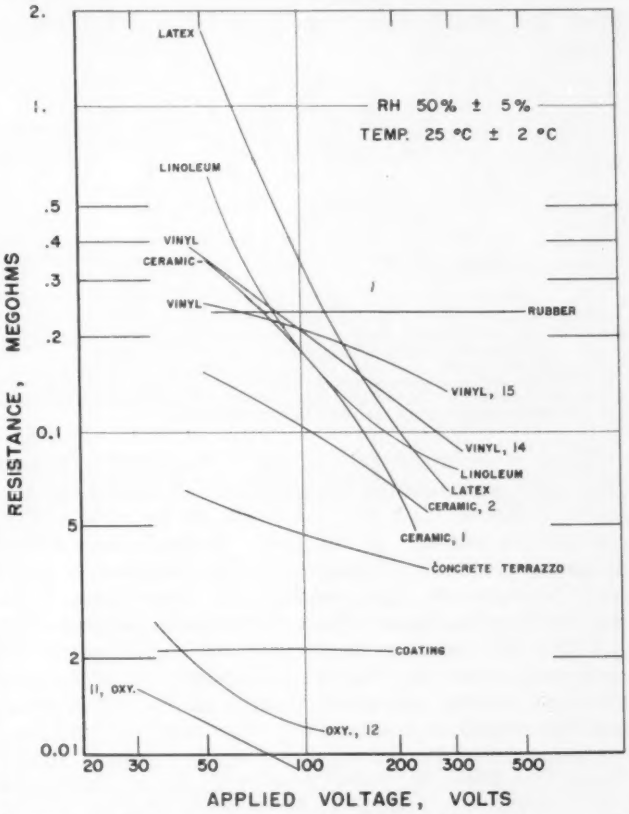

FIGURE 3. *Effect of applied voltage on resistance as measured by the NFPA method.*

5.2. Time

The conventional method of measuring the electrical resistance of an installed floor, for example the method specified in NFPA No. 56, is, in effect, a "steady state" method in which the resistance is measured several seconds after the direct voltage is applied. In practice, static electricity is "generated" (charges are separated) by motions, such as

[3] A commercial megohm bridge with an electronic detector was modified for these tests to measure resistance down to 0.001 meg (1,000 ohms) and to provide an adjustable bridge voltage. It had an effective internal resistance of 50,000 ohms, to limit the current for the protection of the operator and to avoid overheating low-resistance samples. This affects the voltage applied to the sample, as shown in section 5.5 In these tests the voltage actually applied to the sample was measured.

removing a sheet from a table or getting up from a chair, the durations of which are comparatively short, generally in the range from 0.01 to 1 sec [1]. Thus it is the short-time resistance or "surge resistance" of a floor which determines the rate at which the separated charges reunite. For some types of polarization of flooring materials this initial resistance may be less than the steady-state value.

The initial and steady-state resistances of a number of types of flooring materials were evaluated with a cathode ray oscillograph in the circuit shown in figure 4. The oscillograph was connected across a resistor of low inductance to record the current through the sample when the switch, S, was closed. The oscillograph was triggered by the same switch and operated in the single sweep mode, with a sweep time of about 30 msec. After 3 sec the current was read from the milliammeter and the sweep was again repeated without interrupting the current. The ratio of the initial resistance to the steady-state resistance was computed from the initial deflection of the oscillograph (generally observed about 1 msec after the switch was closed), and the deflection at 3 sec.

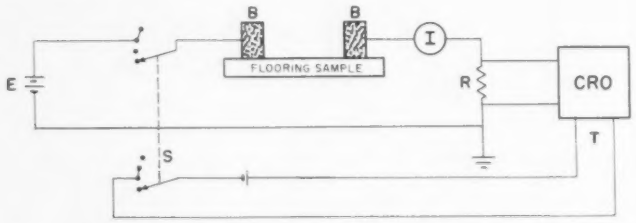

FIGURE 4. *Laboratory circuit for measuring initial and steady-state resistance.*

B, NFPA standard electrode; R, a-c resistor; CRO, cathode-ray oscilloscope and camera, connected to R with coaxial cable, shield at ground potential; T, leads to sweep trigger circuit of CRO; I, milliammeter.

Tests were made at battery voltages of 150 and 400 v, at an ambient temperature of about 25° C, and a relative humidity of 50 to 60 percent. The results are shown in table 3. In most cases the observed difference between the initial and steady-state deflections was small. On this basis it is evident that the 3-sec values of resistance as presently specified for routine tests are not significantly in error and that the fractional changes in resistance for shorter times are not unduly large for the flooring samples tested.

TABLE 3. *Ratio of initial resistance, R_i, to steady-state resistance, R_f, of flooring samples (standard electrodes, relative humidity 50–60%)*

Sample	Type	R_f	R_i/R_f
		meg	
1	Ceramic	0.10	0.8
2	Ceramic	.08	.7
3	Coating	.04	.9
5	Latex	.08	
6	Linoleum	.11	1.0
11	Oxychloride	.04	0.8
13	Rubber	.26	.9
14	Vinyl	.23	.8
15	Vinyl	.41	.8

5.3. Contact Resistance

Experiments have shown that most flooring materials exhibit surprisingly large "contact resistances" at the interfaces between the material and the electrodes which are used to measure the resistance. Because of this the two-terminal method of testing installed flooring (using two electrodes) does not measure the true internal or volume resistance of the flooring material. When necessary, the contact and volume resistivities are best determined by making four-terminal measurements in which two "current" electrodes are used to carry current to the sample under test, with two separate "potential" electrodes between them, connected to a voltmeter whose resistance is much greater than the resistance of the sample. If the electrodes are placed on a rectangular sample as shown in figure 5, the potential electrodes do not disturb the potential gradient in the sample. Then, if the resistance between the current electrodes, the applied voltage, and the voltage between the potential electrodes are measured simultaneously, the average contact resistivity and the internal resistivity can be computed, as shown in appendix B.

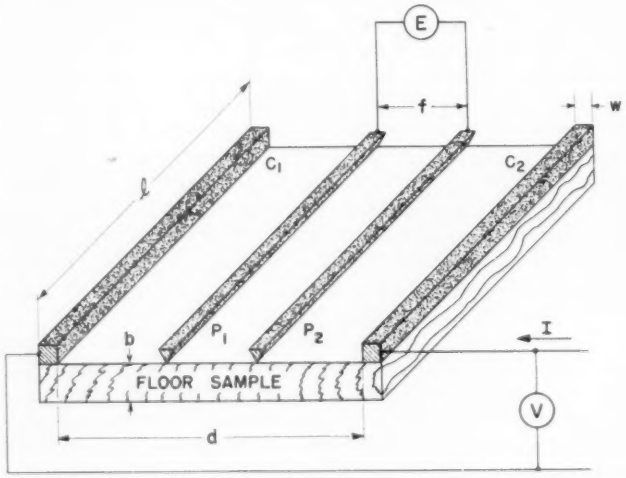

FIGURE 5. *Four-terminal method of measuring contact and volume resistance.*

Several typical samples [4] were measured by this method with the 500-v megohm bridge. The direct voltage from the bridge was applied to two bar-shaped current electrodes, 1½ in. wide and 18 in. long (faced with rubber and covered with foil like NFPA electrodes), with the potential electrodes between them. An electronic voltmeter with an input resistance of 10^{12} ohms was used to measure E. The results are shown in table 4. From this table it is apparent that for each of these materials the contact resistivity with this type of electrode is much greater than the internal resistivity.

It has been argued that the test of an installed floor should be a measurement of the true internal

[4] Samples which had an embedded wire mesh could not of course be evaluated by this method.

TABLE 4. *Contact and internal resistivities*

Sample No.	Type	Contact resistivity	Internal resistivity	Computed resistance between NFPA electrodes	
				1-ft spacing	3-ft spacing
		Ohm-cm²	*Ohm-cm*	*Meg*	*Meg*
1	Ceramic	3×10^6	7×10^4	0.2	0.2
3	Coating	3×10^5	2×10^3	.03	.04
5	Latex	2×10^6	9×10^3	.1	.1
6	Linoleum	2×10^6	2×10^4	.1	.2
13	Rubber	2×16^6	9×10^4	.4	.4
Temperatures					25°±2° C
Relative humidity					50±5%

resistivity of the material and should be made by reducing as far as possible the contact resistivity, for instance by using conductive jelly under the electrodes. However, objects in the operating room must contact the floor, and the principle previously outlined requires that the test electrodes should properly simulate such contacts. In addition, four-terminal measurements show that it is not possible to eliminate contact resistance completely even with wetted electrodes.

The separation of contact and internal resistivity makes it possible to calculate the resistance to be expected for many different configurations of electrodes. In particular, the resistance between two NFPA electrodes on a large floor can easily be determined, as shown in appendix C. The values calculated in this way for several of these flooring samples are given in the last two columns of table 4. These show that the measured resistance is not appreciably affected by the electrode spacing because of the high contact resistivity which is independent of spacing and because the internal resistance of the material between the electrodes is a logarithmic rather than a linear function of the ratio of the electrode diameter to the electrode spacing. Increasing the spacing from 1 to 3 ft increases the internal resistance by less than 50 percent (and does not affect the contact resistance). In addition, the limited area of the 18 by 18-in. samples, which restricts the lines of current flow, increases the internal resistance and somewhat offsets the effect of the reduced electrode spacing.

The computed results agree reasonably well with the values measured for the same samples with NFPA electrodes at approximately the same voltage and ambient relative humidity. The results of these measurements are given in the next section.

5.4. Electrodes

Because of the high contact resistivity it would be expected that the kind and size of electrodes would have marked effects on the measured resistance of conductive floors. From the principle already given, the electrodes should simulate the contacting objects. In an operating room, such objects are of two general types: (a) Soft, resilient materials, such as conductive-rubber shoe soles and heels and conductive-rubber casters and leg tips on furniture; and (b) hard objects such as metal leg tips and gliders. The force on these objects can be expected to vary over a fairly wide range, from perhaps a few pounds (light pail) to several hundred pounds (operating table). Thus no one electrode can be expected to simulate all of these objects.

To evaluate these effects, tests were made of typical materials with several different electrodes and with added weights on each electrode. All measurements were made with the 500-v bridge and at an ambient relative humidity of 30 to 50 percent. Five readings, with the electrodes at different locations, were made on each sample. The average results are given in table 5, along with a key to the types of electrodes used.

TABLE 5. *Results of tests with different electrodes*

Sample No.	Type	Resistance in meg (see key below)						
		S	SW	H	HW	C	CS	B
1	Ceramic	0.055	0.037	0.29	0.24	0.33	0.14	6.5
2	Ceramic	.11	.060	1.4	.80	.65	.34	0.85
4	Concrete [a]	.026	------	0.28	------	.30	.38	.85
5	Latex	.051	.040	.16	.080	.22	.11	------
6	Linoleum	.051	.049	.080	.080	.17	.10	------
7	Oxychloride	.022	.019	.080	.060	2.0	1.0	------
12	Oxychloride	.023	.019	.11	.070	0.25	0.65	------
13	Rubber	.24	.23	.36	.33	.53	.41	------
15	Vinyl	.16	.11	.37	.22	[b] 1.0	1.7	1.0

Key

Symbol	Type of electrode
S	Two 5-lb, 2.5-in. diam electrodes, with flat but resilient contact face on each, conforming to NFPA No. 56.
SW	Same as S with 50-lb additional weight on each electrode.
H	Two 5-lb electrodes with flat steel contact faces, 1-in. diam, having rounded edges.
HW	Same as H with 50-lb additional weight on each electrode.
C	Two conductive casters, 3-in. diam, ¾-in. tread. Weight of each about 1 lb with 5-lb additional weight on each caster.
CS	One type "C" and one type "S" electrode.
B	Two 5-lb electrodes, each having three-legged contacts of ⅛-in. by ⅛-in. brass rods, having flat surfaces and sharp edges.

[a] Sample tested shortly after receipt, before aging.
[b] Moderate variations. Some additional readings up to 100 meg.

The results show that for all materials the resistance measured with the resilient NFPA electrodes is not appreciably affected by large changes in force, so that these electrodes, which weigh only 5 lb and are reasonably portable, can simulate the much heavier objects likely to be encountered in operating rooms. For resilient floors (such as vinyl tile, rubber, linoleum, and the coating with the wood backing) the results with the hard electrodes, which simulate metal leg tips and gliders, are not appreciably higher than with the NFPA electrodes. However, with hard-surfaced materials (oxychloride, concrete terrazzo, and ceramic tile) the actual contact area was much less than with the resilient electrodes, and the measured resistances were greater by factors as large as 10 or more (and in one case by a factor of 100). In general, the scattering in the 5 readings of resistance with each electrode (only the average values are shown in the table) was very much greater with the hard than with the resilient electrodes. The conductive casters, which have a small contact area, showed marked scattering in readings of resistance

on some samples. The differences between results with two standard electrodes and those with two casters were less marked for resilient flooring (except for vinyl tile) than for hard-surfaced materials. (Field tests of a conductive vinyl tile floor of the same manufacture gave nearly equal results with casters and standard electrodes.) The special 3-legged electrodes have been suggested for simulating high-pressure contacts. The resistances were in general comparable with or somewhat higher than those with the 1-in. hard electrodes.

Thus the resilient electrodes simulate well one type of floor contact and give much more uniform and reproducible results than hard-surfaced electrodes. However, when such resilient electrodes are specified, the upper limit of resistance for an installed floor must contain a large factor of safety to allow for hard-surfaced objects which are also widely used. This factor depends upon the resiliency of the floor, so that apparently the specified upper limit with a resilient floor such as conductive rubber or linoleum could safely be 10 times as high, when measured with these electrodes, than the limit for a hard floor such as oxychloride or concrete terrazzo.

5.5. Frequency

The lower limit of resistance specified in NFPA No. 56 for conductive floors is intended to provide some (but not complete) protection from electric shock. Alternating current (120 v, 60 cps) is almost universally used in this country for electrical utilization circuits. Because of this it would appear that the resistance of the floor should be measured at this voltage and frequency to determine compliance with the lower limit. For convenience, however, the same d-c instrument is normally used for both upper and lower limit tests. The instrument commonly specified has an open circuit voltage of 500 v. However, the actual voltage that it impresses on the floor under test depends upon the resistance of the floor and the internal resistance of the instrument, as shown in figure 6. From this figure it is apparent that a 500-v instrument having an internal resistance of almost 0.1 meg will impress about 100 v on a sample near the NFPA lower limit of 25,000 ohms (0.025 meg).

Measurements of several flooring samples were made at 100 v, with alternating and direct current, and with a typical 500-v ohmmeter which has an internal resistance of 0.1 meg. All measurements were made with the standard resilient electrodes at the same location on each sample, and at an ambient relative humidity of about 40 percent. The results given in table 6 shown no really significant differences between the a-c and d-c measurements of a given sample at 100 v. They also show that for samples near the lower limit of 0.025 meg the ohmmeter value agreed reasonably well with others. For samples of higher resistances the ohmmeter impressed more than 100 v on the sample and the measured resistance was, in general, less, as would be expected from the observation that resistance is an inverse function of the voltage, as shown in section 5.1. The 500-v instrument specified in NFPA No. 56 (internal resistance 50,000 to 200,000 ohms)[5] thus can be expected to give results which are reasonably close to those obtained with the somewhat more complex instruments required for a-c measurements, and make it unnecessary to specify two different instruments for measuring installed floors. However, as figure 6 shows, the range of internal resistance specified in NFPA No. 56 could be greatly narrowed. A short circuit current of 5 ± 0.5 ma corresponding to a nominal internal resistance of 100,000 ohms is suggested.

TABLE 6. *Ac-dc comparison tests*

Sample No.	Type	Resistance in meg		
		At 100 v 60 cps, ac	At 100 v dc	With ohmmeter
1	Ceramic	0.20	0.23	0.075
2	Ceramic	.31	.34	.10
4	Concrete	.009	.024	.015
5	Latex	.21	.25	.075
6	Linoleum	.055	.057	.050
8	Oxychloride	.042	.038	.030
11	Oxychloride	.012	.007	.010
12	Oxychloride	.063	.040	.040
13	Rubber	.21	.23	.21
15	Vinyl	.60	.78	.20

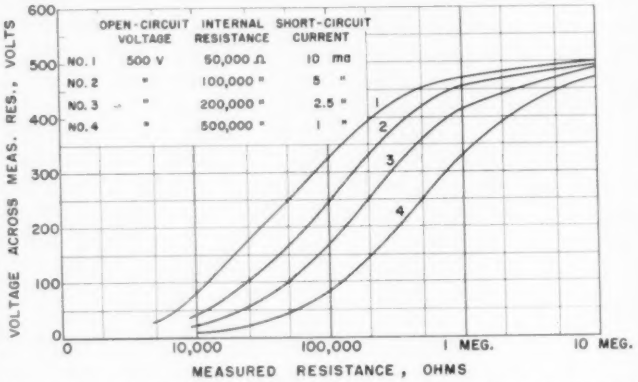

FIGURE 6. *Output voltage of ohmmeters as a function of measured resistance.*

Characteristics of ohmmeters shown in block on graph.

5.6. Instruments

A number of different instruments are commercially available for measuring the resistance of conductive floors. Instruments fall into three general classes: (a) simple ohmmeters; (b) ratio ohmmeters; and (c) Wheatstone bridges [6].

A simple d-c ohmmeter consists of a battery, milliammeter, and a resistor, R, all in series with the unknown resistor, X, to be measured. The current through the milliammeter is adjusted (by shunting the milliammeter or adjusting R) [6] to give full scale deflection of the instrument, which is marked zero on the scale. The current through the instrument is then a function of X and the scale is marked

[5] The internal resistance can usually be computed as the quotient of the open circuit voltage divided by the short circuit current of the instrument.

[6] It is much more desirable to shunt the milliammeter, since the calibration depends on R.

accordingly. Such ohmmeters with 1.5- or 3-v batteries are commonly used in radio or television service instruments. As indicated in section 5.1, these voltages are far too low for meaningful tests of conductive flooring. However, at least one manufacturer has incorporated a vibrator-transformer power supply operated from a dry cell to produce a 500-v conductive-flooring tester.

The moving element in a ratio-type ohmmeter contains a permanent magnet and two rotatable coils fixed at right angles to each other, one of which functions as in the simple ohmmeter while the other carries a current proportional to the applied voltage. With no springs, the coils then take up a position which is a function of the ratio of the voltage to the current, and the scale is laid off in ohms or megohms. The reading is then desirably independent of the voltage, and a zero setting is not necessary. Most ratio ohmmeters also contain handcranked generators to produce the desired voltage.

Wheatstone bridges with electronic detectors have been used occasionally, but are best suited for laboratory work, since a balance must be made before each reading. They are generally capable of greater accuracy and flexibility than ohmmeters.

Table 7 shows the general characteristics of commercially available instruments which are suitable for testing conductive flooring. In accordance with NFPA No. 56, such instruments must have an open circuit voltage of 500 v, a short circuit current of 2.5 to 10 ma, and should have a range of at least 0.01 to 2 meg. Unfortunately, many models of 500-v insulation testers have a higher internal resistance and resistance range than this. Only moderate accuracy is required in field tests of conductive flooring because of the large variations inherent in most materials. An accuracy of 20 percent of the measured resistance in the range 0.025 to 1 meg should be adequate. It can be shown that, because the scale of an ohmmeter is necessarily nonlinear, the markings on the scale must then be accurate to 2 percent of the full-scale length, and the resistors and other component parts must be accurate to better than 10 percent.

The data on the modified megohm bridge are included for reference. The instrument was found to be accurate to 1 percent and well suited for laboratory studies because of its wide voltage and resistance ranges. However, it would not be as convenient as the others for routine tests of installed floors.

TABLE 7. *Characteristics of typical instruments for measuring resistance of conductive floors*

Type	Energy source	Open-circuit voltage	Short-circuit current	Internal resistance	Range [a]		Approximate mid-scale reading
					Low	High	
		v	*ma*	*meg*	*meg*	*meg*	*meg*
Ratio ohmmeter.	Hand-cranked.	0–500	3.5	0.14	0.005	10	0.20
Ratio ohmmeter.	Hand-cranked.	0–500	10	.05	.010	50	.80
Simple ohmmeter.	Internal battery.	500	3	.17	.010	10	.18
Simple ohmmeter.	Internal battery.	500	2.5	.20	.010	10	.23
Ratio ohmmeter.	Hand-cranked.	500	5	.10	.010	50	.50
Megohm bridge.	110 v a-c	500	10	--------	[b] .001	[b] 100	--------

[a] Lowest and highest markings on scale exclusive of zero and "infinity" markings.

[b] At listed short-circuit current; additional ranges to 1,000,000 meg at lower currents.

6. Electrostatic Tests

The electrical tests of conductive flooring samples outlined in sections 4 and 5 have been made under deliberately varied conditions, such as relative humidity and applied voltage, to determine the effect of ambient conditions and of normal use upon the samples, and to evaluate the factors which may be expected to influence the measurements. To substantiate these results, additional experiments were carried out in which each type of floor was actually used as an intercoupler to reunite electrostatic charges. These experiments provided a direct test of the effectiveness of each type of floor in eliminating hazards from static electricity.

Tests in the NBS laboratories have shown that a person rising from a plastic-covered chair while wearing wool clothing causes a separation of charges at as high a time rate (and therefore charging current) as any human action tested. A comparatively low resistance is thus required to keep the voltage between the objects concerned (chair and person rising from it) below the minimum sparking voltage, about 400 v in air at normal pressure. If the voltage is less than this, true electrostatic sparks do not occur [2]. This experiment therefore provides a good test of the actual performance of a floor, if the peak voltage between the objects can be measured.

A few measurements of the voltages produced in such tests have been made in the NBS laboratories by using a high-resistance voltage divider, cathode ray oscillograph, and camera.[7] However, this proved to be too cumbersome for the many tests required for these floors, so that a simple peak-voltage indicator was constructed. It consisted of four small sensitive neon lamps (NE2 or equivalent) connected in series with a 40 $\mu\mu$f capacitor across each. The lamps and capacitors were mounted in a small blackened metal tube having a lens at one end. The capacitors assure that equal transient (or alternating) voltages appear across each lamp until one lamp fires (glows), after which all glow. Tests showed that the firing voltage was about 300 v, somewhat less than the minimum sparking voltage. The "dark" resistance at lower voltages ranged from 5,000 to more than 20,000 meg. Additional tests were made later of some samples, with two neon lamps added to the indicator, so that the firing voltage was about 450 v, approximately that of the standard instrument for measuring floors (500 v).

For these tests a person wearing conductive shoes held the peak-voltage indicator. The other terminal

[7] Since this is a transient voltage an ordinary electrostatic voltmeter can not be used.

of the indicator was connected to the frame of a metal chair (having flat metal gliders ¾ in. diam) which rested on the flooring sample.[8] The person sat in the chair, and then, while observing the indicator, rose from the chair (with a forward sliding motion) with his feet on the same sample and noted whether or not the lamps glowed. At least five such trials were made with each flooring sample. The resistance of the sample between two standard electrodes and between the metal frame of the chair and the subject was measured immediately after each test at three or five different locations on the sample.

Additional tests were made on an insulating floor with a resistor connected between the chair and the subject. The tests were repeated with resistors of successively lower value until the lamps glowed while the person rose from the chair. These tests thus determine the actual safe upper limit resistance for the motion and materials involved.

All of the tests with the flooring samples and the resistors were made at an ambient relative humidity of 20 percent, with a plastic covered chair and a subject who wore a wool suit, conditions which are very favorable to the generation of static electricity.

The results of these tests are given in table 8. The last three rows of the table show that the actual safe limiting resistance to keep the voltage between the chair and subject below the minimum sparking voltage (400 v) for the motion and materials used was about 30 megs. A resistance less than 20 to 30 megs was required to keep the voltage below 300 v, the firing voltage of the 4-lamp indicator.

The range of measured resistances between the chair and subject are given in the fourth column of the table. As indicated in section 5.4 this range is much greater with hard surfaced electrodes such as the leg tips on this chair than with resilient electrodes. (This is one reason why the resilient electrodes are preferred for routine tests.) The results show that except for sample No. 5 the peak voltage was less than 300 v when the measured resistance between the chair and subject was less than about 30 meg, and vice versa.[9] Thus there is excellent correlation between the resistance of a conductive floor as measured with a standard 500-v d-c instrument, and the resistance to the flow of electrostatic charges through the same electrodes (contacting objects).

The upper limit of resistance specified for a conductive floor with the standard electrode is 1 meg. The results show that, for all samples except Nos. 5 and 11, the peak voltage is less than 300 v, if the resistance between the two standard electrodes is less than 1 meg, and vice versa. Thus the specified 1-meg limit with two standard electrodes is a reasonably valid criterion of the performance of these floors.

These tests therefore show that the actual resistance between the objects on which the charges are generated (or transferred by induction) is the important criterion of the effectiveness of a conductive floor as an electrostatic intercoupler, and that this can be measured reasonably well with the specified 500-v instrument. In case of doubt, as for example floors which are slightly above the 1-meg limit with the standard electrodes, measurements of the resistance between objects in the room can provide additional evidence of the safety of the floor (and the contacting objects) with respect to the hazards from static electricity.

These tests indicate that for resilient floors there is an appreciable "factor of safety" (about 10) for the present 1-meg specification, even at this very-low relative humidity, because the resistance of such floors is relatively independent of the hardness of the contacting objects. There would appear to be no such factor for hard-surfaced floors. However, additional tests indicate that there is a very large factor of safety (10 or more) if, as specified in NFPA No. 56, materials such as wool and plastics are prohibited. Such materials are excellent electrostatic generators because of their very high electrical resistivities. In addition, because the resistance of many insulating materials depends upon the ambient relative humidity, there is another very large factor of safety if, as recently specified in NFPA No. 56, a relative humidity of 50 to 60 percent is maintained.

TABLE 8. *Results of electrostatic tests*

Ambient temperature 25° C; relative humidity 20%; plastic chair covering; wool garment (see text)

Sample No.	Type	Resistance (megs) between:		Peak voltage greater than: [a]	
		Two standard electrodes (average)	Chair and subject (min. & max.)	300 v	450 v
2	Ceramic	0.2	0.3 to 0.5	No	
4	Concrete	.9	3 to 30	Yes	No.
5	Latex	.05	0.08 to 0.09	Yes	Yes.
6	Linoleum	.03		No	
7	Oxychloride	6	140 to 260	Yes	
8	Oxychloride	2	15 to 45	Yes	No.
9	Oxychloride	30	200 to 400	Yes	
10	Oxychloride	1.5	7 to 65	Yes	No.
11	Oxychloride	0.3	1 to 50	Yes	Yes.
12	Oxychloride	.6	2 to 5		No.
13	Rubber	.1	0.08 to 0.18	No	
15	Vinyl	.2	.3 to 0.4	No	
	Resistor 20 meg			No	
	Resistor 30 meg			Yes	No.
	Resistor 50 meg			Yes	Yes.

[a] "Yes" signifies that the designated peak voltage was exceeded at least once in five or more trials.

7. Nonelectrical Properties

7.1. Indentation

Indentation studies included the determination of initial indentation under load and residual indenta-

[8] Because of the small size of the sample only the front legs of the chair rested on the sample. Insulators were placed under the rear legs. For some of the tests with the 450-v indicator, two flooring samples of the same type were connected together so that all four legs of the chair rested on the conductive floor.

[9] Additional tests showed that the manufacturer of sample No. 5 had applied a sealer which sometimes effectively insulated the hard-surface gliders of the chair, but not the standard electrodes. With hard electrodes the breakdown voltage of this insulating film ranged from 100 to more than 400 v. This sealer is no longer applied on conductive floors by the manufacturer of this sample.

tion after removal of the load. The initial indentation is sometimes referred to as the "comfort value", in that it expresses the ability of a floor to depress readily under foot. The value of the residual indentation, on the other hand, is an indication of the resistance to permanent deformation due to a concentrated load, such as a table leg. The ideal floor might thus be considered as one which has a high initial indentation or "give" and a low residual indentation or high recovery. In table 9, linoleum, rubber, and vinyl show a much higher initial indentation than the ceramic, concrete, and oxychloride materials. However, other important factors are involved in determining comfort value which are of an indirect nature, but which can be of major importance, e.g., the type of footwear involved. Comparison of these results with those reported in BMS–73 [7] show that the indentation characteristics of the conductive materials are comparable to those of the corresponding nonconductive materials.

TABLE 9. *Indentation characteristics*

Sample No.	Type	Thickness	Initial indentation			Residual indentation			
			A	B	C	1 hr after removal of load			48 hr after removal of load
						A	B	C	C
		in.	*in.*	*in.*	*in.*	*in.*	*in.*	*in.*	*in.*
1	Ceramic	0.25	0.000	0.000	0.000				
2	do	.25	.000	.000	.000				
3	Coating	.035	.011	.007	.009	0.003	0.000	0.000	
4	Concrete	.50	.000	.000	.000				
5	Latex	.443	.009	.007	.014	.002	.000	.000	
6	Linoleum	.134	.024	.005	.007	.003	.000	.002	0.001
7	Oxychloride	.50	.000	.000	.000				
8	do	.50	.000	.000	.000				
9	do	.56	.000	.000	.000				
10	do	.50	.000	.000	.000				
11	do	.50	.000	.000	.000				
12	do	.50	.002	.000	.000	.000			
13	Rubber	.126	.029	.008	.006	.002	.000	.001	.000
14	Vinyl	.121	.043	.021	.024	.006	.007	.007	.000
15	do	.193	.047	.011	.017	.002	.002	.009	.006

A=80-lb load applied 10 min through a 0.178-in.-diam indenter foot (3,200 lb/in.^{2}).
B=100-lb load applied 10 min through a 1.125-in.-diam indenter foot (100 lb/in.^{2}).
C=100-lb load applied 7 days through a 1.125-in.-diam indenter foot (100 lb/in.^{2}).

In the case of sample No. 3 (coating), the results reflected predominantly the indentation characteristics of the plywood backing, because of the thinness of the coating material. The result would undoubtedly have been different if the same material had been applied over concrete.

The indentation tester and procedure used in making the indentation and recovery determinations are described in detail in Report BMS–73 [7] and in Federal Specification LLL–L–367 for Linoleum.

7.2. Scratch Resistance

Precise measurements of scratch resistance, as described in the paragraph below, were made on each sample. This value relates to the ease with which the floor surface can be scuffed and marred by abrasive material carried on shoes. Resistance of conductive flooring materials to surface scratching is of prime importance in operating rooms for the sake of cleanliness as well as the possible effect on electrical contact resistance. In order to establish a basis by which these values can be related to actual service, each sample was placed on the pedestrian traffic test ramp described later.

The Taber Scratch Tester was adapted to measure the scratch width of a diamond point at loads of 250, 500, 750, and 1,000 g. A level plate capable of travel at a uniform rate of 1 ft/min was used in moving the flooring sample under the diamond-point scratch tool. A scratch 2 in. long was made and the width of the scratch was measured at three locations with a 20× Brinell microscope containing a scale graduated in 0.1 mm. The average of the three measurements was converted to the nearest 0.001 in. and recorded as scratch width in mils. The graph, figure 7, illustrates the results.

A pedestrian traffic test ramp was constructed (see fig. 8). Each flooring sample was securely placed on the test ramp and a photoelectric counter was installed to count passages over the ramp. The length of the entrance at each end of the test ramp was altered every 3 months, causing a change in the foot traffic pattern and therefore insuring that each sample received the same amount of wear. The ramp was located on the third floor of the Industrial Building, NBS, away from street grit, gravel, and water, but exposed to light industrial-type dirt and dust. No attempt was made to maintain the samples other than an occasional dry sweeping. These conditions were considered more severe than in hospital operating rooms, resulting in an accelerated test. Photographs taken after 11 months of wear (100,000 passages) were compared with photographs of unexposed flooring to determine the extent of scratching, smudging, and other damage (see fig. 9). A comparison chart of visual appearance of the scratching on the exposed samples is listed below the graph in figure 7.

7.3. Slipperiness

Tests of relative slipperiness of the conductive flooring samples were made with leather and rubber heels under both wet and dry conditions. The method of testing and a description of the instrument used have been previously reported [8]. Slipperiness is not a constant of the walkway surface or of the contact surface of the footwear alone, but is a function of both surfaces and is materially affected by their conditions. Therefore, an unqualified evaluation of a particular floor or floor finish may be very misleading.

The results in table 10 show the antislip coefficients; the higher the value, the less slippery the surface. Comparison of these results show that the antislip characteristics of the conductive materials are comparable to those of the corresponding nonconductive materials.

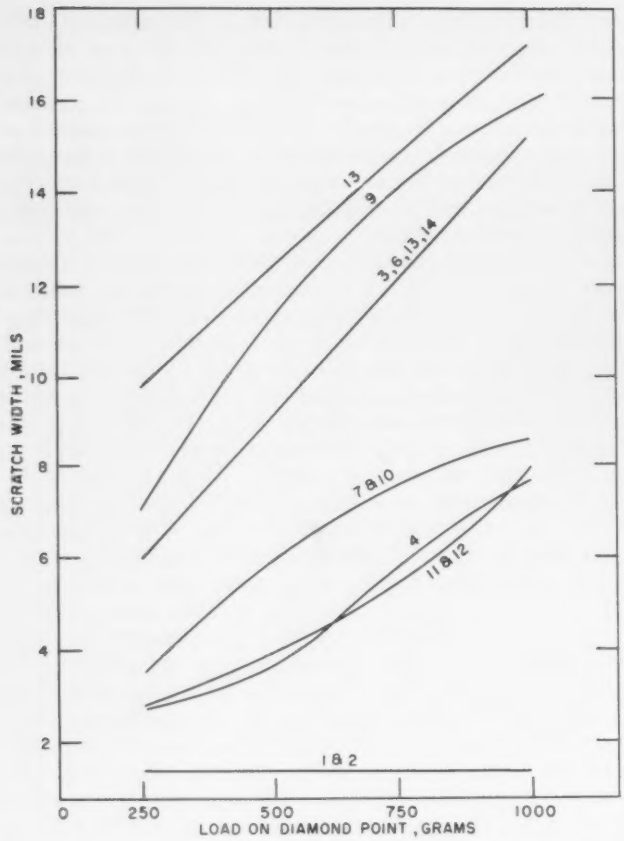
SCRATCH WIDTH, MILS
LOAD ON DIAMOND POINT, GRAMS
13
9
3,6,13,14
7810
4
11812
182
MATERIAL | CERAMIC | COATING | CONCRETE TERRAZZO | LINOLEUM
NBS SAMPLE NO. | 1 | 2 | 3 | 4 | 6
CONDITION AFTER 3 MONTHS SERVICE (33,000 PASSAGES) | GOOD | GOOD | FAIR | GOOD | POOR
CONDITION AFTER 11 MONTHS SERVICE (100,000 PASSAGES) | GOOD | GOOD | FAIR | GOOD | POOR
MATERIAL | OXYCHLORIDE | RUBBER | VINYL
NBS SAMPLE NO. | 7 | 9 | 10 | 11 | 12 | 13 | 14 | 15
CONDITION AFTER 3 MONTHS SERVICE (33,000 PASSAGES) | GOOD | FAIR | GOOD | GOOD | POOR | POOR | FAIR | FAIR
CONDITION AFTER 11 MONTHS SERVICE (100,000 PASSAGES) | FAIR | FAIR | GOOD | GOOD | POOR | POOR | FAIR | FAIR

FIGURE 7. *Resistance to scratching.*

7.4. Scrubbing

The durability of permanent type conductive floorings is quite difficult to assess and no suitable short-term evaluation tests were available. The dry-traffic tests discussed in section 7.2 and the stain-resistance tests in section 7.6 were made in an attempt to judge the relative serviceability of these materials for operating room floors. In addition, because of the frequent washing and cleaning of operating room floors, an apparatus was designed to produce a continuously agitated washing effect. The samples were placed on a plate which rotated at 4 rph and the surface of each sample was kept continuously wet. A brush was used as the scrubber and was rotated at 180 rpm under a total load of 500 g. Each sample was exposed to this continuous wet-brushing action for 52 hr. The samples were examined visually by comparing the exposed with the nonexposed areas, and by electrical conductivity measurements.

Except for one of the oxychlorides the samples were not significantly affected by this severe scrubbing test. Sample No. 8 showed a large amount of wear and erosion, so that the end effect was a removal of the conductive matrix below the level of the nonconductive chips. The electrical resistance of this sample increased to two megohms. In addition, samples No. 9, 10, and 11 showed a slight amount of erosion and pitting, but their electrical conductivity was not affected.

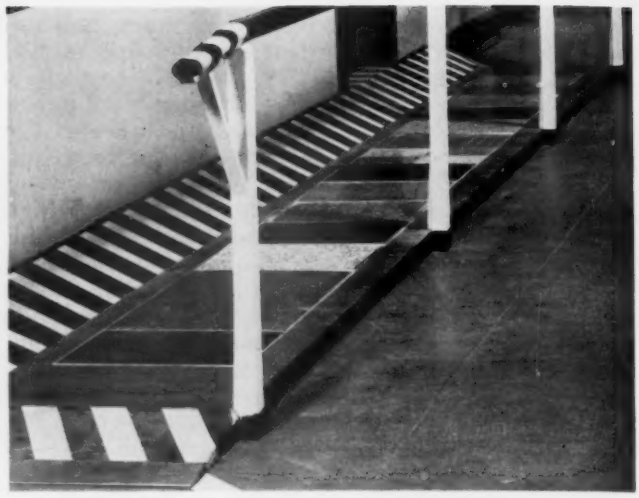

FIGURE 8. *View of pedestrian traffic test ramp.*
Each sample was 18 in. by 18 in.

TABLE 10. *Relative slipperiness*

Sample No.	Type	Antislip coefficient			
		Leather heel		Rubber heel	
		Dry	Wet	Dry	Wet
1	Ceramic	0.37	0.26	0.68	0.44
2	Ceramic	.34	.26	.72	.31
3	Coating	.33	.26	.74	.46
4	Concrete terrazzo	.43	.26	.56	.30
5	Latex terrazzo	.32	.10	.73	.13
6	Lincleum	.37	.18	.68	.37
7	Oxychloride	.39	.38	.68	.48
8	Oxychloride	.36	.15	.62	.21
9	Oxychloride	.21	.18	.58	.24
10	Oxychloride	.37	.14	.58	.22
11	Oxychloride	.37	.12	.55	.16
12	Oxychloride	.34	.13	.54	.39
13	Rubber	.39	.12	.67	.13
14	Vinyl	.26	.16	.46	.10
15	Vinyl	.28	.13	.63	.23

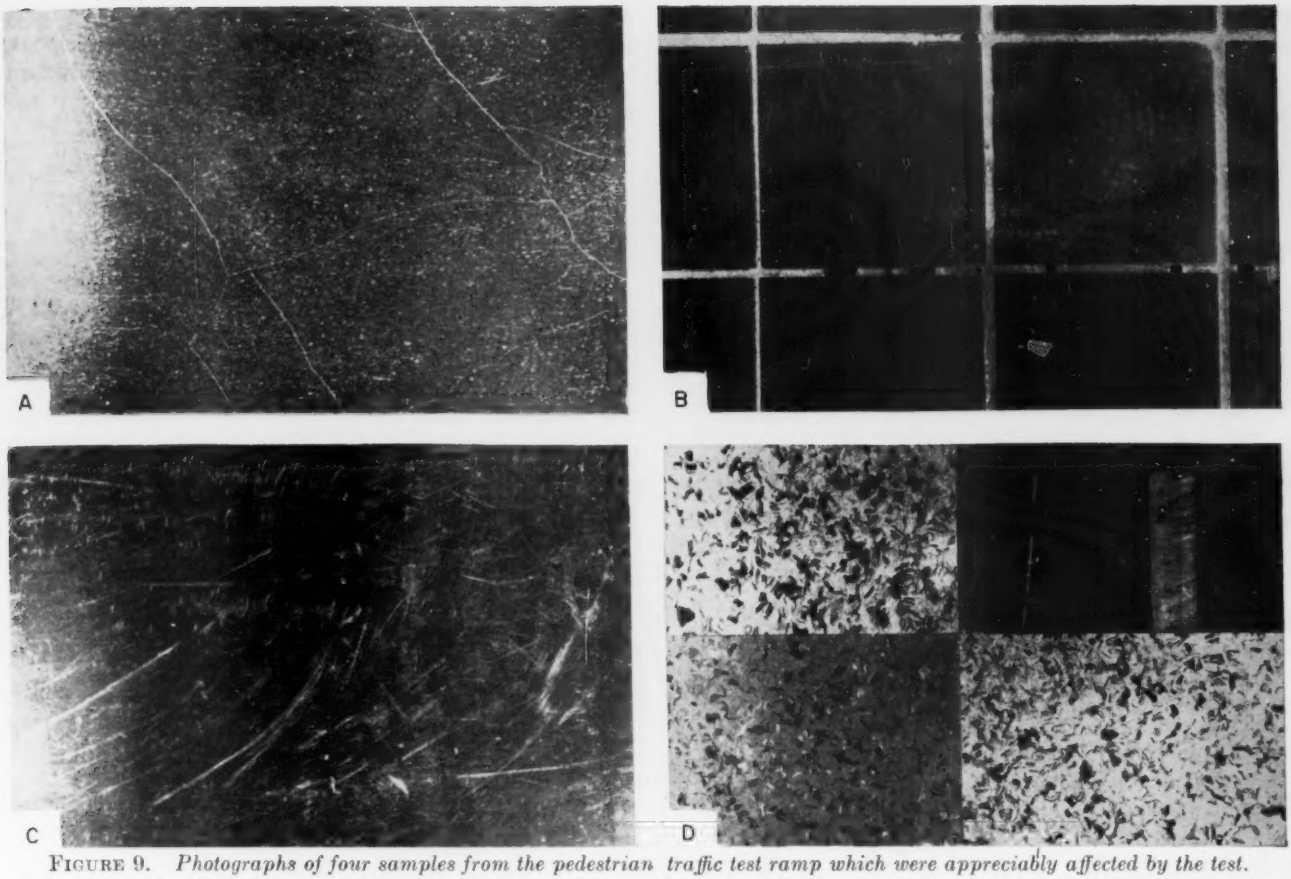

FIGURE 9. *Photographs of four samples from the pedestrian traffic test ramp which were appreciably affected by the test.*

A, Sample No. 8 (oxychloride), showing hairline cracks; B, Sample No. 2 (ceramic), showing pitting in mortar joints; C, Sample No. 13 (rubber), showing extreme scuffing and scratching. No wax was used; D, Sample No. 15 (vinyl), showing extreme soiling of light colored tiles. One tile has been removed to show the copper ribbon which connects the tiles electrically.

7.5. Water Absorption

It has been considered desirable that a flooring material designated for an area subject to frequent washing should have a very low rate of water absorption in order to reduce staining, leaching, and erosion by water and detergents. To establish the rates of water absorption the following test was performed on each sample:

One-tenth milliliter of water was placed on the sample with a pipet and covered with a watch glass. The number of minutes required for complete absorption of the 0.1 ml of water was taken as the time of absorption. Complete absorption was assumed to have taken place when light no longer was reflected from the wetted surface of the sample. All the flooring materials except the five listed below required more than 5 hr for the water to disappear and can therefore be considered fairly impervious to water.

No.	Type	Time of absorption
		min
4	Concrete terrazzo	15
8	Oxychloride	4
9	Oxychloride	6
10	Oxychloride	6
11	Oxychloride	22

7.6. Stain Resistance

A high resistance to staining (or ease of cleaning when stained) is a desirable characteristic of a flooring material intended for use in an area where there is likely to be spillage. Table 11 lists recommended methods for removing certain stains. Care should be used in applying the solutions. For example, acid solutions are usually the most effective means of removing rust stains from concrete; 10 percent solutions of hydrochloric or phosphoric acid are commonly used. Acids should not, however, be allowed to remain in contact with the surface any longer than is necessary to remove the stains. With any such treatment, some roughening of the concrete is inevitable and may be conspicuous. As a precaution it is advisable to carry out a trial on a small area to determine if the resulting appearance is acceptable. Table 12 gives results of tests carried out to determine the effect on the conductive floor samples of various staining agents and the ease or difficulty with which the stains were removed.

8. Summary and Conclusions

1. The conductive floors tested should give satisfactory service in hospital operating suites, with the reservations outlined below. Similar conclusions can be drawn from the results of extensive tests by the staff of the National Research Council of Canada of several types of installed floors [9].

TABLE 11. *Stain-removal methods*

Stain	Linoleum	Ceramic	Concrete terrazzo	Latex terrazzo	Oxychloride	Vinyl	Coating	Rubber
Blood	Apply cool water and rub with cloth. If stain persists, dampen cloth with ammonia.							
Grease or oil	Apply detergent and rub with cloth.	Apply detergent and rub with cloth. If stain persists apply kerosene or varsol on spot, permit to soak, wipe dry and wash with detergent, or mix kerosene or varsol with fuller's earth to form paste. Apply paste to spot and let stand for several hours. Repeat if necessary.				Apply detergent and rub with cloth.		
Ink (washable, writing, and drawing).	Apply detergent and rub with cloth. If stain persists, mix 1 part sodium perborate to 25 parts water. Mix with whiting (calcium carbonate) to form paste. Apply paste to spot and leave until dry.							
Paint or enamel	Remove excess with putty knife and/or No. 0 steel wool. Apply kerosene, turpentine, or varsol. Wash with detergent.						Remove with putty knife and No. 0 steel wool.	
Iodine	Apply alcohol and rub with cloth.		Apply alcohol and cover with fuller's earth.			Same as for linoleum.		
Rust	Rub with No. 0 steel wool and wash with detergent.	Apply water and rub with cloth. If stain persists apply solution of 1 part oxalic acid to 9 parts water. Let remain until dry. Wash thoroughly with water.			Apply water and rub with cloth. If stain persists, dissolve 1 part sodium citrate in 6 parts water. Make a paste with whiting (calcium carbonate) and apply to stain, or wash with sodium citrate solution and add pad of cotton soaked in sodium bisulfite. Wash thoroughly with water.	Same as for linoleum.		
Sole and heel marking.	Apply detergent and rub with cloth.							

TABLE 12. *Results on removal of stains*

Sample No.	Type	Blood	Grease or oil	Ink	Paint or enamel	Iodine	Rust	Sole and heel marks
1	Ceramic [a]	B	B	B	B	B	B	A
2	Ceramic [a]	B	B	B	B	B	B	A
3	Coating	B	B	B	B	B	B	B
4	Concrete terrazzo	B	C	C	B	B	C	B
5	Latex terrazzo with sealer	B	B	B	B	B	B	B
5	Latex terrazzo without sealer	B	B	C	B	F	C	B
6	Linoleum	B	B	B	B	B	B	A
7 & 8	Oxychloride	D	B	D	B	B	F	B
9	Oxychloride	F	F	F	B	B	B	B
10	Oxychloride	B	F	D	B	A	F	B
11	Oxychloride	B	B	D	B	F	B	A
12	Oxychloride	D	F	D	B	B	B	B
13	Rubber	B	B	B	B	B	C	B
14	Vinyl	B	B	B	B	C	B	C
15	Vinyl	B	B	C	B	C	B	C

Note: A, Staining material would not stain or mark floor; B, stain completely removed with little effort; C, stain completely removed, but with difficulty; D, stain completely removed, but floor surface bleached or etched; F, stain not removed.

[a] Results on cement joints same as No. 4, concrete terrazzo.

2. In general, any particular type of conductive flooring may be expected to render service comparable to nonconductive flooring of the same type. Consequently, an architect may base his choice of a conductive flooring material on his knowledge of the behavior of similar nonconductive materials, with the following limitations:

(a) The durability and appearance of at least two of the available materials (linoleum and rubber) may depend on periodic waxing. Conductive waxes containing carbon black which do not deposit an insulating film are available and should be esthetically as well as electrically satisfactory on these uniformly black floors. Sealers should not be used on conductive floors until proven satisfactory by extensive electrical tests.

(b) Since the most commonly used conductive medium (acetylene black) is black, the colors available in most types of conductive floors are limited. However, terrazzo and other pattern effects can be used. Detailed descriptions of some of the available colors and patterns are given in section 3.

(c) The electrical resistance of the oxychloride floors depended on their moisture content, which in turn was governed by the humidity of the air and by water added during washing. The results of the tests given in this report indicate that if this material is used the relative humidity of the air in the room in which it is installed should be controlled and the cleaning schedule for the floor should be carefully established and maintained. The laboratory tests indicate that otherwise the electrical resistance of the floor may fall outside the accepted limits.

3. The results of this investigation indicate that the presently accepted method of measuring the resistance of installed floors, described in NFPA No. 56, reasonably simulates the conditions under which a floor is expected to function as an electrostatic intercoupler.

4. The results also show that current specifications and methods of measuring the physical properties of nonconductive floorings are satisfactory for conductive floorings.

The work described in this report was done under a project sponsored jointly by the Office of the Chief of Engineers, Department of the Army; Bureau of Yards and Docks, Department of the Navy; and Engineering Division, Director of Civil Engineering, Department of the Air Force.

The authors appreciate the cooperation of the staff of the Division of Building Research of the National Research Council of Canada, particularly Mr. P. J. Sereda, in making available their experience with conductive flooring. The cooperation of the numerous manufacturers who generously provided samples is also acknowledged.

9. References

[1] P. G. Guest, V. W. Sikora, and B. Lewis, Static electricity in hospital operating suites: Direct and related hazards and pertinent remedies, Bureau of Mines Report of Investigation 4833, 64 pp. (1952).
[2] F. B. Silsbee, Static electricity, NBS Circ. 438 (June 1942).
[3] F. L. Hermach, Hazards from static electricity, The Military Engineer **44,** 287 (1952).
[4] Recommended safe practice for hospital operating rooms, N.F.P.A. No. 56, National Fire Protection Association (reproduced in part in appendix A of this report).
[5] Robin Beach, Electrostatic safety for hospital operating rooms, Elec. Eng. **72,** 329 (April 1953).
[6] AIEE master test code for resistance measurements, Publication No. 550, Am. Inst. Elec. Engrs., New York, N.Y.
[7] Percy A. Sigler and Myrtle B. Woodward, Indentation of floor coverings, NBS BMS Report 73, 7 pp. (1941).
[8] Percy A. Sigler, Martin N. Geib, and Thomas H. Boone, Measurement of the slipperiness of walkway surfaces, J. Research NBS **40,** 5, 339 (May 1948).
[9] P. J. Sereda, Properties of commercial conductive flooring for hospital operating rooms, Division of Building Research, Nat. Research Council Can., NRC 4031.

10. Appendix A. Excerpts [10] from the 1958 Edition of NFPA Publication No. 56, *Recommended Safe Practice for Hospital Operating Rooms*

6–2. Conductive Flooring.

(a) Resistance.

1. To prevent the accumulation of dangerous electrostatic charges, the surface of the floor . . . shall provide a path of moderate electrical conductivity between all persons and equipment making contact with the floor. No point on a non-conductive element in the surface of the floor shall be more than ¼ inch from a conductive element of the surface.

NOTE: It is not necessary to provide a special floor-to-ground connection unless required by the authority having jurisdiction.

2. The resistance of the conductive floor shall be less than 1,000,000 ohms as measured between two electrodes placed three feet apart at any points on the floor.

3. For additional protection against electric shock, the resistance of the floor shall be more than 25,000 ohms, as measured between a ground connection and an electrode placed at any point on the floor, and also as measured between two electrodes placed 3 feet apart at any points on the floor.

(b) Method of Test.

1. The floor shall be clean and dry and the room shall be free of explosive gas mixtures. Each electrode shall weigh 5 pounds and shall have a dry, flat, circular contact area 2½ inches in diameter which shall comprise a surface of aluminum or tin foil 0.0005 to 0.001 inch thick backed by a layer of rubber ¼ inch thick and measuring 50 plus or minus 10 hardness as determined with a Shore Type A durometer. (American Society for Testing Materials Tentative Method of Test for Indentation of Rubber by Means of a Durometer, ASTM Designation D676–49T, obtainable from ASTM, 1916 Race St., Philadelphia 3, Pa.)

2. A suitably calibrated ohmmeter with a nominal open-circuit output voltage of 500 volts D.C. and a short-circuit current of 2.5 to 10 milliamperes shall be used. Measurements* shall be made at five or more locations in each room and the results averaged. For compliance with Section 6–2(a)2, the average shall be within the limits specified and no value shall be greater than 5 megohms. For compliance with Section 6–2(a)3, no location shall have a resistance of less than 10,000 ohms and the average for not less than five locations shall be greater than 25,000 ohms. Where resistance to ground is measured, two measurements shall be made at each location, with the test leads interchanged at the instrument between measurements, with the average to be taken as the resistance to ground at that location. All readings may be taken with the electrode or electrodes more than 3 ft. from any ground connection or grounded object resting on the floor.

*NOTE: If the resistance changes appreciably with time during a measurement, the value observed after the voltage has been applied for about 5 seconds shall be considered to be the measured value.

13–10. Testing and Maintenance

(a) Conductive Floors

1. The resistance of conductive floors shall be initially tested prior to use, by the method described in Section 6. Thereafter measurements shall be taken at intervals of not more than one month. A permanent record of the readings shall be kept.

2. To be effective the surface of conductive floors shall not be insulated by a film of oil or wax. Any waxes, polishes, or dressings used for maintenance of conductive floors shall not adversely affect the resistance of the floor.

[10] Reproduced by permission of the National Fire Protection Association, 60 Batterymarch Street, Boston, Massachusetts.

3. Cleaning procedures for conductive floors shall be established, then carefully followed to assure that conductivity characteristics of the floors are not adversely affected by such treatment.

A–6–2. Conductive Flooring

In hazardous locations, a conductive floor serves as a convenient means of electrically connecting persons and objects together to prevent the accumulation of electrostatic charges. A resistance not exceeding 5 to 10 megohms between the objects or persons is generally sufficient to prevent dangerous voltages. The upper limit of 1,000,000 ohms for the resistance of the floor has been chosen as meeting this requirement with a reasonable factor of safety and with reasonable provision for other resistances in the conductive path.

The conductive floor produces a definite shock hazard in the absence of an isolated electrical system. The isolating transformers must always be installed simultaneously with or prior to the installation of the conductive floor. Installation in the opposite sequence is definitely dangerous and should not be contemplated.

The resistance of some flooring materials increases with age. Floors of such materials should have an initial resistance low enough to permit increases in resistance with age without exceeding the limits prescribed in Section 6–2(a)2.

A conductive floor need not be provided with a special grounding connection to prevent the accumulation of charges due to the motion of objects or persons resting on it. To be effective it is necessary only that it be conductive and that the persons and objects be electrically connected to it. Considerable conductivity to ground is generally attained in the usual construction, often because of the proximity of grounded conduits and water pipes. This incidental conductivity to ground and the large area, and therefore capacitance of the floor, make any hazard due to the entry of charged persons or objects into the protected zone negligible, provided such persons and objects have proper conductivity to the floor. Grounded objects within the room, such as portable electrical equipment, will be electrically connected to the floor by the requirements of Section 6, and will thus ground the floor, so that such objects do not increase this electrostatic hazard. Therefore, a special grounding connection need not be incorporated in the floor for electrostatic protection, unless desired or otherwise required.

11. Appendix B. Four-Terminal Method of Measuring Contact and Internal Resistivities

If rectangular current electrodes, C_1 and C_2, and very narrow potential electrodes, P_1 and P_2, are placed parallel to each other on the same surface of a rectangular specimen of uniform internal or volume resistivity, r, as shown in figure 5, all equipotential lines are also parallel to the electrodes. Then, if V, E, and the total resistance, R, are measured, we have $I=V/R=E/Q=Elb/rf$ where Q is the resistance between P_1 and P_2. Thus $r=ERlb/Vf$ (in ohm-cm if R is in ohms and all dimensions are in centimeters).

The contact resistivity, s, may be defined as the resistance of a unit area of the interface between the current electrodes and samples. If the internal resistance of the sample under each current electrode is neglected,[11] we may compute the internal resistance, T, of the sample to be approximately $T=rd/lb=ERd/Vf$. The contact resistance under one electrode is $S=s/wl$ where wl is the apparent contact area of the electrode. Since, under these simplifying assumptions, $R=T+2S=T+2s/wl$, we have in ohm-cm^2

$$s=\frac{wlR}{2}\left(1-\frac{Ed}{Vf}\right).$$

12. Appendix C. Calculation of Resistance From Contact and Internal Resistivities

The resistance between two NFPA electrodes of diameter d spaced D centimeters apart ($D>>d$) on a large floor may be evaluated by adding together the contact resistance under both electrodes and the internal resistance of the floor between two imaginary cylinders which form the downward projections of the electrodes through the floor (again neglecting the resistance of the material under the electrodes).[11] The internal resistance may be calculated by using established formulas of the capacitance per unit length between two long cylinders of the same diameter and spacing, and applying a conversion formula to find the internal resistance T. In cgs electrostatic units this capacitance, for a length b (corresponding to the thickness of the floor), is

$$C=\frac{b}{4\ln\frac{2D}{d}},$$

where ln is the natural logarithm.

The conversion formula from which the internal resistance can be computed can be expressed as $T=r/4\pi C$. Thus

$$T=\frac{r}{\pi b}\ln\frac{2D}{d}.$$

The sum of the contact resistances for both electrodes is $2S=8s/\pi d^2$ and the total resistance between electrodes is approximately

$$R=\frac{2.5s}{d^2}+\frac{0.7r}{b}\log\frac{2D}{d},$$

where log signifies the logarithm to the base 10.

The above relations presuppose a uniform material having a negligible voltage coefficient of resistance. Thus, they are only approximate.

[11] Approximate mathematical investigation shows that because of the high ratio of contact to internal resistivity of these flooring materials, the error introduced by this assumption is much smaller than the influence of other factors, such as the nonuniformity and the voltage coefficient of resistivity.

WASHINGTON, D.C. (Paper 63C2–16)

Journal of Research of the National Bureau of Standards—C. Engineering and Instrumentation

Vol. 63C, No. 2, October–December 1959

Measurement of the Aging of Rubber Vulcanizates

J. Mandel, F. L. Roth, M. N. Steel, and R. D. Stiehler

(June 19, 1959)

A study of aging data in the literature and of measurements made at the National Bureau of Standards indicates that ultimate elongation is the best of the tensile properties for characterizing the deterioration of rubber vulcanizates during storage at various temperatures. Ultimate elongation (strain at failure) decreases during aging for all types of rubber vulcanizates; whereas tensile strength and modulus may increase, decrease, or remain essentially unchanged.

This study includes measurements of ultimate elongation of a nitrile rubber vulcanizate after various periods of storage at temperatures of 23°, 34°, 45°, 57°, 70°, 85°, and 100° C. It also includes a study of the published data on ultimate elongation obtained in an interlaboratory test conducted by Subcommittee 15 of ASTM Committee D–11, involving vulcanizates of five different rubbers stored at 25°, 70°, 100°, and 121° C.

The change in ultimate elongation over prolonged periods of storage cannot be expressed by a simple mathematical equation. However, during most of the useful storage life of a rubber vulcanizate, the elongation decreases approximately linearly with the square root of time. The data indicate that for some vulcanizates an estimate of storage life at room temperature can be made from measurements of ultimate elongation at two or more elevated temperatures.

1. Introduction

The aging of rubber vulcanizates has received the attention of many workers and has been the subject of two symposia [1, 2] [1] and a monograph [3]. It has been generally assessed from changes in tensile properties resulting from conditioning at elevated temperatures for specified periods of time. For historical reasons, greater attention has been given to changes in tensile strength than to changes in the other tensile properties. This emphasis probably resulted from the usefulness of this property in predicting the aging behavior of natural rubber vulcanizates.

A study of the results reported in the literature by Schoch and Juve [4], Buist [3], and others reveals that tensile strength is of little or no value in predicting the aging of synthetic rubber vulcanizates. Upon aging or conditioning at elevated temperatures the tensile strength of these vulcanizates may remain essentially unchanged or even increase. Similarly, the change in modulus or stiffness is not a consistent indicator of the aging process. Synthetic rubber vulcanizates generally become harder on aging; whereas natural rubber vulcanizates may become either harder or softer depending on the conditions and the particular vulcanizate. On the other hand, the ultimate elongation or strain at failure of both natural and synthetic rubber vulcanizates consistently decreases on aging. It is surprising that this property has not received more attention since it is unique for distinguishing elastomers from other materials and is the most valuable of the tensile properties for determining the utility of a rubber compound for a particular application. Further, this property appears to change upon aging in some semblance of an orderly manner. This paper presents a study of this change. The study is restricted to an aging test conducted on a nitrile-butadiene rubber (NBR) vulcanizate at NBS and to the results for the various rubber compounds reported by Schoch and Juve [4]. In all tests, the ultimate elongation is measured on dumbbell-shaped specimens having a cross section in the constricted part approximately 0.25 by 0.08 in. and bench marks 1-in. apart (Die C, ASTM Designation D412–51T [5]).

[1] Figures in brackets indicate the literature references at the end of this paper.

2. Experimental Procedures

Vulcanizates of NBR were prepared in accordance with the procedure for formulation 1E in ASTM Designation D15–57T[5]. NBS standard materials for rubber compounding were used except for the rubber which was a sample of Hycar 1042. For each temperature of aging, three mixes were prepared and blended. From the blended batch, 16 standard sheets (approximately $15 \times 15 \times 0.2$ cm) were vulcanized for 40 min at 150° C. Six specimens were cut from each sheet using Die C, ASTM Designation D412–51T[5]. One specimen from each sheet was tested the day after vulcanization. Another specimen from each sheet was tested after each of five prescribed periods of aging at a particular temperature. The position of the specimen in the sheet was noted. The specimens selected for any one period of aging were approximately equally divided among outside, center, and intermediate positions in the 16 sheets. Five periods of aging at each of seven temperatures were used in this study, as shown in table 1.

3. Results

The mean value for each set of 16 specimens comprising the test under each prescribed condition of time and temperature is given in table 2. In order

TABLE 1. *Temperatures and periods of aging*

Aging temp	Period of aging (in days)					
° C	A	B	C	D	E	F
23	0	100	377	(a)	(a)	(a)
34	0	30	120	270	(a)	(a)
45	0	10	41	90	160	359
57	0	4.9	12.9	51	79	113
70 (a)	0	1	4	9	16	25
70 (b)	0	5	20	46	81	148
85	0	1.21	2.71	4.83	12	15.7
100 (a)	0	0.110	0.375	0.90	1.64	2.67
100 (b)	0	.67	2.67	6	10	16.7

[a] Test still in progress.

to have a basis for studying these results, it is necessary to know the magnitude of the error. Table 3 gives the analysis of variance for the nine groups of unaged specimens. It is inferred from this analysis that the standard deviation of a specimen taken at random from one of the 16 sheets comprising a batch is 30 percent elongation or a coefficient of variation of 4.8 percent. Perhaps a more pertinent measure of error is the one derived from the mean square for the interaction between sheets and aging times. Table 4 gives this information for each of the nine batches. The average coefficient of variation of 5.7 percent is somewhat larger than the 4.8 percent noted above since it includes variability introduced by aging. However, it is not larger than the 5.9 percent coefficient of variation for a specimen taken at random from any batch. Thus, the design of test makes the experiment more efficient than a complete random selection of specimens from all batches. Since 16 specimens are used for each aging condition, the overall coefficient of variation is about 1.4 percent.

It is seen in table 1 that two batches were tested at both 70° and 100° C. The purpose of the second batch is to obtain data under conditions of more extensive aging. In the case of the second batch tested at 100° C, the ultimate elongation is reduced much more than that for any of the other batches, being less than 100 percent after the longest period of aging.

Attempts to express the data in table 2 by the standard kinetic equations for a first or a second order reaction were not successful. Other mathematical expressions of the form

$$y=Ae^{-Bt^n} \text{ and } y=Ae^{-Bt}+Ce^{-Dt}$$

were tried. The latter expression described the data well for long periods of aging, but it did not satisfactorily account for the early part of the curve. Further, this equation was difficult to apply. Therefore, the data were empirically fitted to a power series of the form:

$$y=a+bx+cx^2+dx^3+ \ldots . \quad (1)$$

It was observed that when $x=\sqrt{t}$ and y is the ultimate elongation, the first two terms in this series satisfactorily expressed the data in table 2 except for the last three points of the second batch at 100° C where less than half of the original elongation remained. Accordingly, a study was made of the general applicability of the following simplified equation for expressing the change in elongation upon aging:

$$E=E_o-k\sqrt{t} \quad (2)$$

where E=ultimate elongation after aging for time t, and E_o and k are parameters of the vulcanizate.

Table 5 gives the values of the parameters E_o and k calculated by the method of least squares from the data in table 2. This table also gives the standard deviations and coefficients of variation of the points from the linear regression. These coefficients of variation include the inherent error of 1.4 percent, any variability in temperature during the prolonged periods of aging, and deviations of the true aging curve from eq (2). The coefficients of variation in table 4 indicate that eq (2) is quite close to the true aging curve with the possible exception of batch (b) at 70° C. The ultimate elongation of the unaged specimens for this batch does not conform with the rest of the data for this batch at later times.

TABLE 2. *Ultimate elongations of NBR vulcanizate after prescribed conditions of aging*

Aging temp.	Elongation after period of aging [a]					
	A	B	C	D	E	F
° C	%	%	%	%	%	%
23	652	604	528			
34	623	580	534	475		
45	609	576	532	494	465	394
57	614	563	513	436	402	404
70(a)	596	593	548	527	480	433
70(b)	626	496	420	359	305	251
85	609	532	461	419	342	321
100(a)	656	581	548	461	418	371
100(b)	654	489	353	249	152	67

[a] See table 1 for duration of period.

TABLE 3. *Analysis of variance—unaged specimens*

Source of variation	Degrees of freedom	Mean square	Component of variance
Between batches	8	7947	439
Within batches	135	921	921

TABLE 4. *Estimation of variability derived from interaction of sheet and aging time*

Aging temp.	Mean elong.	Mean square	Coefficient of variation
° C	%		%
23	595	1132	5.6
34	553	762	5.0
45	512	667	5.0
57	489	821	5.9
70(a)	530	824	5.4
70(b)	409	899	7.3
85	447	734	6.1
100(a)	506	604	4.9
100(b)	327	494	6.8
		771 avg	5.8 avg

Figure 1 shows the agreement between the experimental observations and eq (2). The straight lines in the figure represent eq (2) using the parameters in table 5.

TABLE 5. *Regression analysis*

NBS data on NBR vulcanizates

Aging temp	E_o	k	Standard deviation	Coefficient of variation
°C	%			%
23	657	6.4	13.5	2.3
34	626	8.9	5.9	1.1
45	608	11.4	3.8	0.7
57	603	21.1	19.0	3.9
70 (a)	613	33.6	14.5	2.7
70 (b)	581	29.8	34.0	8.3
85	600	74.2	16.5	3.7
100 (a), (b)[a]	647	180.4	11.7	2.3

[a] Omitting three longest periods of aging.

4. Interlaboratory Test

The results of the interlaboratory test reported by Schoch and Juve [4,6] were studied. In test A of this report, there were five compounds made from different rubbers. In test B, there were also five compounds, three of which were made from natural rubber (NR), one from NBR, and one from styrene-butadiene rubber (SBR). Since the paper by Juve and Schoch [6] was published, data for test A have become available through Subcommittee 15 of ASTM Committee D–11, on aging at room temperature for 8 yr. Data for the 35- and 180-min cures of the SBR compound have also become available.

Table 6 summarizes the results obtained by applying eq (2) to the ultimate elongation data of test A for aging at room temperature up to 8 yr. Except for the 90-min cure of the SBR compound, eq (2) represents the data quite well. The data for the SBR 90-min cure are very erratic and not consistent with other aging data for this vulcanizate.

TABLE 6. *Regression analysis*

Test A[a]—aging data at 25°C (approximately)

Rubber	Cure		E_o	k	Standard deviation	Coefficient of variation
	Min	°C	%			%
SBR	60	135	601	4.5	16	3.4
	90	135	553	4.9	44	10.9
NR	45	135	669	5.0	16	3.1
	90	135	614	5.9	13	3.0
CR	45	143	528	2.8	15	3.4
	90	143	499	2.9	7	1.8
NBR	45	135	517	2.5	22	4.9
	90	135	485	2.2	6	1.5
IIR	20	149	530	0.4	19	3.6
	30	149	465	1.4	15	3.6

[a] See references [4] and [6].

Examination of the values of k in table 6 for different cures of the same compound indicates that the change in elongation during aging is not dependent on the cure except for butyl rubber (IIR). The k values for the 35- and 180-min cures of the SBR

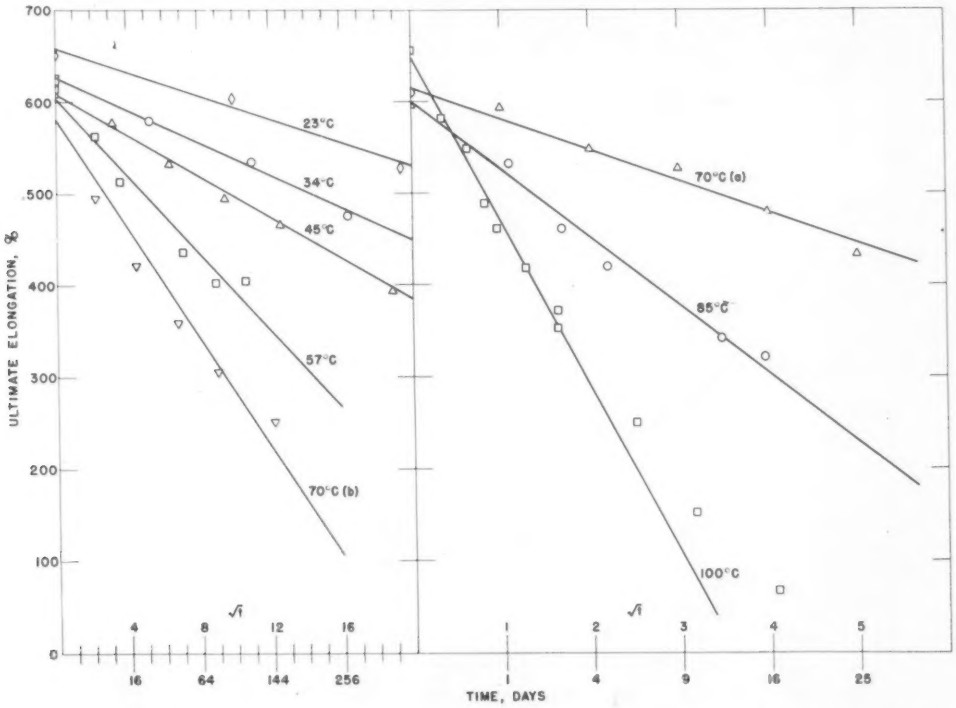

FIGURE 1. *Effect of aging at various temperatures on ultimate elongation of rubber vulcanizates.*

The straight lines represent the least square linear regression for each temperature. The last three points at 100° C are not included in the regression.

compound are about the same as those in table 6 for the 60- and 90-min cures. This independence of k is also observed for all four cures at aging temperatures of 70° and 100° C. At 121° C, k decreases with time of cure possibly as a result of concomitant vulcanization.

Table 7 gives the values of k for the five compounds at the four temperatures of aging. Only the longest cure listed in table 6 is included in table 7. The agreement between the data and eq (2) at the three elevated temperatures is, in general, comparable to that shown in table 6 for aging at room temperature. The anomaly observed for the SBR 90-min cure at 25° C is no longer present at the higher temperatures. On the other hand, the data for the IIR vulcanizate are very erratic. The erratic behavior of these vulcanizates is noted by Juve and Schoch [6].

TABLE 7. *Values of k for test A*[a]

Rubber	Cure		k for temperature of aging			
			25° C	70° C	100° C	121° C
	min	° *C*				
SBR	90	135	4.9	36	117	295
NR	90	135	5.9	54	179	363
CR	90	143	2.9	20	69	162
NBR	90	135	2.2	34	85	172
IIR	30	149	1.4	32	97	186

[a] See references [4] and [6].

Equation (2) expresses the aging data for room temperature of test B fairly well, but not those for elevated aging temperatures. Examination of table 8 shows that the aging periods at the elevated temperatures in test B are much longer than those in test A. As a consequence, the decrease in elongation is so large in test B that eq (2) no longer applies. The data for test B are too limited and erratic to apply the more general eq (1).

TABLE 8. *Aging conditions in interlaboratory tests*[a]

Test	Room temp	70° C	100° C	121° C	125° C	150° C
	yr	*hr*	*hr*	*hr*	*hr*	*hr*
A	1	96	24	6	----	----
	2	168	48	18	----	----
	3	336	96	24	----	----
	4	672	168	48	----	----
	8	----	----	----	----	----
B	1	512	64	----	12	2
	2	1024	128	----	24	4
	4	2048	256	----	48	8
	----	4096	512	----	96	16

[a] See references [4] and [6].

5. Effect of Temperature

If the decrease in ultimate elongation upon aging is the result of a single chemical reaction, the parameter k in eq (2) may be treated as a reaction rate constant. According to the Arrhenius equation

$$\ln k = \frac{-\Delta H}{RT} + c,$$

a plot of the logarithm of k versus the reciprocal of the absolute temperature of aging should be linear. Figure 2 is such a plot of the data in tables 5 and 7,

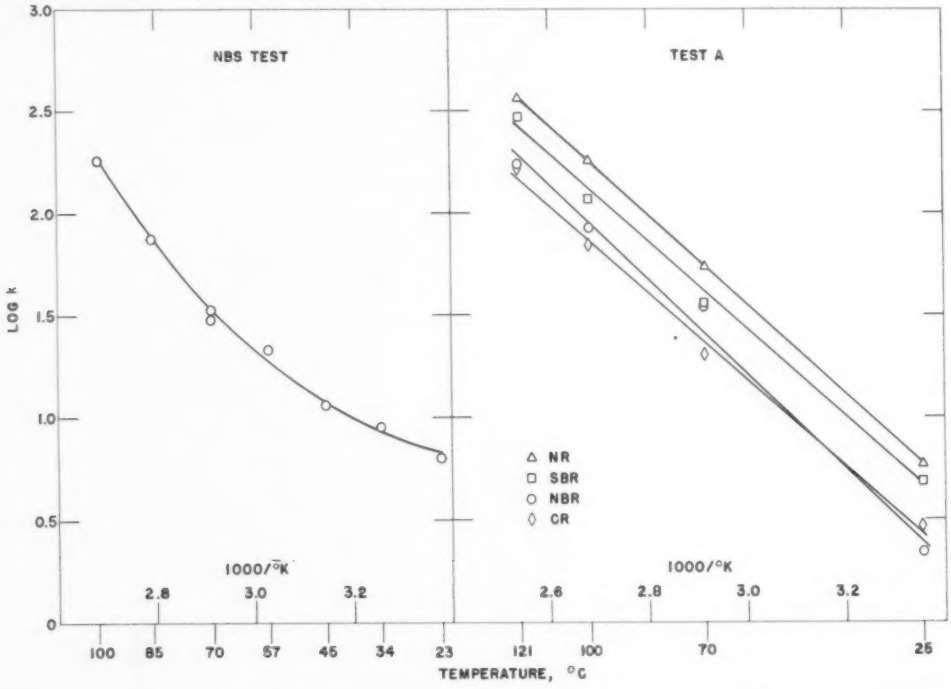

FIGURE 2. *Effect of temperature on aging of rubber vulcanizates.*
The straight lines for test A represent the least square linear regressions.

excluding the IIR compound which behaved erratically at temperatures of 70° C and higher. The curves for the compounds of test A appear to be linear. On the other hand, the curve for the NBR compound studied at NBS definitely is not linear. As the temperature increases, the rate of aging increases much faster than predicted by the Arrhenius equation. When there is curvature, prediction of shelf aging from aging tests at elevated temperature is extremely hazardous.

The slopes in figure 2 are related to the energies of activation. The values calculated for the rubber compounds of test A are: NR 20,500 cal/mole, SBR 19,600 cal/mole, CR 19,400 cal/mole, and NBR 22,100 cal/mole. These values are in reasonable agreement with those reported by Juve and Schoch [6] for the 90-min cures, calculated from equal changes in ultimate elongation.

6. Conclusions

Ultimate elongation (strain at failure) can be used to assess the aging of all rubber vulcanizates. For this purpose, it appears that eq (2) can be used to express the early part of the aging process, corresponding to a period of aging at room temperature of 10 or more years. Prediction of shelf aging from tests at two or more elevated temperatures is only possible if the relationship between aging and temperature is known. For some rubber compounds the Arrhenius equation appears to hold. In these instances, it provides an effective means for esitmating shelf aging.

This study was supported in part by the Bureau of Aeronautics, Department of the Navy, and was presented at the International Rubber Conference, Washington, D.C., Nov. 8 to 13, 1959.

7. References

[1] Symposium on the physical and chemical breakdown of rubbers, Birmingham, England, Trans. Inst. Rubber Ind. **21,** 49–138, 151–157 (1945).
[2] Symposium on aging of rubbers, Chicago, Ill., ASTM STP No. **89** (1949).
[3] J. M. Buist, Ageing and weathering of rubber, I.R.I. Monograph, W. Heffer & Sons Ltd., Cambridge, England (1956).
[4] M. G. Schoch, Jr. and A. E. Juve, Effect of temperature on air aging of rubber vulcanizates, Symposium on aging of rubbers, ASTM STP No. **89**, 59 (1949).
[5] 1958 Book of ASTM Standards, pt. 9, Am. Soc. Testing Materials, Philadelphia, Pa.
[6] A. E. Juve and M. G. Schoch, Jr., The effect of temperature on the air aging of rubber vulcanizates, ASTM Bull. No. **195,** 54 (1954).

Washington, D.C. (Paper 63C2–17)

Selected Abstracts

Pits in metals caused by collision with liquid drops and soft metal spheres, O. G. Engel, *J. Research NBS* **52,** *229 (1959) RP2958.*

An equation is developed to give pit depth as a function of collision velocity for pits formed in soft to medium hard metal plates as a result of collision with liquid drops. The rear face of the target plate must be a free surface. The plate thickness must not be less than 1.5 to 2.0 times the drop diameter nor greater than 4 to 5 times the drop diameter. It is shown that, under the same conditions, on the target plate, the equation is also applicable to pits formed in soft to medium hard metal plates as a result of collision with soft metal spheres that flow radially as a result of the collision. The equation can be used to calculate the dynamic compressive yield strength of soft to medium hard metals.

Lens design: A new approach, O. N. Stavroudis, *J. Research NBS* **63B,** *31 (1959).*

This paper is concerned with the problem of defining and calculating the aberrations of an optical system and their application to lens design. A method of defining total aberrations is presented which involves the derivatives of image space ray coordinates with respect to object space ray coordinates. Their calculation makes use of the properties of Jacobian matrices and Herzberger's fundamental optical invariant.

Analytical integration of the differential equation for water storage, V. U. Yevdjevich, *J. Research NBS* **63B,** *43 (1959).*

The integration of the storage differential equation at present is usually done mostly by graphical or numerical procedures. An approach to the analytical integration of that equation is the subject of this paper. A new method of fitting the given background curves by mathematically tractable expressions is introduced. The storage-outflow discharge relation is expressed in the form of a power function. A general differential equation for water storage $y'+cPy^2-cy^k=0$ is derived, with c and k constants for the given reservoir, and outflow shapes and type of flow, and P being the inflow hydrograph. The analytical solutions of this equation for $P=0$, $P=$const., and certain $P=f(t)$ are given for the integrable cases (tables 1–3, eqs. 12–29). The application of the results obtained is discussed at the end of the paper.

Compressible turbulent boundary layers with heat transfer and pressure gradient in flow direction, A. Walz, *J. Research NBS* **63B,** *53 (1959).*

Derivation of a method of approximate calculation, using integral conditions obtained from basic partial differential equations for viscous compressible fluid. Generalization of semi-empirical laws for turbulent wall friction and dissipation for application in the compressible case with heat transfer.

Power requirements and choice of an optimum frequency for a worldwide standard-frequency broadcasting station, A. D. Watt and R. W. Plush, *J. Research NBS* **63D,** *35 (1959).*

Calculations are presented for the expected transmission characteristics and atmospheric noise levels in the 8 to 100 kc band. When these are combined with carrier-to-noise requirements for a given precision of frequency comparison, it is indicated that a minimum radiated power in the order of 10 to 100 kw for frequencies in the vicinity of 20 kc will be required to provide worldwide coverage.
Minimum observation times of 15 to 30 min appear to be required for these transmitter powers in order to obtain a precision of frequency comparison of one part in 10^9 for typical transmission paths. Carrier-to-noise requirements and the factors determining this ratio are considered for typical receiving systems.

Thermal emf of some thermometric alloys, M. D. Bunch, R. L. Powell, and R. J. Corruccini, *In Low-Temperature Physics and Chemistry; Proc. 5th Internatl. Conf., Univ. of Wis., Madison, Wis., 1957, 484 (1958).*

Measurements of the thermal emf of Au–2.1 at. % Co., Constantan and "normal" silver versus copper have been made from 4° K to 300° K, with reference temperatures at the boiling points of liquid helium, liquid hydrogen and liquid nitrogen. The uniformity of each type of thermo element was tested by simultaneous calibration of several samples from the same melt.

Direct-coupled power amplifier for cryostat heating control, R. D. Goodwin and J. R. Purcell, *Rev. Sci. Instr.* **28,** *No. 7, 581 (1957).*

A direct-coupled amplifier is described which is applicable wherever a steady yet controllable output is required. Input and output circuits employ a comon ground connection. Adjustable output potential is from zero to seventy volts. Voltage gain of the amplifier is unity when utilizing 100 percent feedback for maximum stability. Power gain is in the order of ten thousand. Maximum power of five watts may be increased by adding power tubes.

Multi-factor experiments, M. Zelen and W. S. Connor, *Ind. Quality Control.* **15,** *No. 9, 1 (1959).*

Among the most difficult experiments to conduct is the experiment to investigate the joint effects of several factors on the performance of equipment, or the yield of a product, or the characterstics of a test method, etc. This paper discusses the analysis of such multi-factorial experiments and how one can reduce the number of measurements by selecting a fractional factorial experiment design for planning the experiment.

Note on measurement of sine-wave response of lenses, R. E. Stephens, *J. Opt. Soc. Am.* **49,** *No. 4, 413 (1959).*

In the procedure of Lamberts for measuring the sine-wave response of a lens the phase angle is measured by determining its cosine. For angles less than 45 deg the precision achieved by measuring the cosine is less than is possible by measuring the sine. By displacing the scanning slit one-quarter wavelength transversely data for computing the sine of the phase angle may be obtained.

The elasticity of rubber, L. A. Wood, *Rubber Chem. and Technol.* **31,** *No. 5, 959 (1958).*

Rubbers, natural and synthetic, are unique in being highly extensible and in retracting forcibly and quickly to substantially their original dimensions when released. A summary of what is now known about the nature and origin of the elasticity of rubber is given. It is followed by a statement of some new implications and consequences and an indication of profitable lines of future research.

A dry, static calorimeter for RF power measurement, P. A. Hudson and C. M. Allred, *IRE Trans. Instrumentation* **1–7,** *Nos. 3–4, 292 (1958).*

A new calorimetric type standard rf wattmeter has been developed at the National Bureau of Standards. Its dynamic

range extends from 20 milliwatts to 12 watts and overlaps the range of another standard, a 100μw to 100mw thermistor bridge. The frequency range is from dc to 300 Mc.
The wattmeter is a transfer standard between accurately known values of d-c power and the rf powers to be measured. A complete description of the instrument is given. Analysis of errors indicates a maximum uncertainty of $\pm$ 0.5 percent in the measured rf power. In comparison measurements with other independent methods, agreements of $\pm$(0.5 percent + 2mw) or better were obtained. This accuracy represents an improvement of one order of magnitude over the best presently available commercial instruments designed for the above power and frequency ranges.

Classification and nomenclature for standards of measurement, A. G. McNish, *IRE Trans. Instrumentation* **1-7,** *Nos. 3-4, 371 (1958).*

Standards may be classified and arranged in five categories according to the nature of the standards—Prototype Standards, Derived Standards, Calibration Standards, Standard Instruments, and Standard Materials. Within each category the classification is by orders which show, for standards of a given kind, the way in which they are intercompared.

High-frequency standards of the electronic calibration center, NBSBL, M. C. Selby, *IRE Trans. Instrumentation* **1-7,** *Nos. 3-4, 262 (1958).*

Equipment to calibrate high quality reference standards of power, voltage, attenuation and field strength at 30 kc to 300 Mc and higher frequencies has been developed for use in the Electronic Calibration Center of the NBSBL Radio Standards Division. The major objective is maximum absolute accuracy consistent with the practical expedient of rendering rapid calibration services to government, armed services and private scientific laboratories. Principles involved and special features of this equipment are discussed. This description which covers only a fraction of the equipment planned for the Center, gives a general idea of the type of services anticipated at the National Bureau of Standards for an integrated national rf standardization program, with continuous improvements in the quality and accuracy of primary and reference standards, in general.

High-frequency impedance standards at the National Bureau of Standards, R. C. Powell, R. M. Jickling, and A. E. Hess, *IRE Trans. Instrumentation* **1-7,** *Nos. 3-4, 270 (1958).*

The impedance standards and techniques used at NBS in the frequency range from 30 kc to 300 Mc are described. This paper covers the primary standard and how it is obtained, the comparison methods used in calibrating the working standards and instruments and finally the equipment used in the new Electronic Calibration Center to make measurements for other laboratories. A survey of the field showing the instruments and standards involved, the limitations on standards presently available, in both range and accuracy, and problems involved in accurate calibrations is included.

AC–DC transfer instruments for current and voltage measurements, F. L. Hermach, *IRE Trans. Instrumentation* **1-7,** *No. 3-4, 235 (1958).*

AC–DC transfer instruments provide the vital link between the fundamental d-c standards and the measurement of alternating voltage and current. Electrodynamic, electrostatic and electrothermic transfer instruments can be used for measurements of better than 0.1 percent accuracy at power and audio frequencies. The paper outlines their characteristics, the limitations on transfer accuracy, the methods by which these limitations are overcome, and the useful ranges of voltage, current and frequency. In their best ranges accuracies of 0.01 percent can be achieved with each of these types of instruments.

New apparatus at the National Bureau of Standards for absolute capacitance measurement, M. C. McGregor, J. F. Hersh, R. D. Cutkosky, F. K. Harris, and F. R. Kotter, *IRE Trans. Instrumentation* **1-7,** *Nos. 3-4, 235 (1958).*

Using techniques developed by A. M. Thompson and his group at the National Standards Laboratory of Australia, apparatus for three-terminal capacitance measurements has been constructed at the National Bureau of Standards in Washington. A bridge has been assembled having a least count of 10^{-6} pf when operated at a 20-v level at 1 kc. In terms of NBS facilities, this constitutes both a substantial improvement in precision and an extension of range. The principal elements of the bridge are (a) precise ratio transformers, (b) completely defined three-terminal air capacitors ranging in value from 10^{2} to 10^{-5} pf and (c) a conductance balancing network for injecting quadrature current in the detector branch. Using the theorem recently announced by Thompson and Lampard, a 1-pf calculable cylindrical cross capacitor has been constructed, permitting the assignment of capacitance values with an accuracy essentially limited only by the determination of the length of an end standard gage bar. The constructional features and performances of these various components are described.

Atomic beam sources and the standard of length, K. G. Kessler, R. L. Barger, W. G. Schweitzer, *IRE Trans. Instrumentation* **1-7,** *Nos. 3-4, 181 (1958).*

Three devices which utilize the wavelength of optical transitions in an atomic beam of mercury as a standard of length are described: (1) A beam of atoms excited by electron impact, (2) a beam in absorption which utilizes a Michelson interferometer to produce a narrow line in emission, and (3) a beam in absorption utilized as a narrow band detector.

The ammonia maser as an atomic frequency and time standard, R. C. Mockler, J. Barnes, R. Beehler, H. Salazar, and L. Fey, *IRE Trans. Instrumentation* **1-7,** *Nos. 3-4, 201 (1958).*

The ammonia maser has distinct advantages over atomic beam apparatus in frequency stability, signal to noise ratio and physical size. The maser has, however, the basic shortcoming that the output frequency is not easily reproduced. The effects on the maser frequency resulting from cavity pulling, nonuniform radiation of the beam inside the cavity, hyperfine structure of the spectral line, variations in beam flux, thermal effects and magnetic fields are either avoidable or can be controlled with an adequate degree of precision to fix the frequency to within an estimated 3×10^{-10}.
The measured signal to noise ratio is 10^{4}. The frequency stability for periods of several minutes is 1×10^{-12}. A preliminary frequency for the $J=3$, $K=3$ ammonia transition is 23,870,129,007.$\pm$12 cps (precision) $\pm$100 cps (accuracy).

Testing and operation of ball bearings submerged in liquefied gases, K. B. Martin and R. B. Jacobs, *ASLE Trans.* **2,** *1, 101 (1959).*

The demand for large quantities of liquefied gases has necessitated the development of liquefication turbines and pumping systems. These developments have required studies of bearings and bearing materials suitable for operation in liquid hydrogen and other liquefied gases. The apparatus used to measure frictional torque, wear, and to make life tests on bearings submerged in liquefied gases is described. The information concerning ball bearings obtained from this equipment and some bearing information obtained from an apparatus designed to make basic pump studies is presented. Frictional torque data, wear data, and pictures showing a few of the test ball bearings are included.

Recent developments in the field of microwave power measurements at the National Bureau of Standards, G. F. Engen, *IRE Trans. Instrumentation* **1-7,** *Nos. 3-4 (1958).*

A number of significant advances in the field of microwave power measurement have been recently realized at the Boulder Laboratories of the National Bureau of Standards. These include an improved model of the X-band microwave microcalorimeter, featuring improved accuracy, stability, resolution, and flexibility, which was recently placed in operation, and an improved method of measuring bolometer mount efficiency, using directional couplers, based on the impedance method of Kerns. A preliminary implementation of this second method in waveguide has given agreement of better than 0.5 percent with measurements by the microcalorimetric method which in turn have an absolute accuracy within 0.2 percent.
The problems involved in the intercomparison of bolometer mounts have also been studied, leading to the development of an improved method.

The plasma jet as a spectroscopic source, M. Margshoshes and B. F. Scribner, *Spectrochim. Acta* **138** *(1959).*

The plasma jet utilizes electromagnetic and thermal pinch effects to form an arc plasma into a flame-like cone of high energy. The plasma produced in the discharge chamber is constricted and carried through a circular opening in the cathode by a stream of fluid such as helium, resulting in a jet of hot partially ionized gas. For application as a spectroscopic excitation source, a plasma jet was designed to operate with moderate currents (15–20 A) from a conventional d.c. arc power supply and to include an atomizer to spray a solution through the anode into the discharge. The source excites spark-like spectra, indicating a high excitation temperature. Applied to the spectrographic analysis of stainless steel for iron, chromium and nickel, the results exhibited a coefficient of variation of about 2 percent, including the photometric error. The plasma jet offers promise as a reproducible means of high energy excitation of solutions and of liquids in general.

Reflectors for a microwave Fabry-Perot interferometer, W. Culshaw, *IRE Trans. Microwave Theory Tech.* **MTT-7,** *221 (1959).*

The operation of the Fabry-Perot Interferometer at microwave lengths is discussed, and equations for the transmission and reflection coefficients of the inter-ferometer are derived using transmission line theory. The need for reflectors of high reflectivity and adequate size is indicated, and various methods of reflector design are considered. These consist of lattices of stacked capacitive and inductive rod or strip gratings, as well as perforated metal plate gratings. General equations for the calculation of the reflection and transmission coeffieients of such structures are developed, and the results show that about five such stacked gratings would give high reflectivity. The use of a system of fuzed quartz plates is also considered.

The diode reactance modulator, G. F. Montgomery, *Commun. Electronics, No. 40, 1 (Jan. 1959).*

The reactance modulator that uses one or two diodes to control the current in a capacitor is analyzed with the assumption of lossless circuit elements. Universal curves of susceptance, conductance, and control current, as functions of control voltage, are calculated for three basic circuits.

Recently developed microwave impedance standards and methods of measurement, R. W. Beatty and D. M. Kerns, *IRE Trans. Instrumentation* **1-7,** *Nos. 3-4 (1958).*

Recent developments by the Radio Standards Division of the Boulder Laboratories of the National Bureau of Standards have included microwave impedance standards and measurement methods of greatly increased accuracy.
The concept and analysis of the half-round inductive obstacle in rectangular waveguide as an impedance standard by D. M. Kerns has formed the basis for a series of highly accurate fixed impedance standards.
Advanced techniques for measuring VSWR have permitted measurements of these standards which agree with the calculated values within 0.05 percent, for VSWR's up to 1.5.
In the measuring techniques described, magnified and squared VSWR responses are used as well as directional couplers with auxiliary tuners.

Other NBS Publications*

Section A. Physics and Chemistry, Volume 63A, No. 1, July—August 1959. 70 cents.

Description and analysis of the first spectrum of iodine. C. C. Kiess and C. H. Corliss.
CH in the solar spectrum. Charlotte E. Moore and H. P. Broida.
Infrared studies in the 1- to 15-micron region to 30,000 atmospheres. C. E. Weir, E. R. Lippincott, A. Van Valkenburg, and E. N. Bunting.
Phosphinoborine compounds: mass spectra and pyrolysis. L. A. Wall, S. Straus, R. E. Florin, F. L. Mohler, and P. Bradt.
Experimental and theoretical study of kinetics of bulk crystalization in poly (chlorotrifluoroethylene). J. D. Hoffman, J. J. Weeks, and W. M. Murphey.

Section A. Physics and Chemistry, Volume 63A, No. 2, September–October 1959. 70 cents.

Reflection of fast neutrons from water. Martin J. Berger and John W. Cooper.
Some vibrational-rotational bands of deuterated methanes. Harry C. Allen, Jr., and Earle K. Plyler.
Precise coulometric titration of acids and bases. John K. Taylor and Stanley W. Smith.
Heat of formation of titanium tetraiodide. W. H. Johnson, A. A. Gilliland, and E. J. Prosen.
Reactions of pentafluorohalobenzenes. Walter J. Pummer and Leo A. Wall.
Tritium-labeled compounds I. Radioassay of tritium-labeled compounds in "Infinitely Thick" films with a windowless, gas-flow, proportional counter. Horace S. Isbell, Harriet L. Frush, and Ruth A. Peterson.
Tritium-labeled compounds II. General-purpose apparatus, and procedures for the preparation, analysis, and use of tritium oxide and tritium-labeled lithium borohydride. Horace S. Isbell and Joseph D. Moyer.
Preparation of trichloride and tetrachloride of molybdenum. Dwight E. Couch and Abner Brenner.
Infrared spectra of asphalts. Burton D. Beitchman.

Section B. Mathematics and Mathematical Physics, Volume 63B, No. 1, July–September 1959. 75 cents.

Relations between summation methods and integral transformations. W. Greub.

On a modification of Watson's lemma. F. Oberhettinger.
Principal submatrices of a full-rowed non-negative matrix. K. Goldberg.
Zeros of certain polynomials. A. J. Goldman.
Tables of transport integrals: A supplement. W. M. Rogers, W. J. Hall, and R. L. Powell.
Lens design: A new approach. O. N. Stavroudis. (See abstract above.)
Analytical integration of the differential equation for water storage. V. M. Yevdjevich. (See abstract above.)
Compressible turbulent boundary layers with heat transfer and pressure gradient in flow direction. A. Walz. (See abstract above.)

Section D. Radio Propagation, Volume 63D, No. 1 July–August 1959. 70 cents.

Preliminary results of the National Bureau of Standards radio and ionospheric observations during the International Geophysical Year. D. M. Gates.
Origin of [OI] 5577 in the airglow and the aurora. F. E. Roach, J. W. McCaulley, and E. Marovich.
Comparison of absolute intensities of [OI] 5577 in the auroral and subauroral zones. F. E. Roach, J. W. McCaulley, and C. M. Purdy.
Origin of "very-low-frequency emissions." R. M. Gallet and R. A. Helliwell.
Climatology of ground-based radio ducts. B. R. Bean.
Power requirements and choice of an optimum frequency for a worldwide standard-frequency broadcasting station. A. D. Watt and R. W. Plush. (See abstract above.)
Measurements of phase stability over a low-level tropospheric path. M. C. Thompson, Jr., and H. B. Janes.
System loss in radio wave propagation. K. A. Norton.
Mode expansion in the low-frequency range for propagation through a curved stratified atmosphere. H. Bremmer.
Transmission and reflection by a parallel wire grid. M. T. Decker.
Synoptic variation of the radio refractive index. B. R. Bean and L. P. Riggs.
Low-frequency propagation paths in arctic area. A. D. Watt, E. L. Maxwell, and E. H. Whelan.

Section D. Radio Propagation, Volume 63D, No. 2, September–October 1959. 70 cents.

Stratification in the lower ionosphere. C. Ellyett and J. M. Watts.
Effect of small irregularities on the constitutive relations for the ionosphere. K. G. Budden.
Ionospheric investigations using the sweep-frequency pulse technique at oblique incidence. Vaughn Agy and Kenneth Davis.
Fields in electrically short ground systems: an experimental study. A. N. Smith and T. E. Devaney.
Diffraction of electromagnetic waves by smooth obstacles for grazing angles. James R. Wait and Alyce M. Conda.
Very-low-frequency radiation spectra of lightning discharges. W. L. Taylor and A. G. Jean.
Radio-wave scattering by tropospheric irregularities. Albert D. Wheelon.
Study at 1046 megacycles per second of the reflection coefficient of irregular terrain at grazing angles. Raymond E. McGavin and Leo J. Maloney.
Synoptic study of the vertical distribution of the radio refractive index. B. R. Bean, L. P. Riggs, and J. D. Horn.

On the theory of fading properties of a fluctuating signal imposed on a constant signal, C599, H. Bremmer, 25 cents.
Stark broadening functions for the hydrogen lines, A. B. Underhill and J. H. Waddell, C603, 65 cents.
Maximum permissible body burdens and maximum permissible concentrations of radionuclides in air and in water for occupational exposure, (supersedes H52), H69, 35 cents.
Wind pressures in various areas of the United States, G. N. Brekke, BMS152, 15 cents.
Fractional factorial experiment designs for factors at three levels. W. S. Connor and M. Zelen, AMS54, 30 cents.
Tables of osculatory interpolation coefficients, H. E. Salzer, AMS56, 30 cents.
A double-pulse total-absorption fast neutron spectrometer, L. J. Nicastro and R. S. Caswell, TN1 (PB 151360). 75 cents. (See abstract above.)
World maps of F2 critical frequencies and maximum usable frequency factors, D. H. Zacharisen, TN2 (PB151361), $3.50.
Detwinning quartz crystals, F. P. Phelps, TN3 (PB151362), 50 cents.
The vapor pressures of some hydrocarbons in the liquid and solid state at low temperatures, W. T. Ziegler, TN4 (PB151363), 75 cents.
Tables of median hourly values of the cosine of the solar zenith angle (χ) for thirty-five locations, R. E. McDuffie, TN5 (PB151364), $1.25.
An analysis of propagation measurements made at 418 Mc well beyond the radio horizon, H. B. Janes, J. C. Stroud, and M. T. Decker, TN6 (PB151365), $2.25.
Low- and very low-radiofrequency tables of ground wave parameters for the spherical earth theory: The roots of Riccati's differential equation, (supplementary numerical data for NBS Circ. 573), J. R. Johler, L. C. Walters, and C. M. Lilley, TN7 (PB151366), $2.25.
Mechanized computation of thermodynamic tables at the National Bureau of Standards: The calculation of the equilibrium composition and thermodynamic properties of dissociated and ionized gaseous systems, Proc. of Symposium—Thermodynamic and Transport Properties of Gases, Liquids, and Solids, J. Hilsenrath and J. H. Wegstein, Am. Soc. Mech. Engrs., New York, N.Y., 416 (1959).

Nuclear magnetic reasonance in semiconductors, O. Kraus, J. Phys. Chem. Solids **8,** 504 (1959).

The origin of the current nomenclature for the ionospheric layers, R. Silberstein, J. Atmospheric and Terrest. Phys. **13,** 382 (1959).

A survey of the present knowledge of sporadic-*E* ionization, J. A. Thomas and E. K. Smith, J. Atmospheric and Terrest. Phys. **13,** 295 (1959).

Downcoming radio waves; measurement of characteristics, Electronic and Radio Engr. **36,** 106 (1959).

Experiments on the β decay of polarized nuclei, E. Ambler, R. W. Hayward, D. D. Hoppes, and R. P. Hudson, Physica **24,** S64 (1958), No. 40 (1959).

Standards and measurements for electronics, A. V. Astin, IRE Trans. Instrumentation **1–7,** Nos. 3–4, 134 (1958).

A free precession determination of the proton gyromagnetic ratio, P. L. Bender and R. L. Driscoll, IRE Trans. Instrumentation **1–7,** Nos. 3–4 176 (1958).

A note on the computation of x^2, M. G. Natrella, Am. Statistician **13,** No. 1, 20 (1959).

On the convergence of the Rayleigh quotient iteration for the computation of the characteristic roots and vectors. II, A. M. Ostrowski, Arch. Rational Mech. Anal. **2,** No. 5, 423 (1959).

Un nouveau critere d'univalence des transformations dans un R^n, A. M. Ostrowski, Compt. rend. acad. sci. **248,** 348 (1959).

Modulation studies for VHF ionospheric scattering, J. W. Koch, Record of National Symposium on Extended Range and Space Communications, 114 (Washington, D.C., Oct. 6–7, 1958).

1958 Critique of VHF ionospheric scatter communication, (Survey Paper), R. C. Kirby, Record of National Symposium on Extended Range and Space Communications. 90 (Washington, D.C., October 6–7, 1958).

A statistician and the post office: A case history in operations research, N. C. Severo, Trans. 1959 Conf. Admin. Appl. Div. of ASQC (Milwaukee, Wis., 1959).

Beta-gamma correlations from polarized nuclei, Chapter III. (Interactions Faibles), E. Ambler, R. W. Hayward, D. D. Hoppes, and R. P. Hudson, Compt. rend. Congr. Intern. Phys. Nucleaire, Paris, July 1958 (1959).

The effect of echo on the operation of high-frequency communication circuits, D. K. Bailey, IRE Trans. Antennas and Propagation **6,** No. 4, 325 (1958).

An improved 8-hydroxyquinoline method for the determination of magnesium oxide in portland cement, H. A. Berman, ASTM Bull. No. 237, 51 (1959).

Some radiological applications of gamma-ray transport theory, M. J. Berger and L. V. Spencer, Radiation Research **10,** No. 5, 552 (1959).

Degradation of cellulose acetate films, W. K. Wilson and B. W. Forshee, SPE Journal **15,** No. 2, (1959).

Science fairs, A. T. McPherson, ASTM Bull. No. 237, **29,** (1959).

Selection of glasses for three-color achromats, R. E. Stephens, J. Opt. Soc. Am. **49,** No. 4, 398 (1959).

Thermal decomposition of poly(vinyl chloride), R. R. Stromberg, S. Strauss, and B. G. Achhammer, J. Polymer Sci. **35,** No. 129, 355 (1959).

Thermal and electrical conductivity of aluminum and aluminum alloys, W. J. Hall, H. M. Roder, and R. L. Powell, In Low-Temperature Physics and Chemistry; Proc. 5th Internatl. Conf., Univ. of Wis., Madison, Wis., 1957, 389 (1958).

Thermal and electrical conductivity of pure copper, H. M. Roder, R. L. Powell, and W. J. Hall, In Low-Temperature Physics and Chemistry; Proc. 5th Internatl. Conf., Univ. of Wis., Madison, Wis., 1957, 364 (1958).

Transmission of power in radio propagation, J. R. Wait, Electronic and Radio Engr. **36,** No. 4, 146 (1959).

Formation of ozone from atomic oxygen at low temperatures, R. A. Ruehrwein and J. S. Hashman, J. Chem. Phys. **30,** No. 3, 823 (1959).

The electromotive force method of determining ionization constants: ionization of bisulfate ion, W. J. Hamer, (book) The structure of Electropytic Solutions, edited by W. J. Hamer, 236 (John Wiley & Sons, Inc., New York, N.Y., 1959).

Kinetics of D atom reactions with H_2 CH_4, and D_2CO, R. Klein, J. R. McNesby, M. D. Sheer, and L. J. Schoen, J. Chem. Phys. **30,** No. 1, 58 (1959).

Natural and synthetic rubbers, M. Tryon and F. J. Linnig, Anal. Chem. Appl. Revs. **31,** Part II, No. 4, 767 (1959).

Molecular complexes and their spectra. IX. Infrared absorption by iodine in its pyridine complexes and in benzene, E. K. Plyler and R. S. Mulliken, J. Am. Chem. Soc. **81,** 828 (1959).

The emission of HeI λ 10830, during the great flare of August 26, 1958, E. Tandberg-Hanssen, W. Curtis, and K. Watson, Astrophys. J. **129,** No. 1, 238 (1959).

Tacan coverage and channel requirements, M. T. Decker, IRE Trans. Aeronaut. Navigational Electronics **ANE–4,** 3, 135 (1957).

A phenomenological theory of induced electrical polarization, J. R. Wait, Can. J. Phys. **36,** 1634 (1958).

A study of VLF field strength data: Both old and new, J. R. Wait, Geofis. pure e Appl. **41,** 73 (1958/III).

Near infrared solar radiation measurements by balloon to an altitude of 1,000,000 feet, D. M. Gates, D. G. Murcray, C. C. Shaw, and R. J. Herbold, J. Opt. Soc. Am. **48,** 12, 1010 (1958).

Products of cool flame oxidation of propane-2-^{13}C, R. E. Ferguson and C. R. Yokley, Seventh Symposium (International) on Combustion (London and Oxford, 28 Aug.—3 Sept. 1958) Butterworths Scientific Publications, London (1958).

Emission spectra from mixtures of atomic nitrogen and organic substances, N. H. Kiess and H. P. Broida, Seventh Symposium (International) on Combustion (London and Oxford, 28 Aug.—3 Sept. 1958) Butterworths Scientific Publications, London (1958).

United States planning for the large scale liquefaction and transportation of helium, D. B. Mann and B. W. Birmingham, Physica **24,** S144 (1958).

Transport properties of dilute alloys of copper, R. L. Powell, W. J. Hall, and H. M. Roder, Physica **24,** S176 (1958).

The application of the theory of stochastic processes to chemical kinetics, E. W. Montroll and K. E. Shuler, (Book) Advances in Chemical Physics, Vol. 1 (Interscience Publishers, Inc., New York, N.Y., 1958).

Dense subgraphs and connectivity, R. E. Nettleton, K. Goldberg, and M. S. Green, Can. J. Math. **11,** 262 (1959).

Experiments with the cell Bi, Bi_2O_3, $ZnCl_2/ZnCl_2/ZnCl_2$, Zn between 450° and 510°, R. E. Wood, J. Phys. Chem. **63,** 525 (1959).

Rheology of polyisobutylene. III. Elastic recovery, non-Newtonian flow, and molecular weight distribution, H. Leaderman, R. G. Smith, and L. C. Williams, J. Polymer Sci. **36,** 233 (1959).

Thermal degradation of polyethylene oxide and polypropylene oxide, S. L. Madorsky and S. Straus, J. Polymer Sci. **36,** 183 (1959).

U^{235} fission product decay spectra at various times after fission, A. T. Nelms and J. W. Cooper, Health Phys. **1,** 427 (1959).

Contribution to the theory of Brownian motion, R. W. Zwanzig, Physics of Fluids **2,** 1, 12 (Jan–Feb. 1959).

Low-temperature X-ray studies of Rice's blue material, L. H. Bolz, F. A. Mauer, and H. S. Peiser, J. Chem. Phys. **30,** 1, 349 (1959).

Contribution of annihiliation radiation to the gamma-ray flux in lead, M. J. Berger, J. H. Hubbell, and I. H. Reingold, Phys. Rev. **113,** 3,857 (1959).

On the electromagnetic response of an imperfectly conducting thin dyke, J. R. Wait, Geophysics **24,** 1, 167 (1959).

Temperature dependence of the breakdown field of barium titanate, P. H. Fang and W. S. Brower, Phys. Rev. **113,** 2,456 (1959).

A reexamination of the crystal structures of α and β nitrogen, L. H. Bolz, M. E. Boyd, F. A. Mauer, and H. S. Peiser, Acta Cryst. **12,** Part 3,247 (1959).

A study of the morphology of ionospheric storms, S. Matsushita, J. Geophys. Research **64,** 3, 305 (1959).

Energetic species trapped at 4.2° K from gaseous discharges, G. J. Minkoff, F. I. Scherber, and J. S. Gallagher, J. Chem. Phys. **30,** 3, 753 (1959).

Source function in a non-equilibrium atmosphere. III. The influence of a chromosphere, J. T. Jefferies and R. N. Thomas, Astrophys. J. **129,** 2, 401 (1959).

Theoretical multiplet strengths, F. Rohrlich, Astrophys. J. **129,** 2, 441 (1959).

Oscillatory currents in the ionosphere, (abstract) Astron. J. **64,** 56 (1959).

A new method of checking the consistency of precedence matrices, R. B. Marimont, J. Assoc. Computing Machinery **6,** 2, 164 (1959).

Comments on the structure of 1,1,1-trifluoro-2-butyne, V. W. Laurie, J. Chem. Phys. **30,** 4, 1101 (1959).

Effect of heat-treatment on the constitution and mechanical properties of some hydrated aluminous cements, J. Am. Ceram. Soc. **42,** 4, 185 (1959).

Electronic quenching of OH ($^2\Sigma^+$) in flames and its significance in the interpretation of rotational relaxation, T. Carrington, J. Chem. Phys. **30,** 4, 1087 (1959).

IGY observations of F-layer scatter in Far East, R. Bateman, J. W. Finney, E. K. Smith, L. H. Tveten, and J. M. Watts, J. Geophys. Research **64,** 4, 403 (1959).

Diurnal change of ionospheric heights deduced from phase velocity measurements at VLF (letter), J. R. Wait, Proc. IRE **47,** 998 (1959).

Green coronal line intensity and geomagnetism, C. Warwick, J. Geophys. Research **64,** 5, 527 (1959).

Models of the atmospheric radio refractive index, B. R. Bean and G. D. Thayer, Proc. IRE **47,** 740 (1959).

Sporadic *E* at VHF in the USA, R. M. Davis, Jr., E. K. Smith, and C. D. Ellyett, Proc. IRE **47,** 5, 762 (1959).

**Publications for which a price is indicated (except for Technical Notes) are available only from the Superintendent of Documents, U.S. Government Printing Office, Washington 25, D.C. (foreign postage, one-fourth additional). Technical Notes are available only from the Office of Technical Services, U.S. Department of Commerce, Washington 25, D.C. (Order by PB number.) Reprints from outside journals and the NBS Journal of Research may often be obtained directly from the authors.*

INDEX TO VOLUME 63C

July–December 1959

A

Page

Air lubricated piston gage for pressures below one-half inch of mercury, a tilting ... 47
Aging of rubber vulcanizates, measurement ... 141
Analyzer, stroboscopic vibration ... 97
Asphalt, effect of light and water on the degradation of ... 31

B

Balances, a photoelectric followup and recording system, and its application to remote observations of the beam in high-precision ... 91
Ball bearings at high speeds and extreme temperatures, friction and endurance of prelubricated and unlubricated ... 19
Boone, T. H., F. L. Hermach, E. H. MacArthur, R. C. McAuliff, Conductive flooring for hospital operating rooms ... 125
Bowman, H. A., L. B. Macurdy, A photoelectric followup and recording system, and its application to remote observations of the beam in high-precision balances ... 91
Brooks, R., S. Edelman, S. Saito, E. Jones, E. R. Smith, A stroboscopic vibration analyzer ... 97

C

Capacitors, conical coaxial, and their advantages ... 87
Cathodic protection of steel in a high resistivity environment, current and potential relations for ... 37
Coaxial capacitors, conical, and their advantages ... 87
Coleman, J. W., L. B. Leder, L. Marton, D. C. Schubert, Electron beam magnetometer ... 69
Compact multianvil wedge type high-pressure apparatus ... 59
Conductive flooring for hospital operating rooms ... 125
Conical coaxial capacitors and their advantages ... 87
Coulometer, coulometric-titration ... 65
Coulometric-titration coulometer ... 65
Creep of cold-drawn nickel ... 1
Current and potential relations for the cathodic protection of steel in a high resistivity environment ... 37

D

Darling, W. R., F. E. Washer, Evaluation of lens distortion by the inverse nodal slide ... 105
—, —, Evaluation of lens distortion by the modified goniometric method ... 113
Degradation of asphalt, effect of light and water on the ... 31
Distortion by the inverse nodal slide, evaluation of ... 105
Distortion by the modified goniometric method, evaluation of lens ... 113

E

Edelman, S., R. Brooks, S. Saito, E. Jones, E. R. Smith, A stroboscopic vibration analyzer ... 97
Effect of light and water on the degradation of asphalt ... 31
Electron beam magnetometer ... 69
Engen, G. F., A refined X-band microwave microcalorimeter ... 77
Evaluation of lens distortion by the inverse nodal slide ... 105
Evaluation of lens distortion by the modified goniometric method ... 113

F

Fire tests, proposed criteria for defining load failure of beams, floors, and roof constructions during ... 121
Flooring for hospital operating rooms, conductive ... 125
Friction and endurance of prelubricated and unlubricated ball bearings at high speeds and extreme temperatures ... 19

G

Goniometric method, evaluation of lens distortion by the modified ... 113

H

Hermach, F. L., T. H. Boone, E. H. MacArthur, R. C. McAuliff, Conductive flooring for hospital operating rooms ... 113
High-pressure apparatus, compact multianvil wedge type ... 59
Hospital operating rooms, conductive flooring for ... 125
Hutton, U. O., A tilting air-lubricated piston gage for pressures below one-half inch of mercury ... 47
—, *E. C. Lloyd, D. P. Johnson*, Compact multianvil wedge type high-pressure apparatus ... 59

I

Page

Inverse nodal slide, evaluation of lens distortion by ... 105

J

Jenkins, W. D., C. R. Johnson, Creep of cold-drawn nickel ... 1
Johnson, C. R., W. D. Jenkins, Creep of cold-drawn nickel ... 1
Johnson, D. P., E. C. Lloyd, U. O. Hutton, Compact multianvil wedge type high-pressure apparatus ... 59
Jones, E., S. Edelman, R. Brooks, S. Saito, E. R. Smith, A stroboscopic vibration analyzer ... 97

K

Kleinschmidt, L. R., H. R. Snoke, Effect of light and water on the degradation of asphalt ... 31

L

Leder, L. B., L. Marton, J. W. Coleman, D. C. Schubert, Electron beam magnetometer ... 69
Lens distortion by the inverse nodal slide, evaluation of ... 105
Lens distortion by the modified goniometric method, evaluation of ... 113
Lloyd, E. C., U. O. Hutton, D. P. Johnson, Compact multianvil wedge type nigh-pressure apparatus ... 59
Load failure of beams, floors, and roof constructions during fire tests, proposed criteria for defining ... 121

M

MacArthur, E. H., T. H. Boone, F. L. Hermach, R. C. McAuliff, Conductive flooring for hospital operating rooms ... 125
Macurdy, L. B., H. A. Bowman, A photoelectric followup and recording system, and its application to remote observations of the beam in high-precision balances ... 91
Magnetometer, electron beam ... 69
Mandel, J., F. L. Roth, M. N. Steel, R. D. Stiehler, Measurement of the aging of rubber vulcanizates ... 141
Marton, L., L. B. Leder, J. W. Coleman, D. C. Schubert, Electron beam magnetometer ... 69
McAuliff, R. C., T. H. Boone, F. L. Hermach, E. H. MacArthur, Conductive flooring for hospital operating rooms ... 125
Measurement of the aging of rubber vulcanizates ... 141
Microcalorimeter, a refined X-band microwave ... 77
Microwave microcalorimeter, a refined X-band ... 77
Multianvil wedge type high-pressure apparatus ... 59

N

Nickel, cold-drawn, creep of ... 1
Nodal slide, evaluation of lens distortion by the inverse ... 105

O

Operating rooms, conductive flooring for hospital ... 125

P

Photoelectric followup and recording system, and its application to remote observations of the beam in high-precision balances ... 91
Piston gage for pressures below one-half inch of mercury, tilting air-lubricated ... 47
Prelubricated and unlubricated ball bearings at high speeds and extreme temperatures, friction and endurance of ... 19
Proposed criteria for defining load failure of beams, floors, and roof constructions during fire tests ... 121
Publications of the National Bureau of Standards ... 83

R

Recording system, a photoelectric followup and its application to remote observations of the beam in high-precision balances ... 91
Refined X-band microwave microcalorimeter ... 77
Robertson, A. F., and J. V. Ryan, Proposed criteria for defining load failure of beams, floors, and roof constructions during fire tests ... 121
Roth, F. L., J. Mandel, M. N. Steel, R. D. Stiehler, Measurement of the aging of rubber vulcanizates ... 141
Rubber vulcanizates, measurement of the aging ... 141
Ryan, J. V., A. F. Robertson, Proposed criteria for defining load failure of beams, floors, and roof construction during fire tests ... 121

S

Page

Saito, S., S. Edelman, F. Brooks, E. Jones, E. F. Smith, A stroboscopic vibration analyzer 97

Schubert, D. C., J. W. Coleman, L. B. Leder, L. Marton, Electron beam magnetometer 69

Schwerdtfeger, W. J., Current and potential relations for the cathodic protection of steel in a high resistivity environment 37

Selby, M. C., Conical coaxial capacitors and their advantages 87

Smith, E. F., S. Edelman, F. Brooks, S. Saito, E. Jones, A stroboscopic vibration analyzer 97

Smith, S. W., J. K. Taylor, A coulometric-titration coulometer 65

Snoke, H. F., L. F. Kleinschmidt, Effect of light and water on the degradation of asphalt 31

Steel in a high resistivity environment, current and potential relations for the cathodic protection of 37

Steel, M. N., J. Mandel, F. L. Roth, F. D. Stiehler, Measurement of the aging of rubber vulcanizates 141

Stiehler, F. D., J. Mandel, F. L. Roth, M. N. Steel, Measurement of the aging of rubber vulcanizates 141

Stroboscopic vibration analyzer 97

T

Page

Taylor, J. K., S. W. Smith, A coulometric-titration coulometer 65

Tilting air-lubricated piston gage for pressures below one-half inch of mercury 47

V

Vibration, stroboscopic analyzer 97

W

Washer, F. E., W. P. Darling, Evaluation of lens distortion by the inverse nodal slide 105

—, —, Evaluation of lens distortion by the modified goniometric method 113

White, H. S., Friction and endurance of prelubricated and unlubricated ball bearings at high speeds and extreme temperatures 19

UNITED STATES
GOVERNMENT PRINTING OFFICE
DIVISION OF PUBLIC DOCUMENTS
WASHINGTON 25, D.C.

OFFICIAL BUSINESS

PENALTY FOR PRIVATE USE TO AVOID PAYMENT OF POSTAGE, $300 (GPO)

National Bureau of Standards, Journal of Research Vol. 63C, No. 2 October–December 1959
C. Engineering and Instrumentation

Contents

	Page
Conical coaxial capacitors and their advantages. M. C. Selby.	87
A photoelectric followup and recording system, and its application to remote observations of the beam in high-precision balances. H. A. Bowman and L. B. Macurdy.	91
A stroboscopic vibration analyzer. S. Edelman, R. Brooks, S. Saito, E. Jones, and E. R. Smith.	97
Evaluation of lens distortion by the inverse nodal slide. Francis E. Washer and Walter R. Darling.	105
Evaluation of lens distortion by the modified goniometric method. Francis E. Washer and Walter R. Darling.	113
Proposed criteria for defining load failure of beams, floors, and roof constructions during fire tests. J. V. Ryan and A. F. Robertson.	121
Conductive flooring for hospital operating rooms. Thomas H. Boone, Francis L. Hermach, Edgar H. MacArthur, and Rita C. McAuliff.	125
Measurement of the aging of rubber vulcanizates. J. Mandel, F. L. Roth, M. N. Steel, and R. D. Stiehler.	141
Publications of the National Bureau of Standards.	147
Index to volume 63C, July to December 1959.	153

For sale by the Superintendent of Documents, U.S. Government Printing Office, Washington 25, D.C. Price 75 cents (single copy)
Subscription price: $2.25 a year; 50 cents additional for foreign mailing.

UNITED STATES GOVERNMENT PRINTING OFFICE, WASHINGTON : 1959